



UNIL | Université de Lausanne

Unicentre

CH-1015 Lausanne

<http://serval.unil.ch>

Year : 2020

HIGH RESOLUTION ANALYSIS OF PROTOPHLOEM DIFFERENTIATION IN THE ARABIDOPSIS ROOT TIP

Moret Bernard

Moret Bernard, 2020, HIGH RESOLUTION ANALYSIS OF PROTOPHLOEM
DIFFERENTIATION IN THE ARABIDOPSIS ROOT TIP

Originally published at : Thesis, University of Lausanne

Posted at the University of Lausanne Open Archive <http://serval.unil.ch>

Document URN : urn:nbn:ch:serval-BIB_591954EDE3394

Droits d'auteur

L'Université de Lausanne attire expressément l'attention des utilisateurs sur le fait que tous les documents publiés dans l'Archive SERVAL sont protégés par le droit d'auteur, conformément à la loi fédérale sur le droit d'auteur et les droits voisins (LDA). A ce titre, il est indispensable d'obtenir le consentement préalable de l'auteur et/ou de l'éditeur avant toute utilisation d'une oeuvre ou d'une partie d'une oeuvre ne relevant pas d'une utilisation à des fins personnelles au sens de la LDA (art. 19, al. 1 lettre a). A défaut, tout contrevenant s'expose aux sanctions prévues par cette loi. Nous déclinons toute responsabilité en la matière.

Copyright

The University of Lausanne expressly draws the attention of users to the fact that all documents published in the SERVAL Archive are protected by copyright in accordance with federal law on copyright and similar rights (LDA). Accordingly it is indispensable to obtain prior consent from the author and/or publisher before any use of a work or part of a work for purposes other than personal use within the meaning of LDA (art. 19, para. 1 letter a). Failure to do so will expose offenders to the sanctions laid down by this law. We accept no liability in this respect.



UNIL | Université de Lausanne

Faculté de biologie
et de médecine

Département de Biologie Moléculaire Végétale

**HIGH RESOLUTION ANALYSIS OF PROTOPHLOEM DIFFERENTIATION
IN THE ARABIDOPSIS ROOT TIP**

Rapport de thèse de doctorat ès sciences de la vie (PhD)

présentée à la

Faculté de biologie et de médecine
de l'Université de Lausanne

par

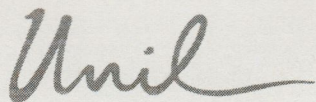
Bernard Moret

Ingénieur diplômé de l'Ecole Polytechnique Fédérale de Lausanne

Jury

Prof. Claus Wedekind, Président
Prof. Christian Hardtke, Directeur de thèse
Prof. Niko Geldner, expert
Prof. Thomas Berleth, expert

Lausanne 2020



UNIL | Université de Lausanne

Faculté de biologie
et de médecine

Ecole Doctorale

Doctorat ès sciences de la vie

Imprimatur

Vu le rapport présenté par le jury d'examen, composé de

Président·e	Monsieur	Prof.	Claus	Wedekind
Directeur·trice de thèse	Monsieur	Prof.	Christian	Hardtke
Expert·e·s	Monsieur	Prof.	Niko	Geldner
	Monsieur	Prof.	Thomas	Berleth

le Conseil de Faculté autorise l'impression de la thèse de

Monsieur Bernard Moret

Master en Sciences et technologies du vivant, EPFL, Suisse

intitulée

**High resolution analysis of protophloem
differentiation in the Arabidopsis root tip**

Lausanne, le 23 septembre 2020

pour le Doyen
de la Faculté de biologie et de médecine

Prof. Niko GELDNER
Directeur de l'Ecole Doctorale

Acknowledgements

First, I would like to thank my supervisor, Professor Christian Hardtke, as well as my committee for accepting to supervise my work. I am also very grateful of having been provided with such a nice work environment, and this is mainly because of my great colleagues in the laboratory. Especially, I would like to show my deepest gratitude to Amelia Amiguet, who taught me everything on the work with plants and made the organization of the lab runs as smoothly as possible. Last, thanks to Pauline Anne for corrections and suggestions about this manuscript.

Lausanne, August 2020.

Abstract

Despite the harmonious growth of the root tip, developing tissues do not differentiate simultaneously. The protophloem, the terminal conductive tissue in the root meristem, may have a crucial role in root meristem maintenance because it is the first tissue to acquire its final functionality. During its differentiation, protophloem sieve elements (PPSE) undergo remarkable modifications occurring in a very short window of space and time.

Mutants with impaired protophloem differentiation such as *brevis radix (brx)* and *octopus (ops)* show not fully differentiated PPSEs, so called gap cells, within a fully differentiated protophloem strand. This interrupts phloem continuity and seems to impair phloem unloading in the root apical meristem. Secondary systemic phenotypes are associated with these local defects, including reduced meristem size and short root, enhanced root branching and deficiencies in hormone and growth factor signaling. This phenotype is called the Disturbed Protophloem Syndrome (DPS).

This project is about the unraveling of a new mechanism in PPSE cell fate determination and shows that a proper PPSE differentiation requires a strong accumulation of auxin in PPSE in comparison to neighboring cells and is mediated by BRX. In *brx* background, the DPS can be partially rescued by increasing the activity of the auxin signaling pathway specifically in the protophloem. Protophloem development requires a feedback-regulated mechanism tuned by two antagonistic actors of auxin efflux, BRX and PROTEIN KINASE ASSOCIATED WITH BRX (PAX). Although, BRX and PAX have opposite functions in the control of auxin efflux, but a loss of BRX or PAX function both lead to the DPS. A deep and precise phenotyping of gap cell occurrence revealed a non-stochastic pattern. A computational approach modelled PPSE development and confirmed that the gap cell pattern occurs according to a biological rule and pointed out that the protophloem differentiation failures originates from an auxin-dependent bi-stability coming from competition among neighboring cells. Those results established a new role of auxin uptake regulation via AUXIN TRANSPORT PROTEIN 1 (AUX1) during PPSE differentiation. The fine-tuned contribution of auxin influx, auxin efflux and local biosynthesis ensures a proper auxin content within the cell and therefore maintains auxin homeostasis which is required for a well-controlled differentiation.

Résumé

Malgré la croissance harmonieuse de la pointe de la racine, les tissus en développement ne se différencient pas simultanément. Le protophloème, le tissu conducteur terminal du méristème racinaire, est le premier tissu à acquérir sa fonctionnalité et a donc un rôle crucial dans le maintien du méristème racinaire. Au cours de leur différenciation, les éléments des cellules criblées du protophloème (CCPP) subissent des modifications uniques se produisant dans une très courte fenêtre d'espace et de temps.

Des mutants, dont la différenciation des protophloèmes est altérée, tels que *brevis radix (brx)* et *octopus (ops)*, présentent des CCPP indifférenciées, appelées « gap cells », contenues dans un protophloème entièrement différencié. Cela interrompt la continuité du phloème et compromet donc la livraison de la sève dans le méristème apical racinaire. Des phénotypes systémiques secondaires sont associés à ces défauts locaux, notamment une taille de méristème et de racine réduite, une densité de racines secondaires plus élevée et des carences en hormones de signalisation et facteurs de croissance. Ce phénotype est appelé syndrome de protophloème perturbé (SPP).

Le projet traite de la découverte d'un nouveau mécanisme de détermination du sort des CCPP et montre que la différenciation des CCPP nécessite une forte accumulation d'auxine dans le protophloème par rapport aux cellules voisines et est médiée par BRX. Dans le contexte *brx*, le SPP peut être partiellement soigné en augmentant l'activité de la voie de signalisation de l'auxine spécifiquement dans le protophloème. Le développement d'un protophloème nécessite un mécanisme régulé par rétroaction et réglé par deux acteurs antagonistes de l'efflux d'auxine, BRX et PROTEIN KINASE ASSOCIATED WITH BRX (PAX). Étonnamment, BRX et PAX ont des fonctions opposées dans le contrôle de l'efflux d'auxine mais une perte de fonction dans BRX ou PAX mène au SPP. Un phénotypage précis des cellules « gap cells » a révélé un schéma non stochastique de leur apparition. Une approche computationnelle a modélisé le développement des CCPP et a confirmé que le modèle d'apparition des cellules « gap cells » se produit en fonction d'une règle biologique et a souligné que les échecs de différenciation proviennent d'une bi-stabilité dépendante de l'auxine due à une compétition entre les cellules. Ces résultats mettent en évidence un nouveau rôle de régulation de l'influx d'auxine via AUXIN TRANSPORT PROTEIN 1 (AUX1) lors de la différenciation des CCPP. La contribution optimisée de l'influx d'auxine, l'efflux d'auxine et de la biosynthèse locale garantit un niveau d'auxine approprié dans la cellule et maintient donc l'homéostasie de l'auxine qui est nécessaire pour une différenciation bien contrôlée.

Contents

Acknowledgements	1
Abstract	3
Résumé.....	4
Chapter 1 Introduction	7
1.1 Plant development	7
1.2 The model organism: The Arabidopsis root	7
1.3 The protophloem tissue as a developmental model	8
1.4 Main regulators of protophloem development	9
1.4.1 Positive regulators of protophloem development	9
1.4.2 The Disturbed Protophloem Syndrome (DPS)	10
1.4.3 Negative regulators of protophloem development	11
1.5 The role of auxin in protophloem development	12
1.6 Thesis context and scope	16
Chapter 2 Material and methods	17
2.1 Plant material and growth conditions	17
2.2 Constructs and generation of transgenic lines	17
2.3 Statistical analysis.....	19
Chapter 3 Investigating impaired protophloem development	21
3.1 Gap cell statistical analysis	21

3.2	Gene expression pattern in mutant background meristems.....	23
3.2.1	Genes expressed specifically in PPSE	24
3.2.2	Differential expression of protophloem related genes in “gap cells”	24
3.3	Realtime imaging of the developing protophloem.....	25
Chapter 4	DPS rescue in <i>brx</i> background	29
4.1	Complementation of <i>brx</i>	29
4.2	DPS rescue in <i>brx</i> mutant background by expressing genes of interest under the control of CVP2 versus CLE45 promoters	31
Chapter 5	The role of auxin biosynthesis in protophloem development.....	35
Chapter 6	Paper #1 (co-author): A molecular rheostat adjusts auxin flux to promote root protophloem differentiation (Marhava et al., 2018).....	37
Chapter 7	Paper #2 (first author): Local auxin competition explains fragmented differentiation patterns (Moret et al., 2020)	43
Chapter 8	Conclusion and future perspectives	45
8.1	Achieved results	45
8.2	Future developments	48
References.....		51
Annex 1: A molecular rheostat adjusts auxin flux to promote root protophloem differentiation (Marhava et al., 2018)	57
Annex 2: Local auxin competition explains fragmented differentiation patterns (Moret et al., 2020)		73

Chapter 1 Introduction

1.1 Plant development

Unlike animal life forms, plant's position is fixed. As consequence, plants constantly need to adapt to their environment to maximize their nutrients, water and energy uptakes. The shoots develop toward the sun whereas the roots grow through the soil. A precise ability to sense the external and internal signals allows a controlled growth since energy can be dynamically allocated to growth, defence or reproduction mechanisms. Such adaptive capacities are controlled by a well-orchestrated cellular differentiation of specific tissues. This fine-tuned differentiation is handled by genetic based molecular processes and explains why post-embryonic development in plants is highly plastic (Sultan et al., 2000). The growth of plant organs is sustained by apical meristems providing them with the stem cells required for tissue development. The meristematic stem cells are pluripotent and commit to a tissue where they will eventually specify in order to acquire their function by differentiation. Once cell/tissue fate is primed, it develops in a stereotypic pattern, like animals (Halle et al., 1986). The maintenance of the stem cell niche of meristems requires sap delivery from source organs (Holbrook et al., 2018; Milne et al., 2018), implying that a functioning phloem is required for the root to develop correctly.

1.2 The model organism: The Arabidopsis root

The primary root of Arabidopsis is a favorite developmental model because of its simple and stereotyped organization of cell types (Dolan et al., 1993; Wildwater et al., 2005; Sarkar et al., 2007). The Arabidopsis root is radially symmetrical, with a xylem axis in the middle of the sieve and in both sides a phloem pole and, symmetrically distributed, the different other tissues. In higher plants, the root has four essential functions: (i) water and nutrients uptake; (ii) anchorage of the plant body into the substrate and supporting the plant body; (iii) storage of nutrients; and for some species (iv) vegetative reproduction. No genetic program restricts root size, meaning that roots exhibit a so-called indeterminate growth, whereas in the shoot, for reproduction means, some tissues will eventually cycle. The appearance of vascular tissues has allowed the sites of nutrition and photosynthesis to be physically separated in the

plant, therefore making the vascular tissues an essential component of the plant. Vascular tissues create a tubular network composed of two independent conducting cell types: the xylem and the phloem. Xylem vessels transport water and minerals acquired from the soil while the phloem ensures the transport of the phloem sap – composed of photosynthates and other molecules such as auxin – from the leaves to the ground and developing tissues. Because of its specific timing of specification, the protophloem is a convenient tissue to investigate differentiation in the root and is technically convenient to work with since confocal microscopy is facilitated by the root's transparency and thinness as each tissue is composed of one cell layer.

1.3 The protophloem tissue as a developmental model

In the root tip, tissues do not differentiate simultaneously. The protophloem, the terminal conductive tissue in the root meristem, may have a crucial role in root meristem maintenance because it is the first tissue to acquire its final functionality. Originating from sieve element-procambium stem cells, protophloem sieve elements (PPSEs) precursor cells undergo two successive periclinal divisions – creating first the phloem precursor and second the procambial cell file, the protophloem and metaphloem cell files, respectively – before dividing anticlinally and ultimately differentiating (**Figure 1a**). During their differentiation, immature PPSEs elongate, concomitantly with cell wall thickening, sieve plates are formed, and cytoplasm follows a complete remodeling including nucleus degradation (Esau, 1965). Since the development of the protophloem follows a stereotypic pattern – two successive periclinal divisions as well as precisely defined meristematic, differentiation and mature zones (**Figure 1b**) – any factors altering protophloem development can be easily isolated (Anne and Hardtke, 2018). Unlike tracheary elements, PPSE do not completely die but will rely on metabolically active adjacent companion cells after differentiation. The decrease in PPSE cellular elements creates an effective conduit through sieve elements. Since PPSEs keep a plasma membrane and some organelles such as the smooth endoplasmic reticulum that localizes near the plasmodesmata, they are connected to their neighboring companion cells, consequently keeping them “alive”. The process of PPSE differentiation is progressive and occurs in a very short window of space and time. This process happens in a context where auxin accumulates around stem cells, then progressively decreases as cells divide and increases again before PPSEs differentiation occurs (**Figure 1c**) (Sabatini et al., 1999; Santuari et al., 2011; Brunoud et al., 2012, Di Mambro et al., 2017). This precise auxin distribution is led by polar auxin transport dynamics, which has been shown to be mediated by plasma-membrane-integral PIN-FORMED (PIN) auxin efflux carriers located at the rootward end of cells (Adamowski et al., 2015; Petrásek et al., 2009).

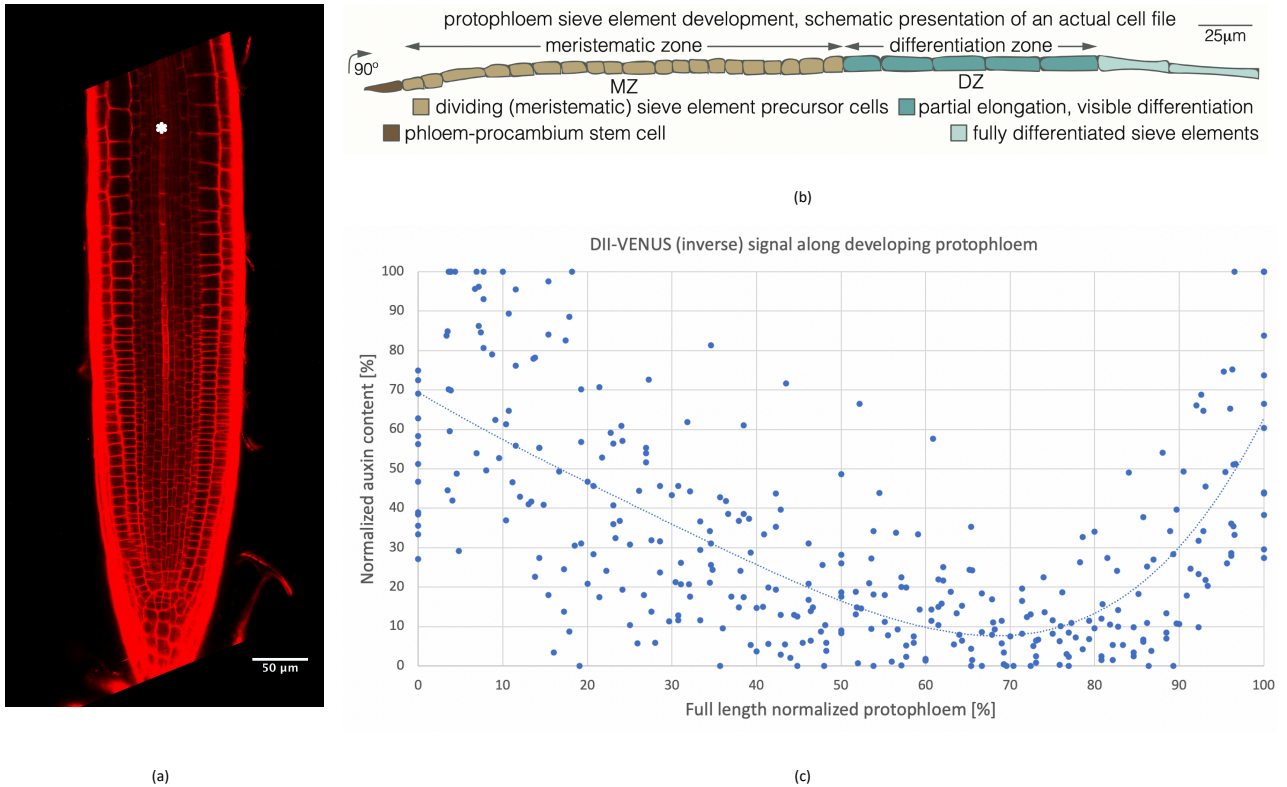


Figure 1: Overview of protophloem development. **a**, Confocal microscopy image of a 7-day-old wild type (WT) root meristem, propidium iodide (PI) cell wall staining (protophloem cell file marked by an asterisk). **b**, Schematic overview of a developing protophloem sieve element (PPSE) cell file in the Arabidopsis root meristem. **c**, Quantification of reporter gene expression levels along developing PPSE cell files, determined cell-by-cell in pertinent regions of interest (nucleus). DII-VENUS is an inverse reporter of cellular auxin levels. The dotted line represents a trendline determined by a polynomial regression of degree 4.

1.4 Main regulators of protophloem development

Protophloem differentiation process was well described since Esau's work (Esau, 1965), however the molecular mechanism are so far poorly understood. Some protophloem specific genes involved in PPSE differentiation are early expressed, suggesting that sieve elements' fate is specified before the appearance of any distinct morphological characteristics (Rodriguez-Villalon et al., 2014; Anne and Hardtke, 2018). Along the past 10 years, research focused more on the genetic understanding of protophloem development. Some essential actors were identified; however, their molecular function still remains unknown.

1.4.1 Positive regulators of protophloem development

Some positive regulators of protophloem development have been identified. ALTERED PHLOEM DEVELOPMENT (APL) has been reported to have a dual role in both promoting phloem differentiation and in repressing xylem differentiation

during vascular development (Bonke et al., 2003). The SMXL gene family is composed of protophloem positive regulators, specifically SMXL3/4/5, since their mutants display strong defects in phloem formation (Wallner et al., 2017).

BREVIS RADIX (BRX) is a plasma-membrane-associated protein, polarly rootward localized and expressed in developing PPSEs (Rodriguez-Villalon et al., 2014). Isolated from a natural genetic variation screen (Mouchel et al., 2004), the *brx* mutation induces a short root phenotype. At the microscopic level this translates into a small meristem compared to WT and the appearance of undifferentiated cells called “gap cells” along the differentiating protophloem (Rodriguez-Villalon et al., 2014). A link between auxin and BRX has been suggested recurrently (Mouchel et al., 2006; Scacchi et al., 2009; Scacchi et al., 2010; Rodriguez-Villalon et al., 2015). *brx* defects could be rescued by second site mutations in the presumed protophloem-specific phosphoinositide 5-phosphatase *COTYLEDON VASCULAR PATTERN 2 (CVP2)*, but not in its homolog *CVP2-LIKE 1 (CVL1)*. Paradoxically, *CVP2* hyperactivity in a WT background recreates a *brx* phenotype, suggesting that a precisely regulated PIP₂ level is essential for proper PPSE differentiation (Rodriguez-Villalon et al., 2015).

OCTOPUS (OPS) is a polarly shootward localized plasma membrane-associated protein with a broad vascular expression that becomes restricted to the phloem upon differentiation (Truernit et al., 2012). Isolated from a gene-trap screen (Bauby et al., 2007), the *ops* mutant phenotype is similar to *brx* (Truernit et al., 2012). OPS function occurs via the repression of the BRASSINOSTEROID-INSENSITIVE 2 (BIN2) protein, a negative regulator of the BR signaling pathway (Anne et al., 2015). OPS and BRX act in parallel in the process of protophloem differentiation, though OPS dosage increase restores defects caused by *brx* loss-of-function (Breda et al., 2017). OPS protein stimulates differentiation of developing PPSEs by inhibiting CLAVATA3/EMBRYO SURROUNDING REGION 45 (CLE45) perception (Breda et al., 2019).

1.4.2 The Disturbed Protophloem Syndrome (DPS)

The protophloem is the final phloem component of the shoot to root vascular system. It feeds the root apical meristem and is thereby essential for root meristem maintenance and differentiation. Phloem unloading occurs in the region where the PPSEs mature and is initially directed towards the neighboring pericycle (Ross-Elliott et al., 2017). Loss-of-function mutants with impaired protophloem differentiation such as *brx* (Mouchel et al., 2004) and *ops* (Truernit et al., 2012) show undifferentiated PPSEs, so called gap cells, within a fully differentiated protophloem strand, compromising phloem transport and unloading in the meristem. Phloem-mediated translocation of carboxyfluorescein diacetate succinimidyl ester (CFDA) dye experiments have shown that phloem sap delivery was strongly reduced in seedlings

affected by the DPS (Marhava et al., 2018). *brx* gap cells indeed display a persisting nucleus as well as a lack of cell wall thickening, as if the PPSEs were not differentiating, the same is observed in *ops* gap cells (Truernit et al., 2012; Rodriguez-Villalon et al., 2015). Secondary systemic phenotypes are associated with these local defects, including reduced meristem size, a short root, enhanced root branching, deficiencies in BR signaling (Kang and Hardtke, 2016) and impaired auxin responses (Marhava et al., 2018). Altogether, these phenotypes represent the Disturbed Protophloem Syndrome (DPS) (Figure 2).

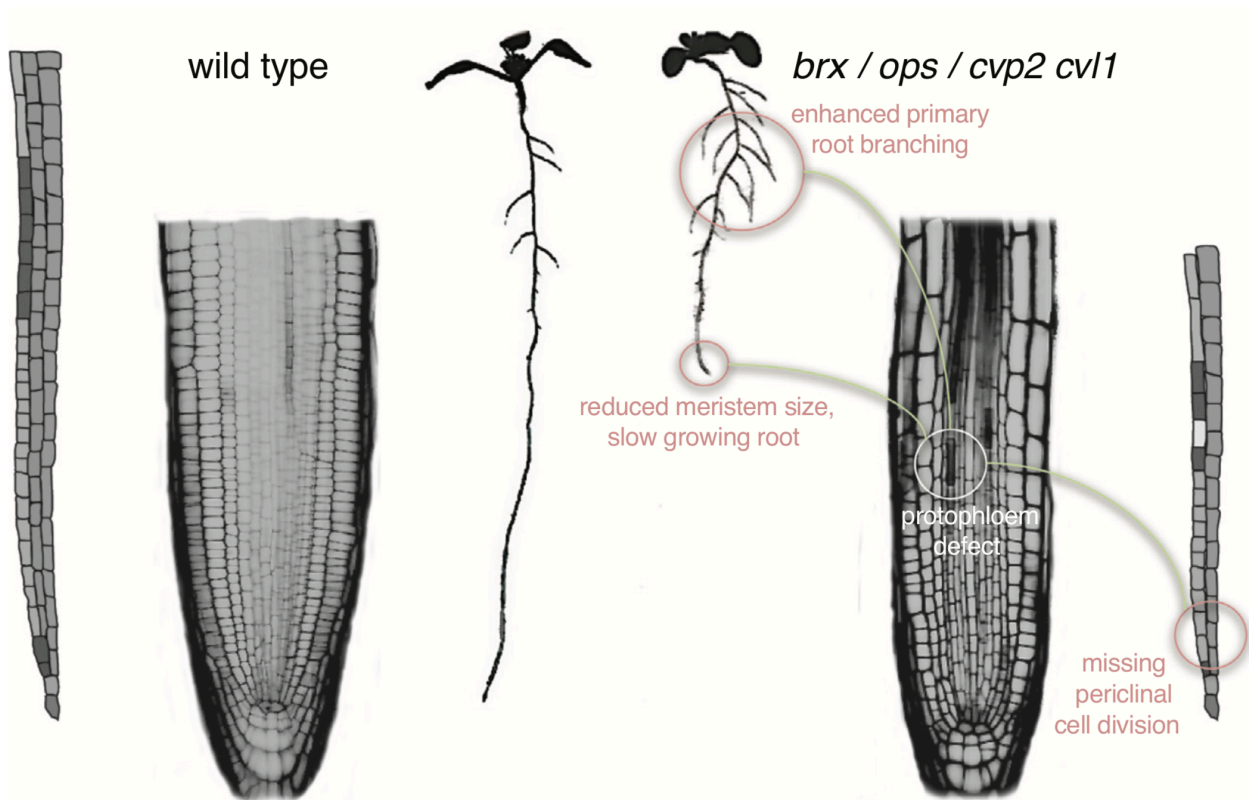


Figure 2: The Disturbed Protophloem Syndrome (DPS). Overview of distinct morphological characteristics (circled) of the Disturbed Protophloem Syndrome (right) as compared to WT (left), such as slow primary root growth, enhanced root branching and a frequently missing second periclinal division of the phloem lineage, as a systemic consequence of a local defect, that is, stochastically perturbed sieve element differentiation in the protophloem of the primary root meristem. (Anne and Hardtke, 2018)

1.4.3 Negative regulators of protophloem development

In order to better understand the BRX pathway, a suppressor screen was performed on *brx* mutants, looking for a rescue of the short root phenotype as a macroscopic visual selection argument. Some homologue proteins in signaling pathways involving receptor-like kinases (RLKs) have been identified: BARELY ANY MERISTEM 3 (BAM3) (Depuydt et al., 2013) and MEMBRANE-ASSOCIATED KINASE REGULATOR 5 (MAKR5) (Kang and Hardtke, 2016). Lately, CORYNE (CRN),

CLAVATA 2 (CLV2) (Hazak et al., 2017) and CLE-RESISTANT RECEPTOR KINASE (CLERK) (Anne et al., 2018) joined the signaling complex as they all contribute to CLE45 signaling in the root.

The receptor-like kinase BAM3 is required for CLE45 suppression of Arabidopsis protophloem differentiation and root meristem growth (Depuydt et al., 2013). Indeed, external CLE45 peptide application represses protophloem differentiation in WT, but not in *bam3* mutants (Depuydt et al., 2013). *BRX*, *BAM3*, and *CLE45* are expressed in a similar spatiotemporal trend along the developing protophloem, up to the end of the transition zone (Rodriguez-Villalon et al., 2014). Several cues such as the fact that *BAM3* expression is induced by CLE45 treatment and ectopically overexpressed in *brx* root meristems suggest that the regulatory activity of *BRX*, *BAM3*, and *CLE45* together could be responsible for the proper transition of PPSE from proliferation to differentiation (Depuydt et al., 2013).

MAKR5 is a post-transcriptionally regulated amplifier of the CLE45 signal that acts downstream of BAM3. MAKR5 belongs to the protein family of BRI1 KINASE INHIBITOR 1 (BKI1), which is an essentially negative regulator of BR signaling (Jaillais et al., 2011). By contrast, MAKR5 is a positive effector of CLE45 signaling (Kang and Hardtke, 2016). CLV2 and the pseudokinase CRN are necessary to fully sense root-active CLE peptides. CRN stabilizes BAM3 expression and is therefore required for proper BAM3-mediated CLE45 signaling. Moreover, protophloem-specific *CRN* expression restores sensitivity to root-active CLE peptides in *crn* mutants, suggesting that the protophloem is the principal site of action of the CLE peptides (Hazak et al., 2017). CLERK gene is required for full sensing of root-active CLE peptides in early developing protophloem and acts genetically independently of *CLV2-CRN* (Anne et al., 2018).

1.5 The role of auxin in protophloem development

The variation of auxin levels between the quiescent center (QC), the differentiating zone and the meristematic zone (**Figure 1c**) made me focus on the role of auxin in protophloem development. Meristems affected with the DPS have displayed reduced auxin levels compared to WT as illustrated by the inverse auxin sensor DII-NLS-VENUS (Gujas et al., 2012 and **Figure 3**). Whether this is due to impaired auxin transport or biosynthesis in roots affected with the DPS is still unknown.

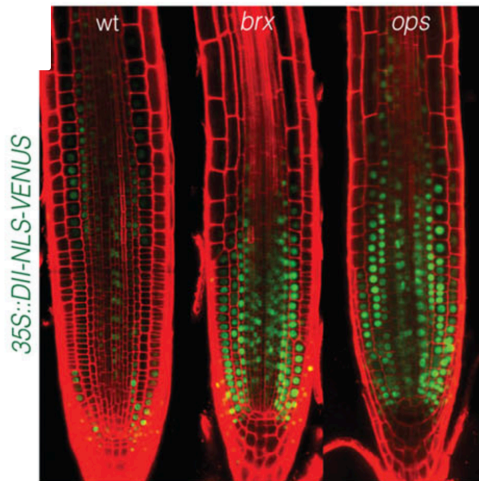


Figure 3: Altered auxin levels in protophloem differentiation mutants. Confocal microscopy images of PI stained root meristems of 5-day-old seedlings of indicated genotypes that constitutively express the fluorescent DII-NLS-VENUS inverse auxin activity reporter protein. Confocal images were obtained with a 63× magnification objective (Rodriguez-Villalon et al., 2015).

Root growth plasticity is possible thanks to growth factors acting as intrinsic signaling molecules and modulates root growth in response to external signals. In order to characterize growth factors function, physiological assays using synthetic hormones can indeed strongly deregulate root growth and disturb the meristem activity. This approach was the foundation of many genetic screens that allowed the identification of mutants impaired in hormone biosynthesis or downstream signaling pathway.

Indole-3-acetic acid (IAA) has been identified as the main natural auxin in the early 20th century (Thimann and Koepfli, 1935). The plant hormone auxin is an important regulator of growth and developmental processes and plays a key role in plant architecture (Vanneste and Friml, 2009). Auxin is generally described as produced in the shoot apical meristems and distributed throughout the plant via the phloem highway, acting as a long- and short-distance signaling molecule controlling multiple developmental processes, including root patterning (Sabatini et al., 1999; Friml et al., 2002; Petersson et al., 2009), cell division, and cell elongation in roots (Ding and Friml, 2010; Baster et al., 2013).

The auxin signaling machinery is composed of three protein families such as Transport Inhibitor Response 1 / Auxin Signaling F-Box (TIR1/AFB), Auxin Response Factors (ARFs), and Auxin/Indole Acetic Acid (Aux/IAA) transcriptional repressors. At low auxin level, Aux/IAA proteins binds to ARFs and repress their activity and therefore preventing the transcription of auxin-responsive genes. Conversely, the F-box protein TIR1/AFB binds to Aux/IAA proteins in presence of auxin and induce their degradation, removing the inhibition applied on ARFs, thus inducing ARF-mediated expression of auxin-responsive genes (Ljung, 2013; Wang and Estelle, 2014). The ARFs are transcription factors composing the final component in auxin signal transduction. They are responsible for regulating gene expression and are therefore likely to be the components responsible to confer precision to auxin response via the selection of the genes they will be specific

to. This could explain why the ARF family is composed of 23 members in Arabidopsis, and more than 10 in the moss *Physcomitrella* (Finet et al., 2013). The ARF genes are expressed with a precise dynamic and display distinct patterns of expression revealing their specificity during various developmental processes (Guilfoyle and Hagen, 2007; Rademacher et al., 2011, 2012; Weijers et al., 2005). For example, ARF1 and 2 are responsible for senescence and floral organ abscission (Ellis et al., 2005) while ARF5/MONOPTEROS is required for embryonic root and flower formation (Berleth and Jürgens, 1993; Przemeck et al., 1996). Notably, the *arf5/mp* mutants are not able to develop an embryonic root and, as a consequence, grow as rootless seedlings (Hardtke and Berleth, 1998).

In addition to the widespread expression of the different genes involved in auxin signaling, auxin gradients modulate auxin activity. Since the auxin signaling pathway is taking place in the cytosol, transport mechanisms are required in order to get auxin there. The first proposed model of auxin transport was dependent on the auxin protonation state. As a weak acid, the protonation state of auxin is modulated by the pH of its environment (Rubery and Sheldrake, 1973, 1974; Goldsmith and Goldsmith, 1981; Goldsmith et al., 1981). In a cell wall acidic environment (pH ~5.5), ~20% of auxin is in a protonated form (IAAH). IAAH diffuses across cell membranes. In the cytoplasm, the pH is neutral (pH ~7) and most of the auxin is anionic (IAA⁻), preventing auxin to diffuse across cell membranes. 1-Naphthaleneacetic acid (1-NAA) is a lipophilic synthetic form of auxin used in *in vitro* assays. The specific characteristics of this synthetic auxin allows it to reach intracellular compartments without any active transport limitations (Marchant et al., 1999).

Auxin application triggers rapid cell wall acidification and elongation of plant aerial organs. Auxin-induced acidification arises by local activation of H⁺-ATPases. This auxin-stimulated acidification and growth require TIR1/AFB-Aux/IAA nuclear auxin perception and auxin-induced gene transcription and specifically Small Auxin Upregulated RNA (SAUR) proteins are crucial downstream mediators of this growth (Fendrych et al., 2016). A higher apoplastic pH would make a higher proportion of auxin being anionic and require the influx carriers to enter the cell (Band et al., 2014).

Additionally, auxin is also transported through the plasma membrane thanks to Polar Auxin Transport (PAT). This transport is slower than phloem transport but is controlled and dependent on auxin intracellular concentration. PAT is coordinated by AUXIN RESISTANT (AUX1)/LIKE-AUXs (LAXs) uptake permeases and PINs auxin efflux carrier proteins and ABCB/MULTIDRUG RESISTANCE (MDR)/PHOSPHOGLYCOPROTEIN (PGPs) transporters (reviewed in Adamowski and Friml, 2015).

PIN1 was first shown to encode a membrane localized protein at the basal side of stem xylem cells (Gälweiler et al., 1998) and second to transport auxin directly from the cytosol the outer cell (Petrásek et al., 2006). The morphogenic auxin gradients necessary for proper plant developments are generated by the polar distribution of PINs, enabling the directional auxin flow from the shoots to the roots (Wisniewska et al., 2006).

AUX1 localization has been described to be tissue specific and providing directionality of intercellular auxin flow together with PIN efflux transporters (Swarup et al., 2001; Kleine-Vehn et al., 2006). The presence of AUX1 is essential for the root's gravitropic response (Marchant et al., 1999). Mutations in *AUX1* or *LAX3* produces auxin-related developmental defects: mutants are agravitropic and have delayed or reduced number of lateral roots. Together, AUX1 and LAX3 act alongside to control lateral root development by regulating initiation steps (Marchant et al., 2002) and emergence (Swarup et al., 2008). No root growth-related defects are detected in either *lax1* or *lax2* mutants. Unlike *aux1*, mutations in *lax1* or *lax2* do not display any agravitropic behavior (Péret et al., 2012). *AUX1* expression in the lateral root cap and epidermal tissues of *aux1* roots can fully restore the *aux1* agravitropic phenotype (Swarup et al., 2005). The root meristem has been proposed to recycle auxin coming from the root tip via the root cap (Blilou et al., 2005), and the auxin transport to this area also involves AUX1 (Swarup et al., 2001; Swarup et al., 2005). Removing AUX1 would as a consequence produce an accumulation of auxin in the QC and its surrounding cells, with a reduced variance between the auxin levels in the diverse tissues.

AUX1, as nonpolar influx carriers control which tissues receive auxin and therefore has high auxin levels whereas PIN carriers, as polar efflux carriers control the direction of auxin transport within these tissues. Auxin has been thought to be present in roots only because it was transported there but several studies have challenged that believe by showing that auxin can also be synthesized locally in roots (Ljung et al., 2005).

IAA is mainly produced from L-tryptophan (Trp) via indole-3-pyruvic acid (IPyA) in a two-step pathway (reviewed in Brumos et al., 2014). IPyA is then converted into IAA by the YUCCA (YUC) family of flavin monooxygenases (Zhao et al., 2001) consisting in Arabidopsis of 11 YUCCA enzymes. Even if auxin transport, signaling and response have been intensively studied, little is known about the contribution of the local *de novo* auxin biosynthesis in the generation and maintenance of the morphogenic auxin maxima. Therefore, a better understanding about how and where auxin is produced is critical to precisely define auxin sources and sinks and refine our knowledge of auxin distribution within a plant. Thus, if it is known that auxin cell level gradients are dependent on auxin diffusion, transport and biosynthesis, it is now required to investigate how transporters activity is fine-tuned by complementary actors as well as to precisely

define the local biosynthesis contribution on auxin concentration in a tissue specific or cell specific manner during protophloem development.

1.6 Thesis context and scope

The “gap cells” occurring in developing protophloems of mutants affected with the DPS are intriguing. They are thought to be undifferentiated cells since they lack the hallmarks of differentiated PPSE (mainly thickening of the cell wall and loss of nucleus). They have been described as companion cells by a recent study (Gujas et al., 2020). Our first focus was to investigate the role of auxin in the differentiation of PPSE. Clues such as reduced auxin levels in DPS affected root meristems (Rodriguez-Villalon et al., 2015) and the presence of a “valley” of auxin in the protophloem cell strands (Santuari et al., 2011) pointed out to a putative role of auxin in shaping PPSE differentiation. Auxin levels were therefore assessed in detail in WT and in protophloems affected with the DPS (**Chapter 5**). Also, auxin signaling was manipulated specifically in the protophloem in order to test the effects of deregulated auxin signaling in WT as well as a possible rescue aptitude of increased auxin signaling in mutants affected with the DPS (**Chapter 5**). The deep evaluation of the pattern of expression of a set of genes involved in protophloem development in WT and DPS affected root meristems (**Chapter 2**) allowed us to identify promoters that were expressed or not in gap cells. We were therefore able to express genes (**Chapter 3**) or increase auxin signaling (**Chapter 4**) specifically in the protophloem, including or not the gap cells, in order to have an elegant control in DPS rescue. Next, we went deeper in the assessment of the relation between auxin and protophloem development by looking into the actors responsible for auxin levels control in the root meristem (**Chapter 6**). After confirming that gap cells occurrence was not stochastic but following a pattern (as suggested in **Chapter 2**), we explored the role of AUX1-mediated auxin influx as well as auxin biosynthesis in the protophloem and confirmed the experimental results with computational modelling (**Chapter 6**).

Chapter 2 Material and methods

2.1 Plant material and growth conditions

The *Arabidopsis thaliana* WT line used in this study was Col-0, which was also the genetic background for the mutants and transgenic lines. For plant tissue culture, seeds were surface-sterilized, stratified for 2 days in the dark at 4 °C, and germinated in vertically placed Petri dishes on 0.7% agar and 0.5 × Murashige and Skoog (½ MS) medium (Duchefa) with 0.3% sucrose at 22 °C under continuous light. Seedling grown completely in medium were germinated on magentas with ½ MS medium and 0.3% agar. The following transgenic and mutant lines have been described elsewhere: *CVP2::MP^A* and *CLE45::MP^A* (Marhava et al., 2018), *BRX::BRX-CITRINE* (Rodriguez-Villalon et al., 2014), *CVP2::NLS-VENUS* and *CLE45::NLS-VENUS* (Rodriguez-Villalon et al., 2015), *35S::DII-NLS-VENUS* and *35S::mDII-NLS-VENUS* (Brunoud et al., 2012), *AUX1::YFP-AUX1* and *PIN1::PIN1-GFP* (Swarup et al., 2004; Benková et al., 2003), *brx* (Rodriguez-Villalon et al., 2014), *ops* (Truernit et al., 2012).

2.2 Constructs and generation of transgenic lines

Transgenes for plant transformation were created in suitable binary vectors and produced through standard molecular biology procedures and/or NEBuilder HiFi DNA Assembly Reaction Protocol.

For the cloning of the *CVP2::SYP122-3xmCherry* construct, the promoter of *CVP2* was inserted into a pDONR P4P1r from the Gateway system using restriction sites XmaI and KpnI, and amplified with the forward primer 5'- ATT GGT ACC GGT TTG TGG CAA TTT GTA TCC -3' and the reverse primer 5'- ATT CCC GGG GCT TTT AAA TTC CAT GAA GAT GGG C -3'. For the cloning of the *CLE45::SYP122-3xmCherry* construct, the promoter of *CLE45* was inserted into a pDONR P4P1r from the Gateway system using restriction sites XmaI and KpnI, and amplified with the forward primer 5'- ATT GGT ACC AAC ATT CAA GAT TTC ACT ATC -3' and the reverse primer 5'- ATT CCC GGG GCT CTT AGG CAG ACA AG -3'. The *SYP122-3xmCherry* reporter in a pDONR 221 was kindly provided by the laboratory of Professor Geldner. The DNA fragments described above were combined into the pH7m24GW binary vector.

For the cloning of the ***pX::NLS-3xVENUS*** constructs, the following primer combinations were used to insert the amplified promoters into a version of the pCAMBIA1305.1 binary vector containing a *NLS-3xVENUS* reporter downstream of a multi cloning site. The restriction sites were added to the sequence of interest for further uses. The restriction sites that were used are KpnI or Eco53kI for the forward primers and SbfI for the reverse primers.

	Forward primer	Reverse primer
pAUX1 (KpnI/SbfI)	5'- CTC GGT ACC CAA GAG ATT TTG AAG ACT CTT C -3'	5'- CAG CC TGC AGG TTT TTT AGC TTC TAG ATC TGA GA -3'
pCLE26 (KpnI/SbfI)	5'- CTC GGT ACC TTC GAG CAA ATT TTC TCG TTG GG -3'	5'- CAG CC TGC AGG GGT TTC TAG CCT TTG TGG ATA TG -3'
pBRX (KpnI/SbfI)	5'- CTC GGT ACC GAA ATG AAC ATG ACA AAC AAA CAC ATC -3'	5'- CAG CC TGC AGG TTT TGG TCT CTT TTT TGA GTT GTT CTC -3'
pMAKR5 (Eco53kI/SbfI)	5'- TTC GAG CTC CTA AAG AGG CGT AGT AAG AAC C -3'	5'- CAG CC TGC AGG TTA GAA AGA GAG AAA GAG AGT AAT GG -3'
pOPS (KpnI/SbfI)	5'- CTC GGT ACC CAT AGG CGT ATA GTA CTT GTC GG -3'	5'- CAG CC TGC AGG GAC GGG AAA TGG TGG TTA ATC C -3'
pBAM3 (KpnI/SbfI)	5'- ATT GGT ACC GAT CAC ATA CCA CAT TGA TCT GC -3'	5'- CAG CCT GCA GGT GTA ACA TCA GAA AAA TAA AAA C -3'

Table 1: List of the primers used for promoter amplification prior to integration into *NLS-3xVENUS* pCAMBIA1205.1 construct templates.

The ***CLE45/CVP2::YUC1(-GFP6)*** constructs were generated using the NEBuilder® system. The fragments were amplified using the primers listed on table 2. The first part of the primer name corresponds to the overlap sequence (in lowercase letters in the primer sequence) and the second part corresponds to the annealing sequence (in uppercase letters in the primer sequence).

Primer name (overlap – ANNEAL)	Primer 5'-3' sequence
pCAMBIA – pCVP2 FW	5'- atgaccatgattacgaattcgagctGAATCTAAGGACGAGAAGTATC -3'
YUC1 – pCVP2 RV	5'- gatgagactccatTGTGCTTCTTCTCTGCAAG -3'
pCVP2 – YUC1 FW	5'- agaagaagcaacaATGGAGTCTCATCCTCAC -3
pCAMBIA – YUC1 RV	5'- tgaacgatcggggaattcgagctTTAGGATTTAGAGGTAAGACAAAAC -3'
GFP6 – YUC1 RV	5'- ctctttactcatGGATTTAGAGGTAAGACAAAAC -3'
YUC1 – GFP6 FW	5'- tacctctaaatccATGAGTAAAGGAGAAGAAGACTTTTCACTGG -3'
pCAMBIA – GFP6 RV	5'- tgaacgatcggggaattcgagctTCAGGCGCCTTTGTAT -3'
pCAMBIA – pCLE45 FW	5'- atgaccatgattacgaattcgagctCAAACCAATTTTAGGAAAATTATAG -3'
YUC1 – pCLE45 RV	5'- gatgagactccatTTCTGCTTTAGGCAGAC -3'
pCLE45 – YUC1 FW	5'- cctaagagcagaaATGGAGTCTCATCCTCAC -3'
pCAMBIA – YUC1 RV	5'- tgaacgatcggggaattcgagctTTAGGATTTAGAGGTAAGACAAAAC -3'

Table 2: List of the primers used for fragments amplification necessary for the *CLE45/CVP2::YUC1(-GFP6)* constructs generation using the NEBuilder® system.

The complementation lines were generated using the Gateway[®] system. Promoters pDONR P4P1r containing plasmids were the same as described above. *PAX* pDONR 221, *D6PK* pDONR 221 (Marhava et al., 2018), *BRX* pDONR 221 (Rodriguez-Villalon et al., 2014), *BAM3* pDONR 221 (Depuydt et al., 2013), *OPS* pDONR 207 (Breda et al., 2017), *CLV2* pDONR 221 (Hazak et al., 2017) and *MAKR5* pDONR 207 (Kang and Hardtke, 2016) containing vectors were as previously described. The DNA fragments described above were combined into the pH7m34GW binary vector.

The binary constructs were introduced into *Agrobacterium tumefaciens* strain GV3101 pMP90 and transformed into *Arabidopsis thaliana* using the floral dip method (Clough and Bent, 1998). At least three independent transgenic lines were used for each construct to perform experiments and verify reproducibility.

2.3 Statistical analysis

One-way ANOVA with post-hoc Tukey HSD Test analyses were carried out using the web tool (https://astatsa.com/OneWay_Anova_with_TukeyHSD/), $p < 0.05$.

Chapter 3 Investigating impaired protophloem development

The protophloem being the final vascular component in the transport of sap from the shoots to the roots and consequently the first root tissue to differentiate, its proper development – and therefore the correct differentiation of individual cells – is required for a sustainable root meristem maintenance. Altogether, it suggests that any disturbance in protophloem development could lead to catastrophic systemic consequences for the plant root system. In the case

- A slow growing root
- A reduced meristem size
- An enhanced primary root branching
- A missing second periclinal division

In addition to the latter symptoms, some developing sieve elements display differentiation defects. The subsequently undifferentiated protophloem cells, the gap cells, are putatively interrupting the continuity of the protophloem sieve tube. This discontinuity in phloem transport could explain the different symptoms of the DPS, because of hormones accumulation/depletion in the root, lack of nutrients delivery in the meristem, etc.

3.1 Gap cell statistical analysis

The appearance of gap cells has always been assumed to be stochastic. To assess if there is any pattern in the appearance of the gap cells, a statistical analysis of their occurrence was performed. The existence of a pattern in gap cells occurrence would mean that their occurrence is not random but governed by an underlying biological mechanism. The characterization of a pattern would help us understand what kind of biological mechanism is triggering the gap cells' incapacity to differentiate. A deep analysis of developing protophloems was therefore performed, in Col-0

background as WT control, and in *brx* and *ops* mutant backgrounds. The quantification of the gap cell occurrence was done assessing:

- The number of gap cells and gaps (multiple gap cells together) per plant and per protophloem.
- The number of differentiated cells flanking a gap cell – 0, 1 or 2. (Do a gap cell need to be in contact with any differentiated cell?)
- The position in the developing protophloem cell file of the first gap cell of a gap. (Are gaps arising in early or late differentiating protophloem?)
- The number of differentiated cells between two gaps within a protophloem. (How frequent in a protophloem cell file can gaps arise?)

More than 100 seedlings per genetic background (**Table 3**) were analyzed and allowed the drawing of the following conclusions (for more see Moret et al., 2020):

- A gap is usually made of 2 gap cells (rarely only one gap cell in a gap).
- There are gaps in half of the protophloems.
- There are usually 2 gap cells per protophloem.
- There are no more than 3 gaps per protophloem (usually only one).
- Plants have usually not more than 4 gaps per primary root.
- Gaps arise in the early differentiating protophloem (position 2 to 7).
- There are usually not more than 3 differentiated cells between two gaps.

According to the collected data, the pattern of gap cells occurrence is as follow: a root has one of the two protophloems affected with one or two gaps. When two gaps are present, the first gap is located in the early differentiating protophloem and is composed of two gap cells. The second gap is separated by three differentiated cells from the first gap and is composed of two cells too, making a total of 4 gap cells per protophloem and per root. Comparing the two DPS affected backgrounds, in *ops* there can be slightly more gaps/gap cells per protophloem and more cells between gaps compared to *brx*. Overall, gaps in *ops* span a broader region than in *brx* but are mainly similar in terms of occurrence, size and position. Altogether, these data highlight a trend in the emergence of gaps – in two distinct mutant backgrounds – indicating that the process is probably not stochastic.

Background	# of protophloems	# of gap cells	# of gaps	# of protophloems with gaps
Col-0	150	0	0	0
<i>brx</i>	182	210	111	97
<i>ops</i>	190	244	134	95

Table 3: Simplified data set of gap cells quantification in seedlings grown vertically on regular petri dishes.

In order to investigate whether the gap occurrence pattern was influenced by external conditions such as air/medium contact and nutrients uptake, the same experiment was performed using three distinct conditions. The first condition with the seedling growing as usual on a vertical plate complemented with sucrose (as control), a second condition with the seedling growing with the root completely plunged in the medium without any sucrose and a last condition with the seedling growing with the root completely plunged in the medium again, but this time the medium was complemented with sucrose. Even if the number of gaps, number of protophloem with gaps and position of the gaps remained similar in the three conditions – confirming the pattern in gaps occurrence – more gap cells and therefore bigger gaps were present in roots grown completely plunged in the medium (**Table 4**). Since gaps interrupt sap transport and therefore impair the delivery of nutrients to the root meristem, a tolerance to starving conditions could be acquired since nutrients can be provided by the medium when the root is completely immersed in it.

Background	# of protophloems	# of gap cells	# of gaps	# of protophloems with gaps
Col-0	150	0	0	0
<i>brx</i>	182	210	111	97
<i>brx</i> <i>in medium</i> <i>without sugar</i>	56	105	35	26
<i>brx</i> <i>in medium</i>	56	153	50	33

Table 4: Simplified data set of gap cell quantification in seedlings grown vertically on regular petri dishes and completely in the medium.

3.2 Gene expression pattern in mutant background meristems

To better understand the mechanisms underlying protophloem development, reporter lines were generated using promoters of genes known to be expressed in the protophloem and/or in the root meristem and therefore supposed to have a role in protophloem development. The expression pattern of the following genes was studied in Col-0 and in DPS affected mutant backgrounds such as *brx* and *ops*.

3.2.1 Genes expressed specifically in PPSE

Of the studied genes, three were found to be protophloem specific: *OPS*, *CLE45* and *CVP2*. Although BRX protein localization is known to be specific to the protophloem (Scacchi et al., 2010; Marhava et al., 2018), slight activity of its promoter was observed in the surrounding tissues of the protophloem, in the epidermis and in the columella. *CLE26*, *MAKR5* and *BAM3* were all expressed in the protophloem, but some promoter activity could be found in the surrounding cells (**Figure 4**). Interestingly, the positive regulators of protophloem differentiation were pretty specific to the protophloem whereas negative regulators such as *CLE26*, *CLE45*, *MAKR5* and *BAM3* displayed a broader expression, suggesting an underlying mechanism to restrict the protophloem specification to a single cell file.

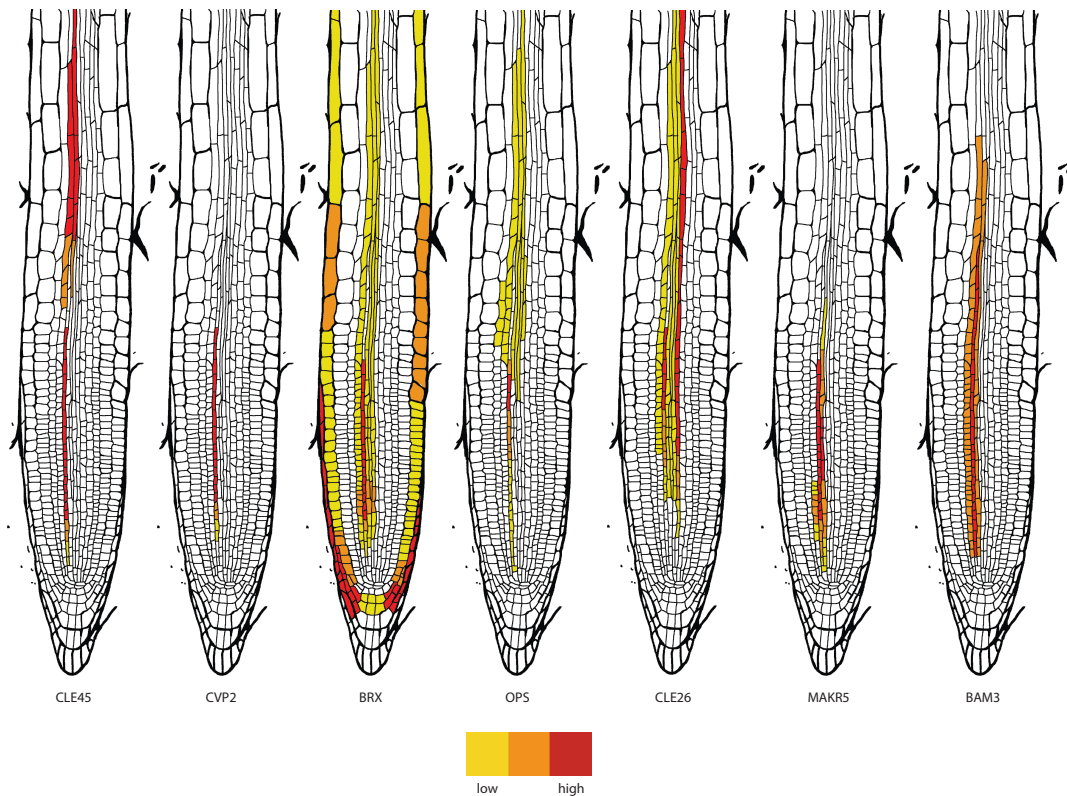


Figure 4: Expression pattern of genes implicated in PPSE development. Schematic representation of the expression pattern of meristematic genes related to protophloem in Col-0 background.

3.2.2 Differential expression of protophloem related genes in “gap cells”

The expression of protophloem related genes was assessed in gap cells exhibiting mutants such as *brx* and *ops* since they could present deregulated gene expression. *CVP2* was expressed in gap cells while *CLE45* was not (**Figure 10n**). The expression of *AUX1*, *BAM3* and *BRX* was downregulated in gap cells whereas the expression of *MAKR5* was upregulated

in gap cells (**Figure 5**). The reduced expression of *CLE45*, *BAM3* and *AUX1* suggested that the differentiation process was impaired (absence of the *CLE45/BAM3* set of differentiation negative regulators) and that auxin influx transport was diminished in the gap cells (reduced *AUX1* expression). Also, *BRX* downregulation in *ops* gap cells suggested a requirement for low *BRX* expression in gap cells and a putative cross-talk between the *OPS* and *BRX* signaling pathway.

<i>X::NLS-VENUS</i>	<i>brx</i>	<i>ops</i>
<i>BRX</i>		-
<i>CVP2</i>	o	
<i>CLE45</i>	x	x
<i>BAM3</i>	-	
<i>MAKR5</i>	+	+
<i>AUX1</i>	-	-

+: elevated expression
 o: identical expression
 -: reduced expression
 x: no expression

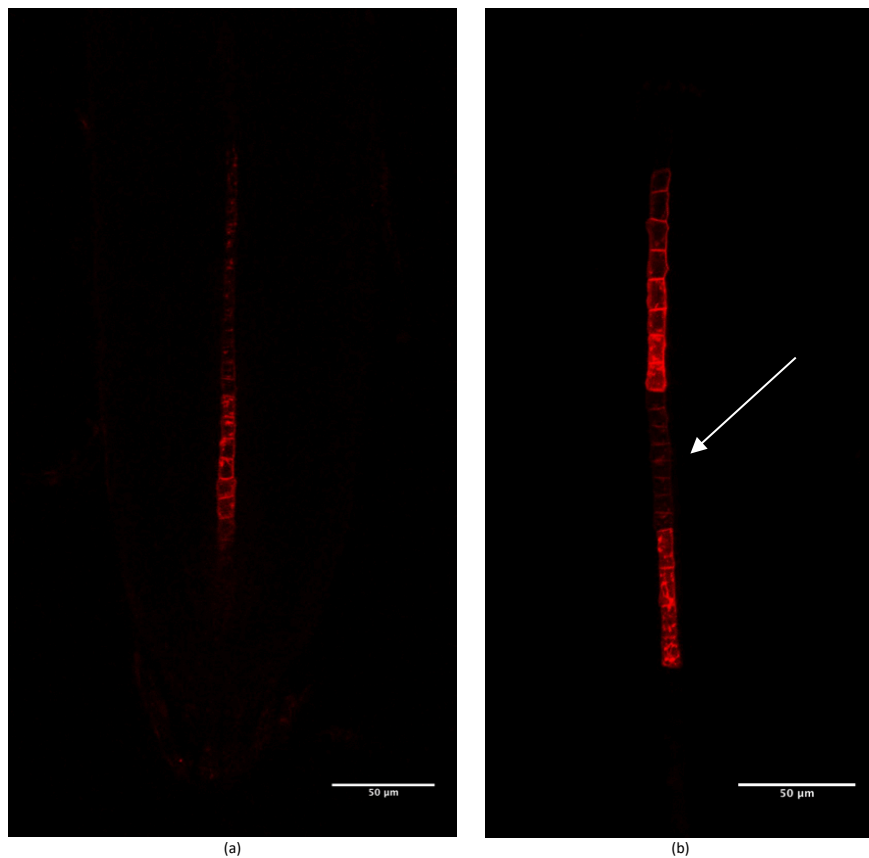
Figure 5: Summary of the variation of the expression of protophloem genes in gap cells. Expression levels of protophloem related genes in gap cells compared to their expression in normally differentiating protophloem cells in *brx* and *ops* mutant backgrounds. Transcriptional reporters were generated using the promoters of the genes listed and fused to NLS-3x-VENUS reporter constructs.

3.3 Realtime imaging of the developing protophloem

To further investigate the mechanisms underlying gap cells appearance, transgenic lines specifically expressing reporters under the control of protophloem specific promoters were generated and allowed us to live image protophloem cells during their journey through protophloem differentiation. The *CVP2* and the *CLE45* promoters – the first being expressed in gap cells whereas the latter not – were used to drive the expression of SYP122, a membrane associated protein, tagged with a triple mCherry fluorescent protein (**Figure 6a, b**). The purpose of such a marker line was to replace the toxic PI staining with a protophloem specific membrane staining. Growing meristems were imaged during several hours under a confocal microscope to follow protophloem cells divisions and differentiation steps.

The observations were that divisions occur each 5-6 hours in the developing protophloem and that protophloem differentiating cells spend around a day to go from a stem cell to a completely differentiated PPSE. Because of the horizontal orientation of stages in conventional confocal microscopes, growing meristems could not be observed for

more than 5-6 hours. The use of vertical confocal microscope would hopefully remove such time limits and allow us to visualize gap cells appearance in DPS affected backgrounds such as *brx* and *ops* gap and follow them in time. We tried to combine such a membrane reporter expressed under the control of the *CLE45* promoter with a nuclear protophloem marker (*CVP2::NLS-3xSCARLET*) to follow gap cells in a longer time range and with a clear tool to discriminate between differentiating protophloem cells and gap cells (*CVP2* vs *CLE45*). Using the same logic, we also combined a *CVP2::NLS-3xSCARLET* with a *CLE45::NLS-VENUS* to have the reporters all nuclear (**Figure 6c, d, e**). We collaborated with the laboratory of Prof Jiri Friml to image those lines in a vertical microscope, but the quality of the results was not sufficient to deduce more facts about protophloem differentiation dynamics.



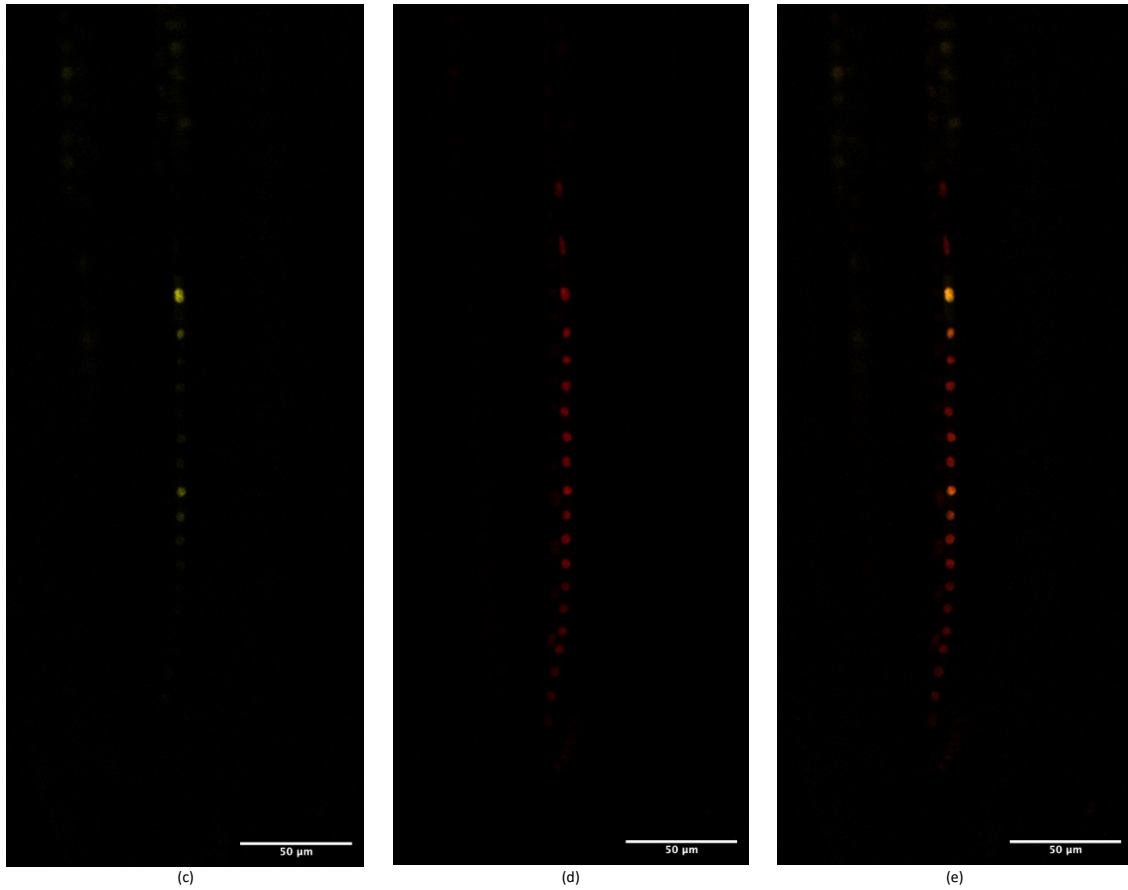


Figure 6: Protophloem specific marker lines. Confocal microscopy of *CVP2::SYP122-3xmCherry* (a) *CLE45::SYP122-3xmCherry* (b) and specifically expressed in the protophloem of 7dag *brx* background lines. The arrow highlights a gap in (b). Confocal microscopy of *CLE45::NLS-VENUS* (c), *CVP2::NLS-3xSCARLET* (d) and the corresponding composite image (e) in the protophloem of 7dag Col-0 background lines.

Chapter 4 DPS rescue in *brx* background

Genes are differentially expressed in gap cells compared to normally differentiating PPSEs. This raises the question of the identity of the gap cells and whether mutant backgrounds such as *brx* and *ops* could be rescued by the expression of gap cells specific turned off genes and whether this expression is needed in the gaps. In order to answer this, *brx* mutant background seedlings were complemented using the *CVP2* and the *CLE45* promoter. The first candidate genes would have been the ones with a reduced expression in gaps as seen in 2.2.2 (**Figure 5**) but all protophloem related genes were tested. We investigated here if expressing PPSE related genes in the protophloem – in the gaps or not – is sufficient to rescue the DPS.

4.1 Complementation of *brx*

In order to investigate the necessity of *BRX* to be expressed in the gaps to successfully complement *brx*, *BRX* was expressed under the control of its native promoter as a control, under the control of the *CVP2* promoter in order to be expressed in the protophloem and in the gap cells, and under the control of the *CLE45* promoter in order to exclude *BRX* from the gap cells but still express it in the normally differentiating PPSEs. *brx* mutants were successfully complemented expressing *BRX* under the control of its native promoter and under the control of the *CVP2* promoter as seen by the rescue of root length (**Figure 7d**), suggesting a requirement of *BRX* being expressed in the gaps in order to see a proper rescue of the short root phenotype. The CITRINE signal was correctly localized and expressed according to the predicted expression pattern for the *BRX* promoter (**Figure 7a**) while for the *CVP2* promoter the signal was surprisingly restricted to the early developing protophloem (**Figure 7b**) not exactly matching the expected pattern of expression observed in 3.2.1. The expression pattern for the *CLE45* promoter did match the expected expression pattern (**Figure 7c**). Even if the *brx* mutants short root phenotype was completely rescued with the expression of *BRX* under the control of the *CVP2* promoter (**Figure 7d**), some gap cells were still present (**Figure 7b**).

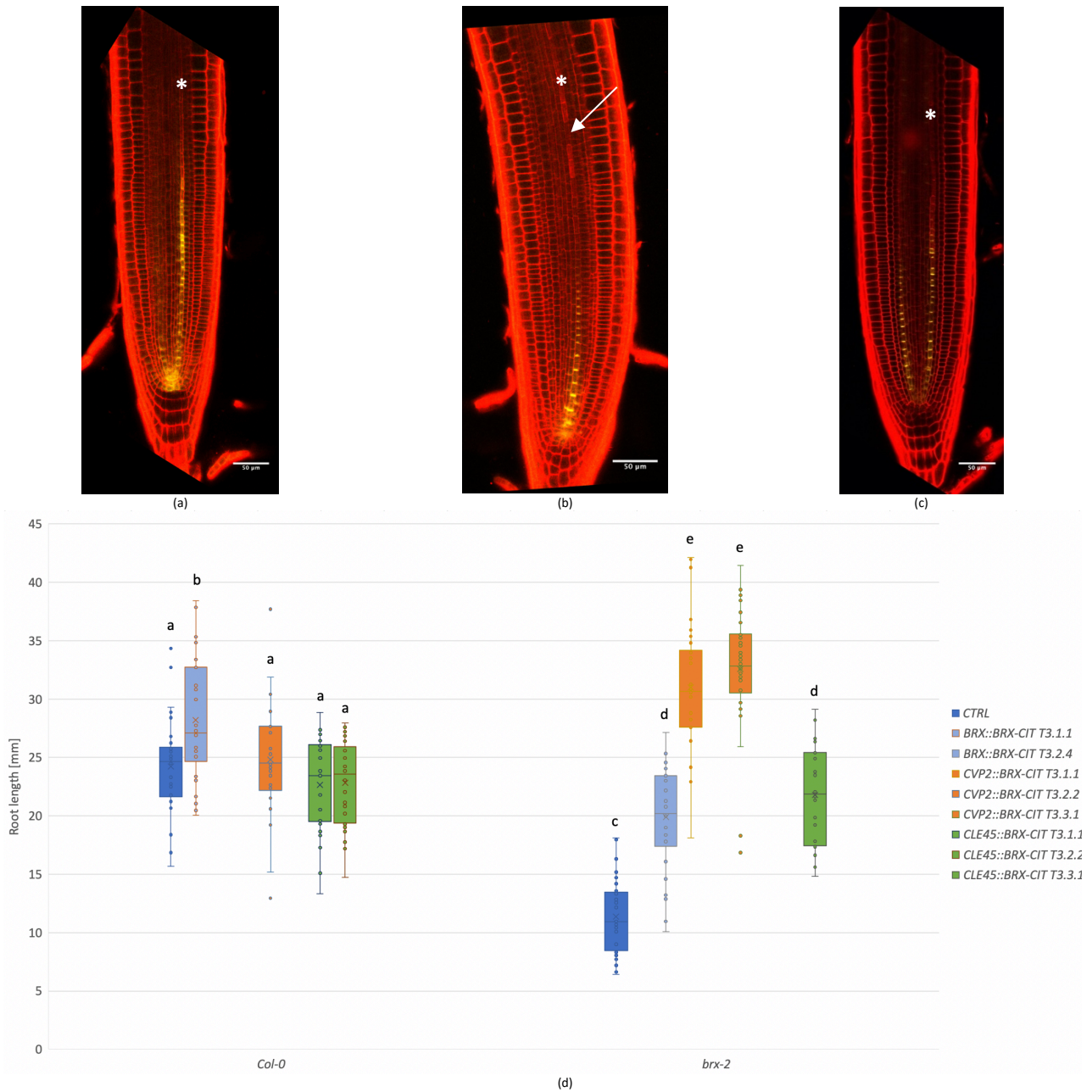
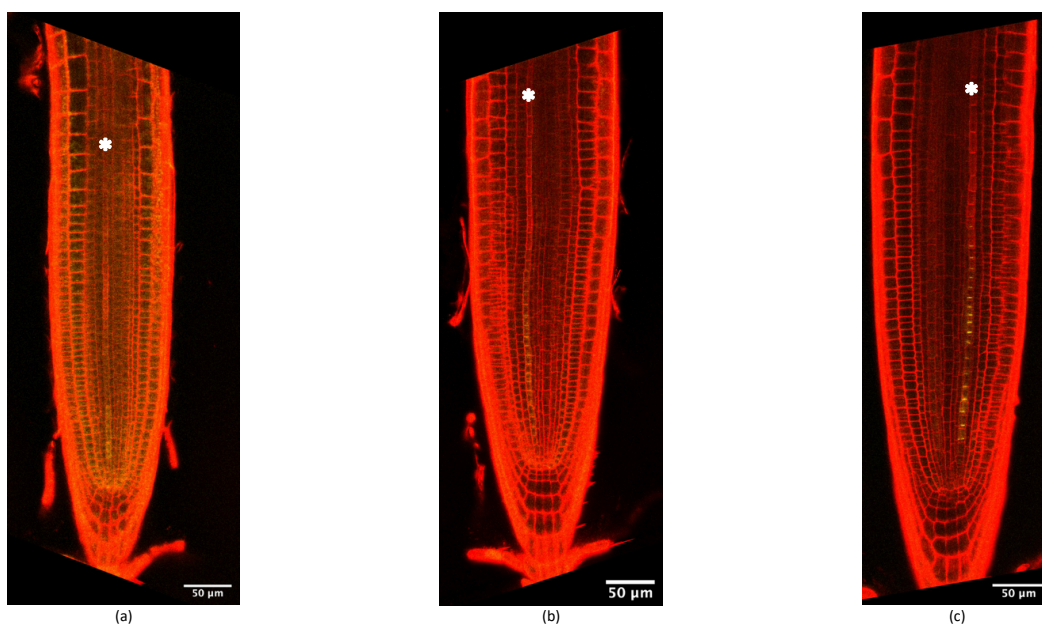


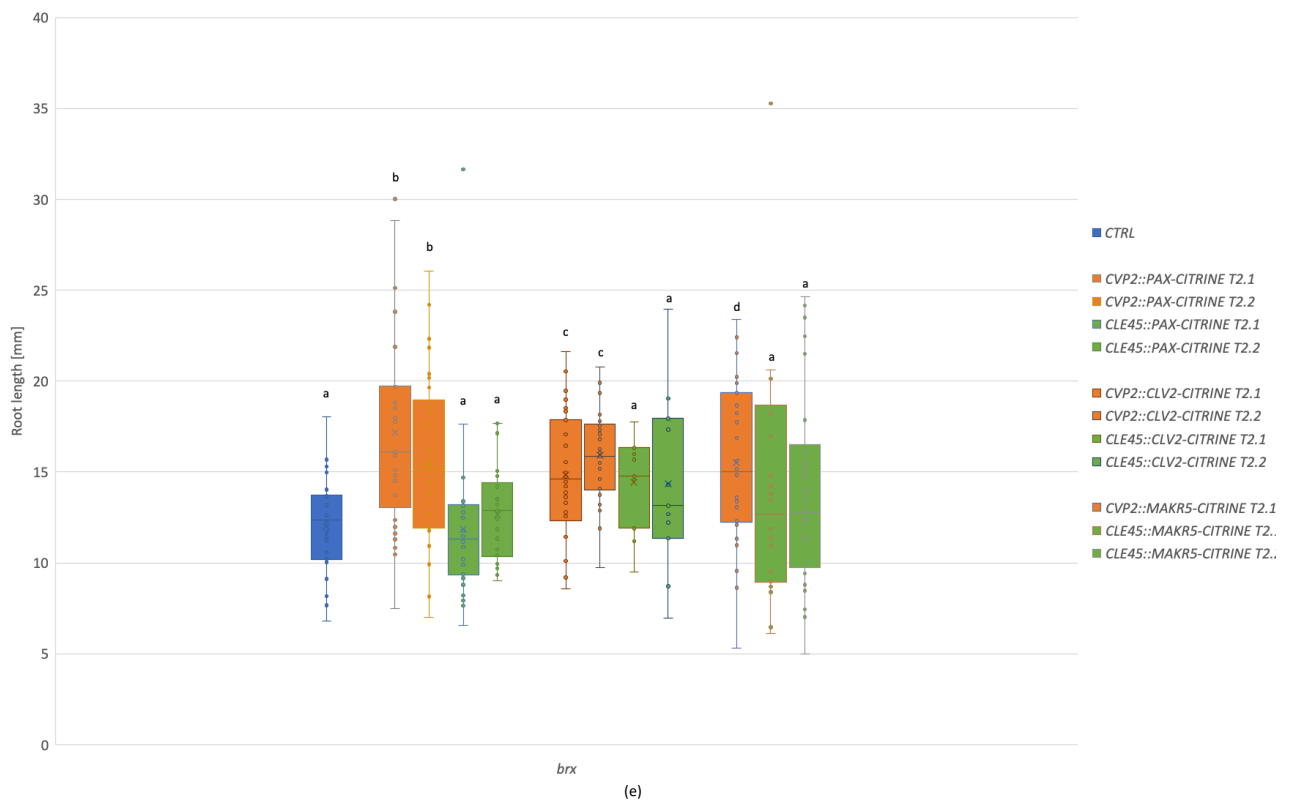
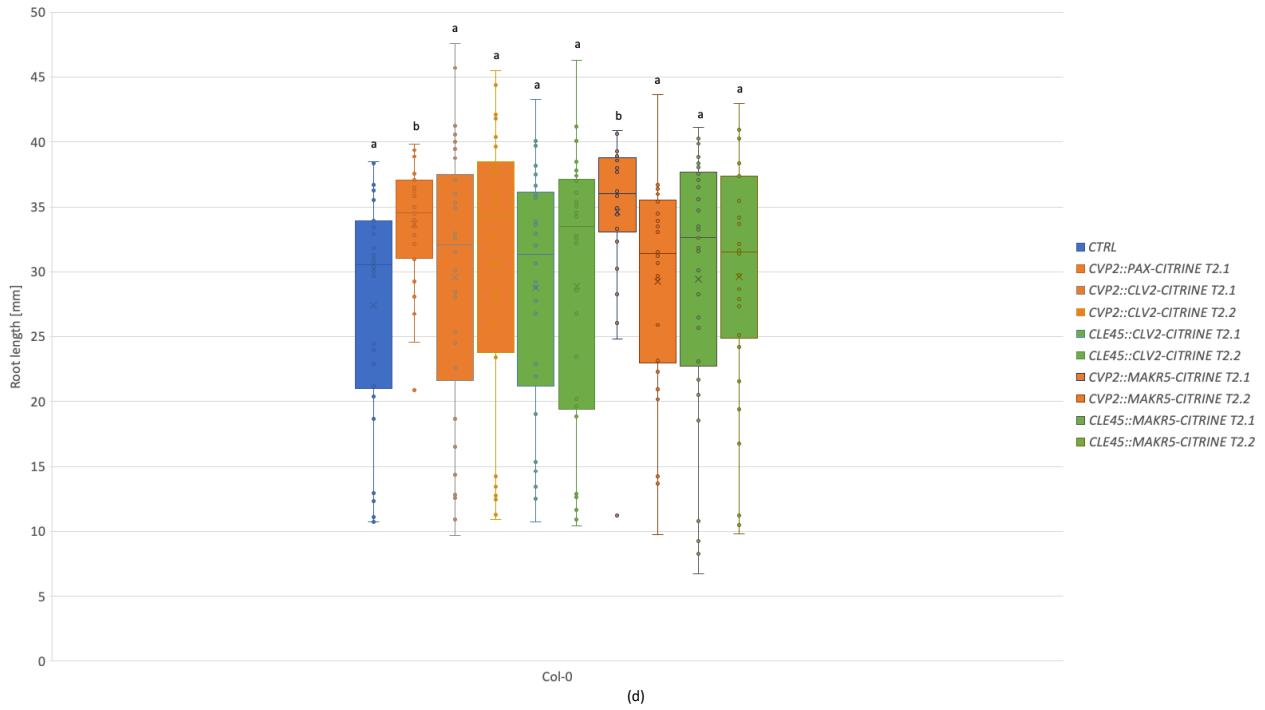
Figure 7: Complementation of *brx* mutants using the *BRX*, *CVP2* and *CLE45* promoter. a, b, c, PI counterstained confocal microscopy of *BRX::BRX-CITRINE* (a), *CVP2::BRX-CITRINE* (b) and *CLE45::BRX-CITRINE* (c) reporter fusion protein lines in *brx* mutant background, focused on a plane containing the protophloem cell file highlighted by stronger PI signal as a consequence of the PPSE differentiation associated cell wall thickening. Asterisks indicate the protophloem cell file and the arrow highlights a gap. **d**, Root length quantification of *brx* complemented lines and *Col-0* lines expressing an additional copy of *BRX*. Plots display individual values (dots), the median (horizontal line), the mean (cross) and the standard error of the mean (whiskers). See Material and Methods section for statistical test details.

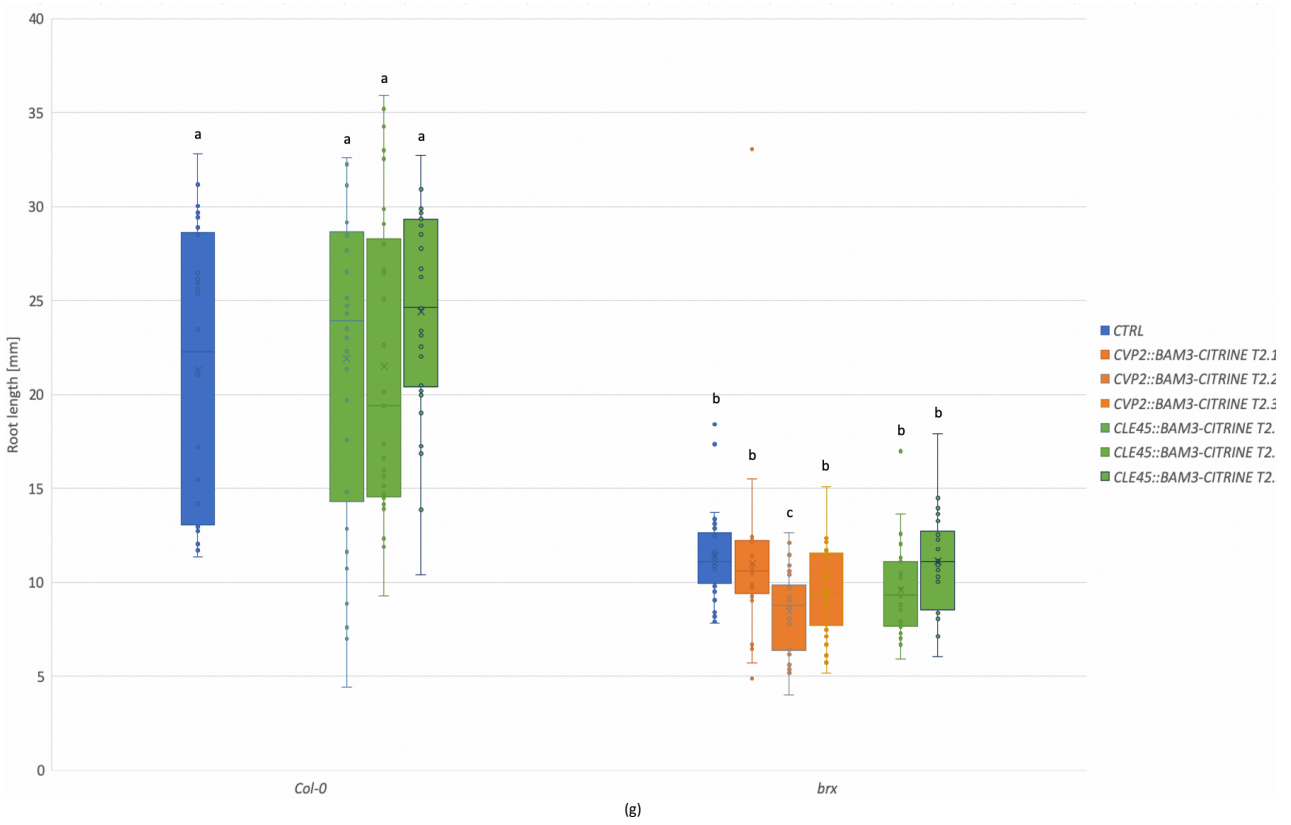
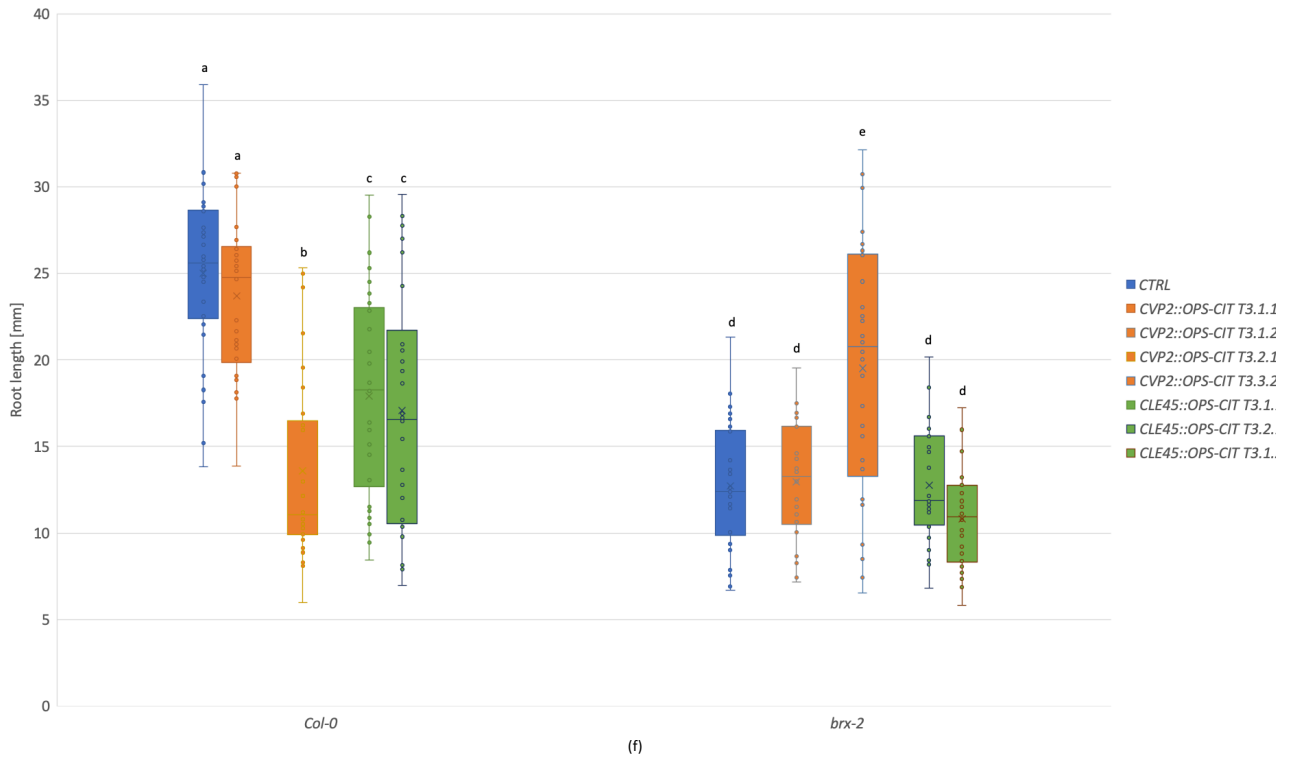
4.2 DPS rescue in *brx* mutant background by expressing genes of interest under the control of CVP2 versus CLE45 promoters

To test whether the *brx* mutant background could be rescued by the expression of gap cell specific turned off genes, some genes of interest were cloned downstream of the *CVP2* and the *CLE45* promoter and fused to a *CITRINE* fluorescent protein. Preliminary results obtained from T2 and T3 seedlings expressing *CLV2*, *MAKR5*, *OPS*, *BAM3*, *PROTEIN KINASE ASSOCIATED WITH BRX (PAX)* and *D6 PROTEIN KINASE (D6PK)*, a homologue of *PAX* (Marhava et al., 2018), are presented in the **Figure 8**. The protophloem specific expression was confirmed by the presence of the *CITRINE* signal (**Figure 8a-c**). Although no change in Col-0 root length was observed (**Figure 8d**), *brx* root length appeared to be partially rescued by the expression of *PAX*, *CLV2* and *MAKR5* in the protophloem when expression was driven by the *CVP2* and *CLE45* promoter except for the *PAX* expression under the control of the *CLE45* promoter which showed no rescue (**Figure 8e**). An additional copy of *OPS* in Col-0 background seemed to have a negative effect on root growth whereas when expressed under the *CVP2* promoter in *brx* mutants, a slight rescue could be observed (**Figure 8f**). *BAM3* did not have any effect on root length in either Col-0 and *brx* mutant background (**Figure 8g**) and *D6PK*, did display a slight rescue when expressed under the *CVP2* promoter in *brx* mutants (**Figure 8h**).

The expression of genes supposedly important for PPSE differentiation may be rescuing partially the DPS when expressed in gaps using the *CVP2* promoter. The high variability in root length measurements due to T2 seedlings don't allow us to make any solid conclusions but proposes *PAX*, *MAKR5*, *OPS* and *D6PK* as candidates for DPS rescue.







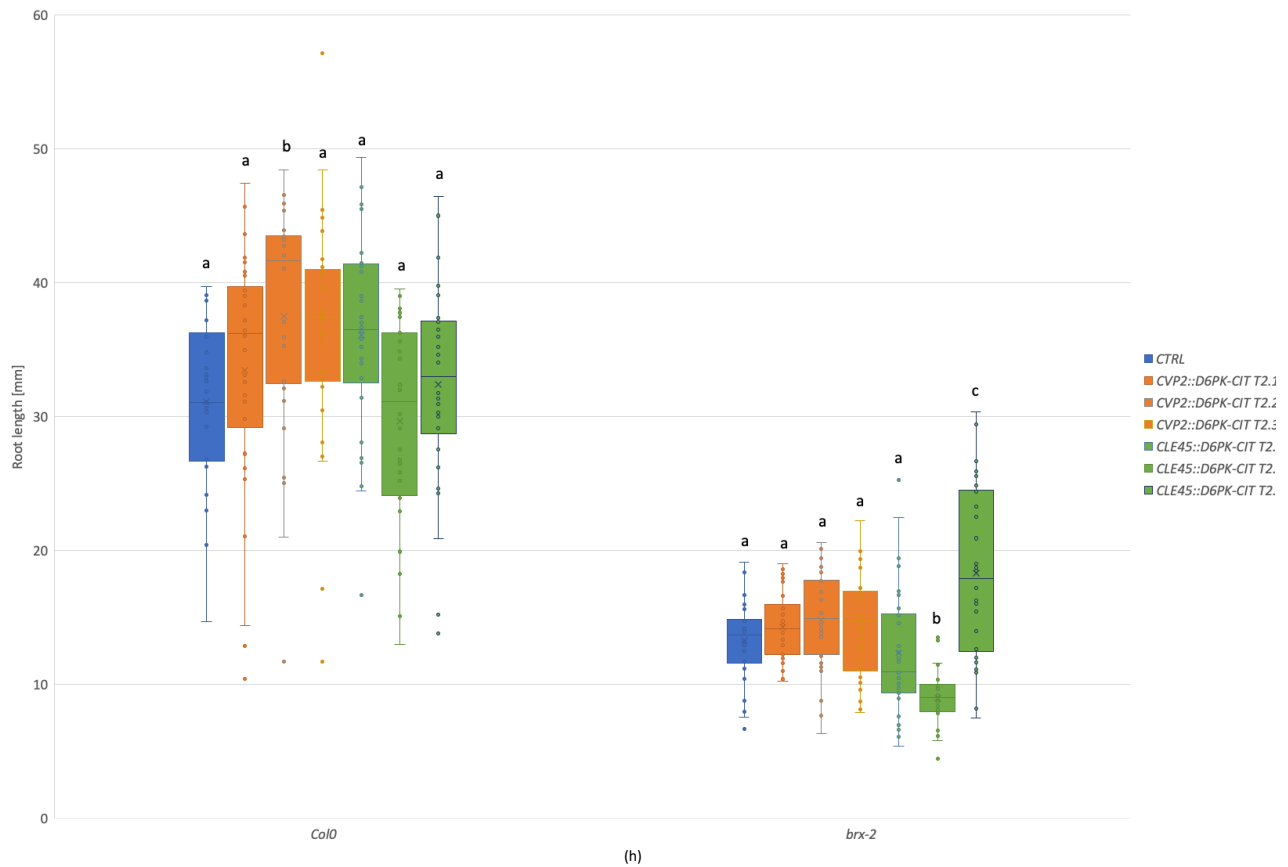


Figure 8: Complementation of *brx* mutants using protophloem specific promoters. a-c, PI counterstained confocal microscopy of *CLE45::CLV2-CITRINE* (a), *CLE45::MAKR5-CITRINE* (b), and *CLE45::PAX-CITRINE* (c) reporter fusion protein lines in Col-0 background, focused on a plane containing the protophloem cell file highlighted by stronger PI signal as a consequence of the PPSE differentiation associated cell wall thickening. Asterisks indicate the protophloem cell file. d-h, root length quantification of T2 and T3 transgenic lines in Col-0 and *brx* mutant background. Plots display individual values (dots), the median (horizontal line), the mean (cross) and the standard error of the mean (whiskers). See Material and Methods section for statistical test details.

Chapter 5 The role of auxin biosynthesis in protophloem development

To further investigate protophloem development and study the different actors of this process, the role of auxin in protophloem development was explored, starting with auxin biosynthesis. Auxin biosynthesis was induced specifically in developing PPSEs in order to evaluate the effect of increased auxin levels on protophloem development in various backgrounds. The auxin biosynthesis rate limiting enzyme YUCCA1 (*YUC1*) – which is the most widely represented YUCCA family member in the root meristem and is not expressed in the protophloem (**Supplementary Figure 6, Moret et al., 2020**) – was expressed under the *CVP2* and *CLE45* protophloem specific promoters, consequently increasing auxin levels in PPSEs of Col-0 and *brx* roots. The expression of *YUC1* was effectively restricted to the cytoplasm of developing PPSEs (**Figure 9a**), and absent of gap cells in *brx* mutant background when the expression was driven by the *CLE45* promoter (**Figure 9b, c**).

Seedlings expressing *YUC1* under the *CVP2* promoter displayed a reduced root length in Col-0 and *brx* backgrounds whereas when expressed under the *CLE45* promoter, *YUC1* had no effect on root length (**Figure 9d, e**). This suggests that *YUC1* – by increasing auxin levels in developing PPSEs – induces the premature differentiation of the protophloem, leading to a short root phenotype.

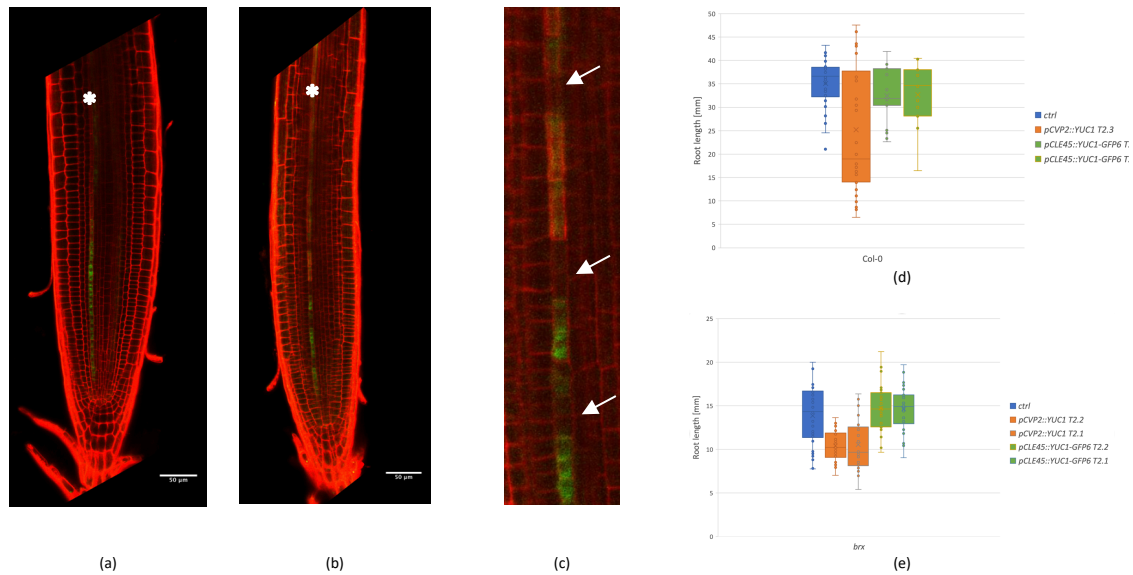


Figure 9: Protophloem specific *YUC1* expression. **a, b**, PI counterstained confocal microscopy of *CLE45::YUC1-GFP6* in Col-0 (**a**) and *brx* (**b**) mutant background. Asterisks indicate the protophloem cell file. **c**, higher magnification of (**b**) and gaps highlighted with arrows. **d, e**, Root length quantification of seedlings expressing *YUC1* specifically in Col-0 (**d**) and *brx* (**e**) protophloems. Tagged protein function was confirmed by the macroscopic phenotype.

The strong expression of *YUCCA5* (*YUC5*), an homologue of *YUC1*, in the last three cells prior to the full PPSE differentiation confirms that auxin biosynthesis has a great role in elevating the auxin levels required for the proper transition of PPSEs from a proliferation to a differentiation state (**Supplementary Figure 6, Moret et al., 2020**). Auxin has therefore a role in tuning protophloem differentiation timing and this is achieved by the expression of *YUC5* in the differentiating PPSEs. The role of auxin in PPSEs is developed later on in **Chapter 5**.

Moreover, as shown in 2.2.2 (**Figure 5**), *AUX1* expression is reduced in gap cells of *brx* mutants, resulting in a reduced influx transport of auxin and suggesting that auxin is either depleted in gap cells or accumulating in adjacent cells, deregulating the normal auxin mediated differentiation process. The role of *AUX1* in PPSE differentiation is discussed in **Chapter 6**.

Chapter 6 Paper #1 (co-author): A molecular rheostat adjusts auxin flux to promote root protophloem differentiation (Marhava et al., 2018)

A precise auxin distribution in post-meristematic developing protophloem is necessary for a proper timing of PPSE differentiation and requires controlled PIN activity (Santuari et al., 2011). In DPS affected backgrounds such as *brx* and *ops*, levels of auxin are reduced in the root meristem compared to Col-0 (Rodriguez-Villalon et al., 2015). Nevertheless, how differential auxin activity is achieved in PPSEs and its role in cell differentiation remains unclear.

In this paper we show that a “molecular rheostat” is created by the collaboration of two antagonistic regulators of auxin efflux, BRX and PAX. They are two polar plasma-membrane-associated proteins that co-localize with PINs in developing PPSEs. While PAX is responsible for the stimulation of PIN-mediated auxin efflux, BRX is inhibiting this activation via an auxin threshold that negatively regulates BRX plasma membrane association and therefore stimulates PAX activity. This dynamic steady state equilibrium provides a fine-tuned PIN activity and thus a proper auxin flux through PPSE cell files.

The first phase of my investigation into the role of auxin in protophloem is summarized in my contribution to Marhava et al., 2018 (**Figure 10a-n, q**):

The proximo-distal auxin profile in root meristems intersects with differential auxin activity in the radial dimension. For example, developing PPSEs display higher auxin accumulation than surrounding cells (**Figure 10a–d**) and differentiate faster than the neighboring cells that remain in meristematic state (**Figure 10e**). To explore whether PPSE differentiation depends on auxin activity, the auxin response was manipulated by expressing a constitutively active variant of an auxin-

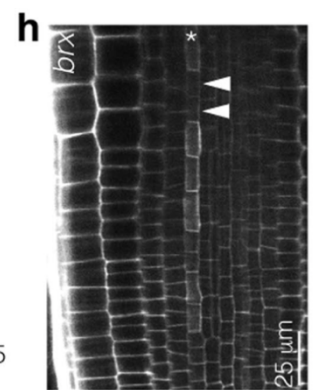
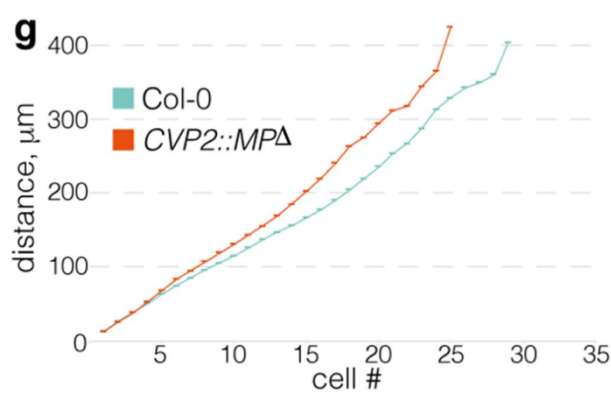
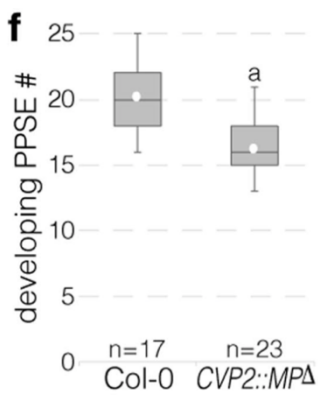
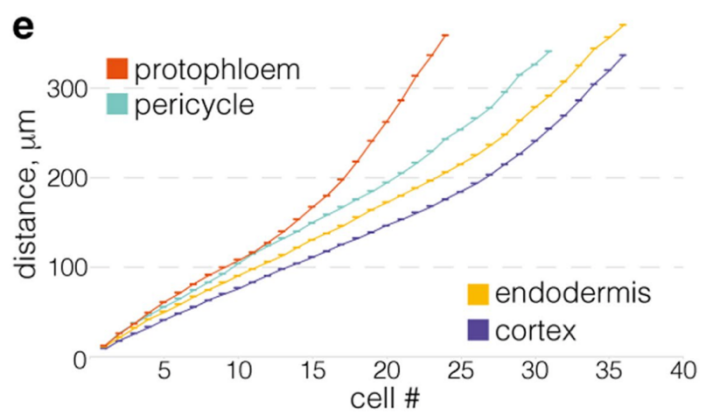
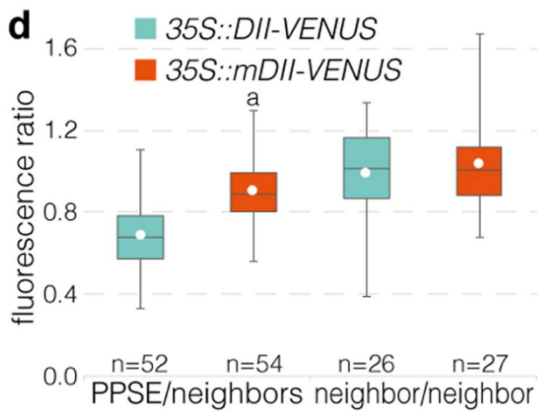
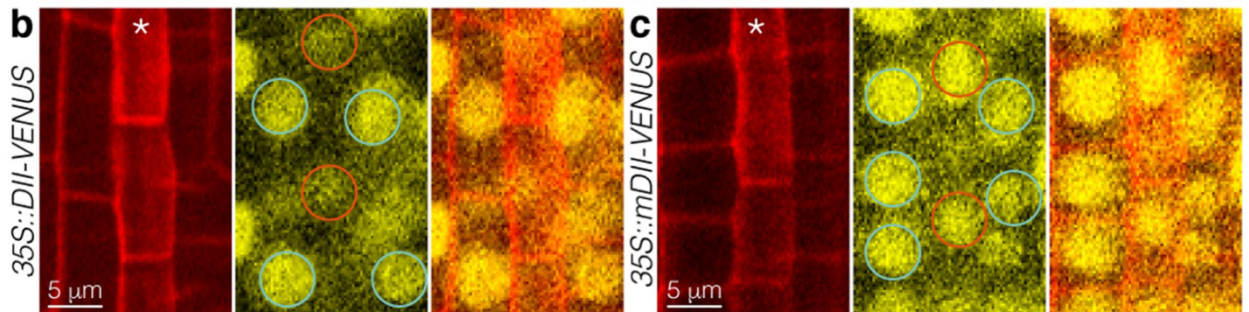
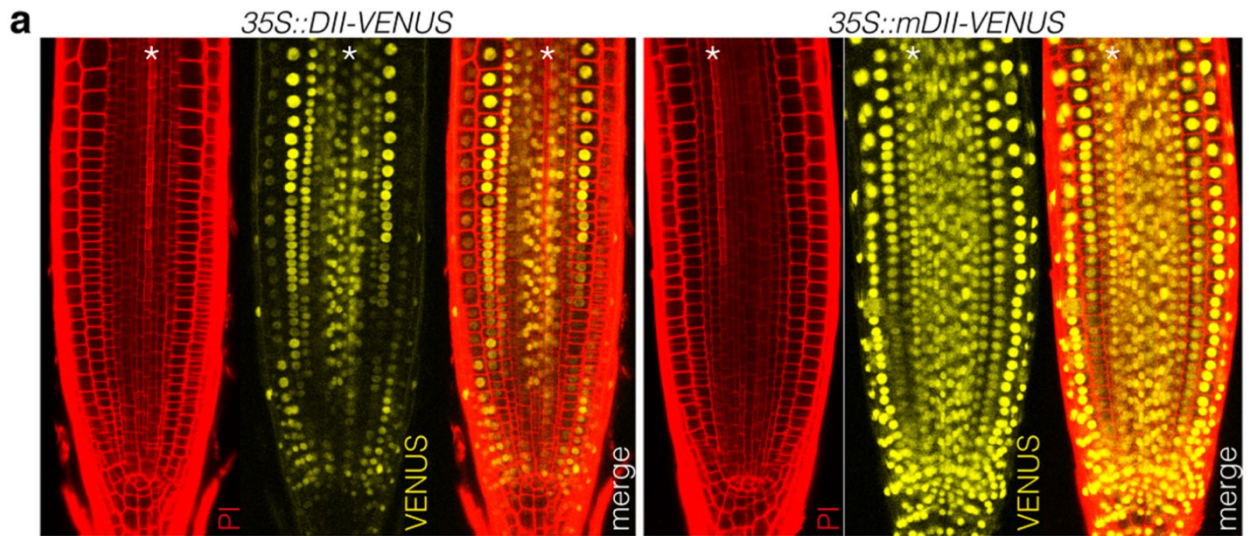
response factor, MONOPTEROS (MP^{Δ}), under the control of PPSE-specific *CVP2* promoter. *CVP2::MP^{\Delta}* accelerated PPSE differentiation, indicating that auxin responses critically determine the differentiation process (**Figure 10f, g**).

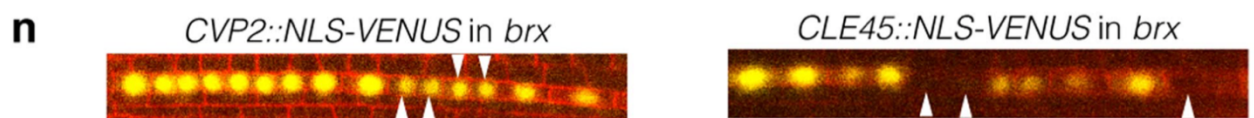
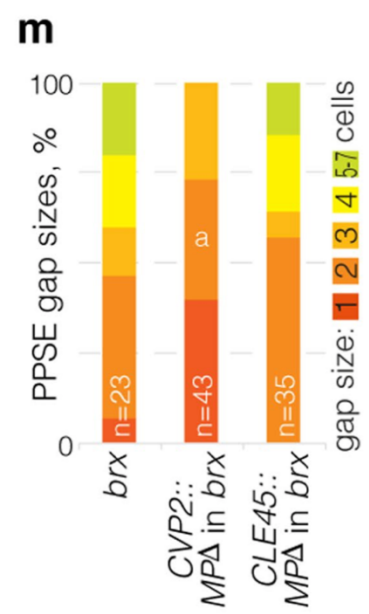
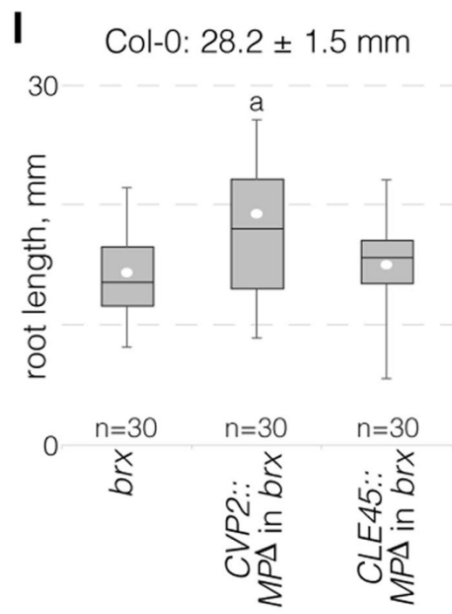
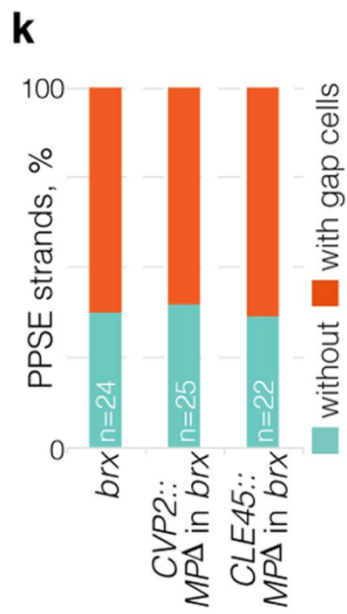
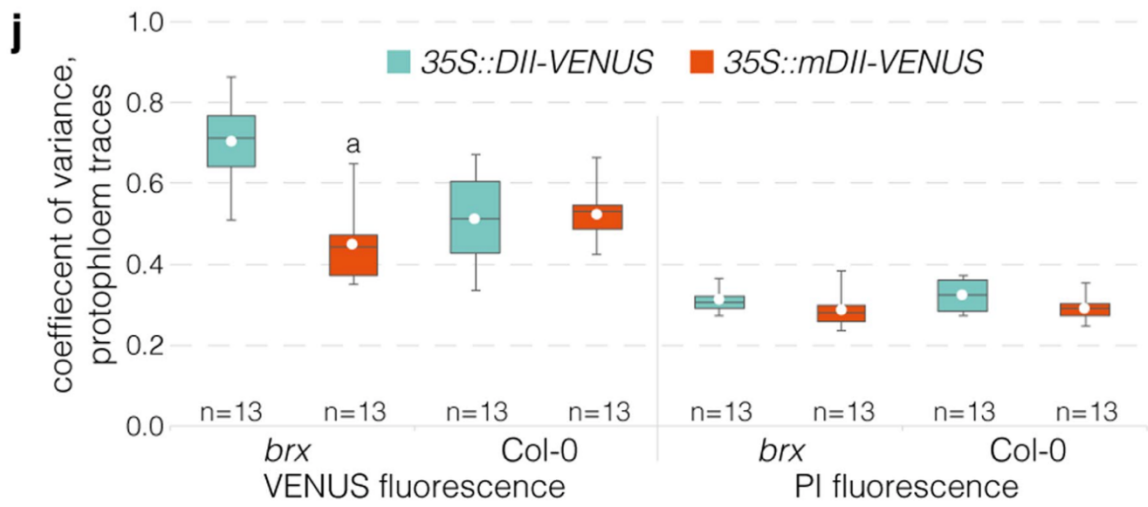
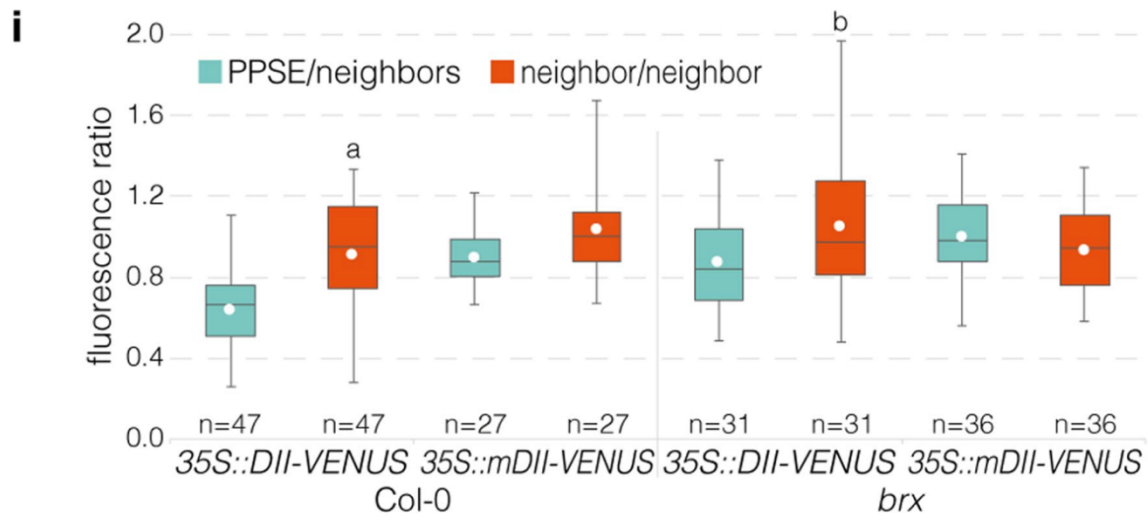
In *brx* mutants, PPSEs frequently fail to differentiate, giving rise to gap cells. These cells lack the characteristic cell-wall changes and appear as gaps in the PPSE differentiation zone (**Figure 10h**). Auxin negatively regulates BRX protein abundance and plasma-membrane association, but induces BRX transcription (Scacchi et al., 2009; Mouchel et al., 2006). Thus, BRX is a candidate for mediating auxin effects in PPSE differentiation.

In *brx* PPSEs, auxin accumulation as compared to neighboring cells was markedly lower and more variable than in the WT, putatively because of impaired auxin transport in gap cells (**Figure 10i, j**). Although the promotion of auxin activity by expressing *CVP2::MP^{\Delta}* in *brx* did not reduce the proportion of PPSE strands with gaps (**Figure 10k**), it significantly stimulated root growth (**Figure 10l**), reduced gap size (**Figure 10m**) and enhanced cell elongation and differentiation (**Figure 10g**). Such partial rescue was not observed with another PPSE-specific promoter that was inactive in gap cells (**Figure 10k–n**). Moreover, *brx* protophloem defects were aggravated by genetic interference with auxin uptake (**Figure 10q**). These observations support the hypothesis that finely tuned auxin activity contributes to proper PPSE differentiation.

The relation between PAX and BRX was further investigated and the result was published recently: Plasma membrane localization and polarity of PAX and indirectly BRX mostly rely on phosphatidylinositol-4,5-bisphosphate. Indeed, mutants in phosphatidylinositol-4-phosphate 5-kinases (PIP5Ks) display protophloem differentiation defects mimicking *brx* mutant phenotype. PIP5Ks form a complex with BRX and exhibit “muffin-like” polar localization. The BRX-PAX module recruits PIP5Ks to reinforce PAX polarity. This leads to a reinforcement of the polarity of all three proteins, which is needed to keep a local PIN minimum. PAX abundance at the plasma membrane is more variable in *brx* mutants in comparison with WT but is also overall reduced. PAX plasma membrane abundance was increased in *brx cvp2* double mutants compared to *brx* single mutant, although the increase did not strictly correlate with the extent of phenotypic rescue (Marhava et al., 2020).

Whether influx facilitators or local biosynthesis also contribute to this auxin distribution remains unclear. This was therefore assessed, and the results are discussed in **Chapter 6**.





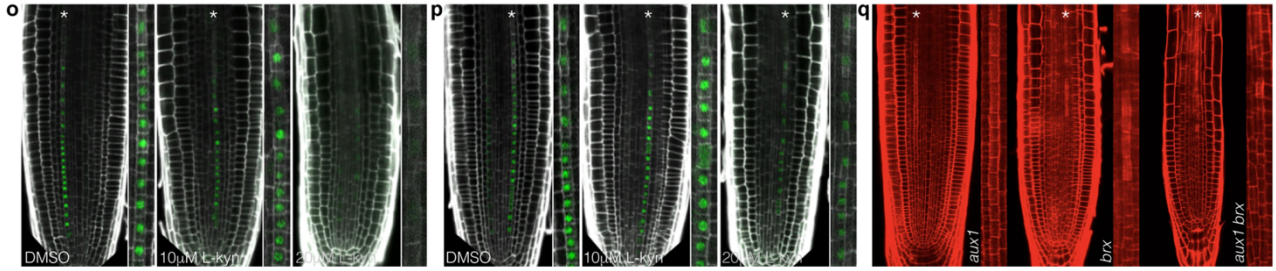


Figure 10: Auxin activity in developing PPSEs. **a**, Confocal microscopy of the inverse auxin activity reporter DII-VENUS and its negative control mDII-VENUS (yellow fluorescence) in the root meristem (PI staining, red) of WT Col-0 plants. Asterisks indicate sieve element cell files. **b**, Confocal microscopy of constitutively expressed DII-VENUS in developing PPSEs and neighboring cell files. Left, PI cell-wall staining (red); middle, DII-VENUS fluorescence (yellow; PPSE nuclei marked with red circles, nuclei in neighboring cell files with blue circles); right, overlay. **c**, As in b, for mDII-VENUS. **d**, Relative intensity of the DII-VENUS reporter and its mDII-VENUS control in the nuclei of Col-0 PPSEs as compared to the nuclei of directly neighboring cells. The statistically significant difference between DII-VENUS and mDII-VENUS in the PPSE/neighbors group is indicated (two-sided Student's t-test; a, $P = 5.86 \times 10^{-11}$). **e**, Cumulative average cell length in different root cell files, starting from the respective first stem-cell daughters (cell #1) ($n = 11$ WT Col-0 roots). **f**, Number of developing PPSEs from the first stem-cell daughter up to the first transition zone PPSE (protophloem length) in seven-day-old Col-0 seedlings, and transgenic seedlings expressing a constitutively active derivative of the auxin response factor *MONOPTEROS* (MP^{Δ}) under control of the PPSE-specific *CVP2* promoter. a, $P = 3.16 \times 10^{-6}$; two-sided Student's t-test. **g**, Cumulative average cell length in the developing protophloem, starting from the first stem-cell daughter (cell #1) ($n = 23$ each). Elongation occurs prematurely in *CVP2::MP^{\Delta}* plants. **h**, Confocal microscopy of a *brx* root meristem, focused on one of the sieve element strands (asterisk). Arrowheads point out gap cells, which fail to build up the characteristic PPSE cell wall owing to a failure to differentiate. **i**, Relative intensity of the DII-VENUS reporter and its mDII-VENUS control in the nuclei of Col-0 and *brx* PPSEs as compared to nuclei of cells in directly neighboring files. Statistically significant differences between PPSE/neighbors and neighbor/neighbor in the Col-0 and *brx* DII-VENUS groups are indicated (two-sided Student's t-test; a, $P = 2.49 \times 10^{-7}$; b, $P = 0.026$). **j**, Coefficient of variance for fluorescence traces of the DII-VENUS reporter and its mDII-VENUS control (left) and PI staining (right) along protophloem cell files. The statistically significant difference in VENUS fluorescence in the *brx* group is indicated (two-sided Student's t-test; a, $P = 2.30 \times 10^{-7}$). **k**, Quantification of PPSE strands with gaps in roots of indicated genotypes. **l**, Root length in seven-day-old seedlings for indicated Δ genotypes. The statistically significant differences between *CVP2::MP^{\Delta}* in *brx* and *brx* alone ($P = 0.0017$) and between *CVP2::MP^{\Delta}* in *brx* and *CLE45::MP^{\Delta}* in *brx* ($P = 0.0052$) are indicated by the character a. **m**, Distribution of gap size in protophloem strands of seven-day-old seedlings with gaps of indicated genotypes. The statistically significant differences between *CVP2::MP^{\Delta}* in *brx* and *brx* alone ($P = 0.0008$) and between *CVP2::MP^{\Delta}* in *brx* and *CLE45::MP^{\Delta}* in *brx* ($P = 0.0051$) are indicated by the character a (two-sided χ^2 test). **n**, Expression of fluorescent NLS-VENUS reporter in PPSEs of *brx* mutants, driven by either *CVP2* or *CLE45* promoter. Arrowheads indicate gap cells. **o**, **p**, Expression of *CVP2::NLS-VENUS* reporter (green fluorescence) in PPSE cell files (asterisks) of six-day-old Col-0 root meristems (PI staining, white) grown in the presence of (o), or transferred for 48 h onto (p), increasing amounts of the auxin biosynthesis inhibitor l-kynurenine (l-kyn). On the higher concentration, PPSE cell files (magnified) were barely distinguishable. **q**, Confocal microscopy of seven-day-old root meristems (PI staining, red). Asterisks indicate sieve element cell files (magnified, barely distinguishable in *aux1 brx*). (Marhava et al., 2018)

Chapter 7 Paper #2 (first author): Local auxin competition explains fragmented differentiation patterns (Moret et al., 2020)

Counter-intuitively, both *brx* and *pax* loss-of-function mutants show discontinuous protophloems, which results in short root phenotypes as well as other systemic effects (Rodriguez-Villalon et al., 2014; Marhava et al., 2018; Anne and Hardtke, 2018). This phenotype arises from apparently stochastic failure of developing PPSEs to differentiate. Such cells stand out as “gaps” that interrupt transition zone continuity because they retain their nucleus and do not reinforce their cell wall (Rodriguez-Villalon et al., 2014). Taking advantage of the different elements in our knowledge we collaborated with the laboratory of Prof. Kirsten ten Tusscher in Utrecht in order to computationally model protophloem development and predict gap cells occurrence.

We first showed that the differentiation defects observed in *brx* and *pax* are non-random and emerge in a characteristic pattern that can be simulated by defining a differentiation failure probability of an individual cell, total or split, as a function of differentiation failure in the preceding cell (**Figure 1g, Moret et al., 2020**). The observed pattern turned out to be a consequence of the presence of the auxin-sensitive auxin influx facilitator AUX1 (**Figure 4, Moret et al., 2020**).

Localization of AUX1 has been described to be cell type dependent and, together with PIN efflux transporters, it provides directionality of intercellular auxin flow (Swarup et al., 2001; Kleine-Vehn et al., 2006). The basal meristem has been proposed to recycle auxin coming from the root tip via the root cap (Blilou et al., 2005), and the basipetal transport towards this region also involves AUX1 (Swarup et al., 2001; Swarup et al., 2005). AUX1 is expressed in a subset of columella, lateral root cap, and stele tissues (Swarup et al., 2001).

AUX1 is specifically enriched in the developing protophloem, both at the transcriptional and translational level (**Figure 2, Moret et al., 2020**). We also confirmed AUX1 localization by immunolocalization and could show that AUX1

distribution is apolar, all around developing PPSEs (**Supplementary Figure 2, Moret et al., 2020**). The presence of AUX1 triggers a local auxin competition between neighboring cells. The cells accumulating auxin go on to differentiate normally, while the auxin depleted cells fail to differentiate (**Figure 3 & 5, Moret et al., 2020**). In WT, this competition is prevented by auxin efflux regulation via BRX and PAX (Marhava et al., 2018).

Chapter 8 Conclusion and future perspectives

8.1 Achieved results

By a meticulous approach, I could demonstrate that gap cells occurrence is not stochastic. In a root affected by the DPS, one of the two protophloems usually displays two gaps. The first gap occurs in the early differentiating protophloem area and is composed of two consecutive gap cells. The second gap is separated from the first gap by three differentiated cells and is also composed of two gap cells. Thus, each root usually exhibits a total of 4 gap cells in a protophloem strand, the second strand staying continuous. When analyzing different DPS mutants such as *brx* or *ops*, the occurrence, size and the position are mainly the same, however *ops* seems to show more and bigger gaps. Nevertheless, *pax* – that has a milder short root phenotype compared to *ops* and *brx* – exhibits gaps composed of more than two cells. The double mutant *brx pax* displayed comparable number of gaps compared to *brx* mutants (Marhava et al., 2018). This inverse proportionality between the bigger size of the gaps and the milder short root phenotype suggests that the size of the gap is not so relevant for the macroscopic phenotype, once a gap is present, whatever its size, it interrupts protophloem continuity. In order to test the effect of interrupting sap transport on root meristems fitness, roots of *brx* seedlings were grown completely plunged in sucrose complemented medium. Interestingly, roots plunged in sucrose complemented medium displayed more and bigger gaps, indicating a tolerance for big gaps as nutrients could be acquired from the medium easily. In addition, roots excessively affected by the DPS are possibly negatively selected when their environment has limited amounts of sugar. This suggests that the disruption of proper phloem transport by the gap cells is limiting the nutrients delivery in the root meristem and that stress can be relieved when roots are grown plunged in a rich medium.

The previously described gap cells phenotyping is based on a PI staining of the cell wall and therefore relies on the thickening of the cell wall, which is not happening in gap cells of DPS backgrounds. In order to address a better

characterization of gap cells, describe their identity and understand if the transcriptional regulation of genes involved in protophloem development is affected in mutants affected with the DPS, I investigated the expression pattern of various root meristematic genes in WT and in DPS affected mutants.

BRX, *OPS*, *AUX1*, *CVP2*, *BAM3*, *CLE45* and *MAKR5* are expressed in the early developing protophloem, suggesting they play a role in PPSE development. The positive regulators of protophloem differentiation (except for *CLE45*) are relatively specific to the protophloem whereas negative regulators such as *MAKR5* and *BAM3* display a broader expression pattern, suggesting a mechanism to restrict protophloem specification to a single cell file. Indeed, whereas positive regulators are specific to the protophloem, determining PPSE identity, negative regulators, seemingly in a quantitative manner, are there preventing surrounding cells to differentiate into PPSE.

The expression of some genes was found to be deregulated in gap cells, emphasizing the importance of these genes for proper protophloem differentiation. *CVP2* and *CLE45* are specific to the protophloem with overlapping expression pattern in WT. However, in gap cells, *CVP2* remains expressed whereas *CLE45* is shut down. Counterintuitively, this observation could suggest that *CLE45* would be required for a proper protophloem differentiation. Recently shown to be restricting PPSE identity to the protophloem position via RECEPTOR LIKE PROTEIN KINASE 2 (RPK2), *CLE45* signaling has been also suggested to give phloem cells the ability to re-determine their fate when protophloem fails to form (Gujas et al., 2020).

The expression of various genes known to be involved in protophloem differentiation were expressed in *brx* mutants in order to assess their ability to rescue the DPS. Using the *CVP2* and the *CLE45* promoter we tested if when putting back those genes of interest in the protophloem, in the gap cells or not respectively, a rescue of the DPS could be observed. The expression of genes supposedly important for PPSE differentiation are rescuing partially the DPS when expressed in gaps using the *CVP2* promoter, but this is not always the case when they are not expressed in the gaps, suggesting that their presence is indeed required in the gaps to rescue the DPS.

The downregulated expression of *CLE45*, *BAM3* and *AUX1* in gap cells suggests that the differentiation process might be impaired because of the absence of the set of differentiation negative regulators *CLE45/BAM3* and a reduced auxin influx transport. I therefore focused my work on the role of auxin in protophloem development.

I could show that along differentiating protophloem, auxin reaches two maxima: one close to the QC and one just before cells are completely differentiated, suggesting a dual role of auxin in the protophloem, preventing cell division and

inducing differentiation, respectively. Furthermore, auxin accumulates in the developing protophloem proposing that auxin could provoke differentiation earlier than in the surrounding tissues. Supporting that hypothesis, a constitutive activation of auxin signaling pathway in the protophloem by the expression of a truncated version of *MP* led to the premature differentiation of PPSEs and could even reduce the number of gaps in *brx* background. In addition, the modulation of auxin biosynthesis in the protophloem shows that *YUC1* – by increasing auxin levels in developing PPSEs – induced premature differentiation, leading to a short root phenotype.

In WT, the final auxin push is generated by *YUC5*. *YUC5* is a protophloem specific component of the auxin biosynthetic pathway expressed in three cells right before the first PPSE is fully differentiated, where auxin accumulates before triggering protophloem's switch from proliferation to differentiation. This confirms the importance of auxin for protophloem development, and more precisely auxin biosynthesis regulation at the tissue level. Still, *yuc5* loss-of-function mutants exhibits at best slightly delayed PPSE differentiation, but no gap cells or root phenotype could be so far identified. *yuc5* mutation also did not aggravate *brx* defects, consistent with strongly reduced *YUC5* expression in *brx* protophloem.

Furthermore, auxin biosynthesis and transport are deregulated in gap cells in the PPSE differentiation zone in *brx* mutant background. This suggests that auxin is either missing in gap cells or accumulating in adjacent cells, deregulating the normal auxin mediated differentiation process. In addition, *aux1* mutations are aggravating the *brx* phenotype. Even if auxin is massively transported from the shoot to the root by the phloem, there seems to be a great importance for proper PPSE differentiation of a tightly regulated active transport and biosynthesis in the protophloem.

Lastly, our combined experimental-modelling approach could explain why opposite effects on auxin homeostasis – *brx* VS *pax* mutant – trigger a similar protophloem phenotype: gap cells. The results suggest that once auxin homeostasis is affected in protophloem, PPSEs lose out the auxin concentration competition with surrounding tissues. This prevents their proper timed differentiation therefore leading to the DPS. Oppositely, a too early high auxin signaling activation leads to early protophloem differentiation. The switch from division to differentiation occurs before the cells could have enough time to renew the mother cells stock, the root gets shorter by exhaustion of the meristem.

In this scenario of auxin-dependent bi-stability, transported auxin gains in importance, and explains the non-random gap pattern observed in the DPS affected mutants. Still, our data also shows that as long as auxin efflux homeostasis is conserved, impaired auxin influx or local biosynthesis have little effect on differentiation.

8.2 Future developments

The literature and the conclusions of my project imply that auxin, cell division and CLE45 are linked and work together to coordinate PPSE development (Rodriguez-Villalon et al., 2014). However, the link(s) between auxin and CLE45 signaling pathways remain unknown. The regulation of PIN1 activity is now well described (Marhava et al., 2018), but what about AUX1? Do protophloem cells require low auxin to divide? What is the link between division and CLE45 in the protophloem? Why does CLE45 inhibit protophloem differentiation but seems to be required for proper PPSE differentiation?

In order to assess more deeply PPSE differentiation, dynamic analysis along time lapse becomes a priority. First, having an inducible system allowing one to complement *brx* mutant roots would allow us to understand the cell fate determination dynamics. We could see if – by putting back at some point a functional BRX in a *brx* mutant background – some already primed gap cells could be complemented and revert their cell fate into a normally differentiating PPSE. Since *BRX* is expressed at very low levels, it is yet hard to implement such an inducible system with really limited levels of leakiness, avoiding the unintentional complementation of *brx* mutants.

Such a time lapse analysis would need the technology – vertical microscopes – to capture growing roots in a long term (min. 24h) to be able to follow an individual cell from the division zone to the differentiation zone. Real time imaging of a developing PPSE would indeed allow a better understanding of the dynamics of cell differentiation in that context. What does an initial cell need to fully differentiate and acquire its function? What is the time ratio between division and differentiation? At what point is a gap cell fate defined and how does it evolve through the differentiating protophloem? In that perspective, the reporter genes toolbox I generated will be a powerful tool to visualize protophloem establishment during long time lapse and avoid the use of toxic staining chemicals such as PI. Therefore, live imaging would capture the dynamics of gene expression through time for a particular cell. In combination with an auxin marker, this could unravel the link between some specific gene expression and cellular auxin concentration. One could also try to see if gap cells could be induced by the expression of gap cells specific genes. Besides, what is the effect of *CLE45* when expressed under a gap cell specific promoter in a *brx* mutant background? Is *CLE45* expression sufficient to rescue gap cells?

So as to identify more gap cells specific genes, one could use single cell RNA sequencing. By analyzing data with our present knowledge, we could look at cells expressing known protophloem specific genes and search for other

protophloem specific genes. Additionally, we could compare normally differentiating protophloem cells with gap cells in order to identify new genes that are specifically expressed in gap cells. This could allow us to link their identity to known other cell types or characterize them better.

The recent advances in the CRISPR technology could be beneficial for protophloem gene network characterization. For example, PINs single mutants do not show obvious protophloem phenotypes probably because of compensation effects. Yet, high order mutants could be lethal or show pleiotropic effects, but they are crucial to better understand the role of PINs in protophloem development. In that context, mutation of all the PINs specifically in the protophloem would bypass the pleiotropic obstacle and would help to understand their function in that context.

References

- Adamowski M, Friml J** (2015). PIN-dependent auxin transport: action, regulation, and evolution. *Plant Cell* 27(1):20-32.
- Anne P, Amiguet-Vercher A, Brandt B, Kalmbach L, Geldner N, Hothorn M, Hardtke CS** (2018). CLERK is a novel receptor kinase required for sensing of root-active CLE peptides in Arabidopsis. *Development* 145(10).
- Anne P, Azzopardi M, Gissot L, Beaubiat S, Hématy K, Palauqui JC** (2015). OCTOPUS Negatively Regulates BIN2 to Control Phloem Differentiation in Arabidopsis thaliana. *Curr Biol* 25(19):2584-90.
- Anne P, Hardtke CS** (2018). Phloem function and development-biophysics meets genetics. *Curr Opin Plant Biol* 43:22-28.
- Band LR, Wells DM, Fozard JA, Ghetiu T, French AP, Pound MP, Wilson MH, Yu L, Li W, Hijazi HI, Oh J, Pearce SP, Perez-Amador MA, Yun J, Kramer E, Alonso JM, Godin C, Vernoux T, Hodgman TC, Pridmore TP, Swarup R, King JR, Bennett MJ** (2014). Systems Analysis of Auxin Transport in the Arabidopsis Root Apex. *Plant Cell* 26(3):862-75.
- Baster P, Robert S, Kleine-Vehn J, Vanneste S, Kania U, Grunewald W, De Rybel B, Beeckman T, Friml J** (2013). SCF(TIR1/AFB)-auxin signalling regulates PIN vacuolar trafficking and auxin fluxes during root gravitropism. *EMBO J* 32(2):260-74.
- Bauby H, Divol F, Truernit E, Grandjean O, Palauqui JC** (2007). Protophloem differentiation in early Arabidopsis thaliana development. *Plant Cell Physiol* 48(1):97-109.
- Benková E, Michniewicz M, Sauer M, Teichmann T, Seifertová D, Jürgens G, Friml J** (2003). Local, efflux-dependent auxin gradients as a common module for plant organ formation. *Cell* 115(5):591-602.
- Berleth T, Jurgens G** (1993). The role of the monopteros gene in organising the basal body region of the Arabidopsis embryo. *Development* 118(2):575-587.
- Blilou I, Xu J, Wildwater M, Willemsen V, Paponov I, Friml J, Heidstra R, Aida M, Palme K, Scheres B** (2005). The PIN auxin efflux facilitator network controls growth and patterning in Arabidopsis roots. *Nature* 433(7021):39-44.
- Bonke M, Thitamadee S, Mähönen AP, Hauser MT, Helariutta Y** (2003). APL regulates vascular tissue identity in Arabidopsis. *Nature* 426(6963):181-6.
- Breda AS, Hazak O, Hardtke CS** (2017). Phosphosite charge rather than shootward localization determines OCTOPUS activity in root protophloem. *Proc Natl Acad Sci U S A* 114(28):E5721-E5730.
- Breda AS, Hazak O, Schultz P, Anne P, Graeff M, Simon R, Hardtke CS** (2019). A Cellular Insulator against CLE45 Peptide Signaling. *Curr Biol* 29(15):2501-2508.e3.
- Brumos J, Alonso JM, Stepanova AN** (2014). Genetic aspects of auxin biosynthesis and its regulation. *Physiol Plant* 151(1):3-12.
- Brunoud G, Wells DM, Oliva M, Larrieu A, Mirabet V, Burrow AH, Beeckman T, Kepinski S, Traas J, Bennett MJ, Vernoux T** (2012). A novel sensor to map auxin response and distribution at high spatio-temporal resolution. *Nature* 482(7383):103-6.
- Chen Q, Dai X, De-Paoli H, Cheng Y, Takebayashi Y, Kasahara H, Kamiya Y, Zhao Y** (2014). Auxin overproduction in shoots cannot rescue auxin deficiencies in Arabidopsis roots. *Plant Cell Physiol* 55(6):1072-9.
- Ckurshumova W, Smirnova T, Marcos D, Zayed Y, Berleth T** (2014). Irrepressible MONOPTEROS/ARF5 promotes de novo shoot formation. *New Phytol* 204(3):556-66.
- Clough SJ, Bent AF** (1998). Floral dip: a simplified method for Agrobacterium-mediated transformation of Arabidopsis thaliana. *Plant J* 16(6):735-43.
- Depuydt S, Hardtke CS** (2011). Hormone signalling crosstalk in plant growth regulation. *Curr Biol* 21(9):R365-73.

- Depuydt S, Rodriguez-Villalon A, Santuari L, Wyser-Rmili C, Ragni L, Hardtke CS** (2013). Suppression of Arabidopsis protophloem differentiation and root meristem growth by CLE45 requires the receptor-like kinase BAM3. *Proc Natl Acad Sci U S A* 110(17):7074-9.
- Di Mambro R, De Ruvo M, Pacifici E, Salvi E, Sozzani R, Benfey PN, Busch W, Novak O, Ljung K, Di Paola L, Marée AFM, Costantino P, Grieneisen VA, Sabatini S** (2017). Auxin minimum triggers the developmental switch from cell division to cell differentiation in the Arabidopsis root. *Proc Natl Acad Sci U S A* 114(36):E7641-E7649.
- Ding Z, Friml J** (2010). Auxin regulates distal stem cell differentiation in Arabidopsis roots. *Proc Natl Acad Sci U S A* 107(26):12046-51.
- Dolan L, Janmaat K, Willemsen V, Linstead P, Poethig S, Roberts K, Scheres B** (1993). Cellular organisation of the Arabidopsis thaliana root. *Development* 119(1):71-84.
- Ellis CM, Nagpal P, Young JC, Hagen G, Guilfoyle TJ, Reed JW** (2005). AUXIN RESPONSE FACTOR1 and AUXIN RESPONSE FACTOR2 regulate senescence and floral organ abscission in Arabidopsis thaliana. *Development* 132(20):4563-74.
- Esau K** (1965). FIXATION IMAGES OF SIEVE ELEMENT PLASTIDS IN BETA. *Proc Natl Acad Sci U S A* 54(2):429-37.
- Fendrych M, Leung J, Friml J** (2017). TIR1/AFB-Aux/IAA auxin perception mediates rapid cell wall acidification and growth of Arabidopsis hypocotyls. *Elife* 5. pii: e19048.
- Finet C, Berne-Dedieu A, Scutt CP, Marlétaz F** (2013). Evolution of the ARF gene family in land plants: old domains, new tricks. *Mol Biol Evol* 30(1):45-56.
- Friml J, Benková E, Blilou I, Wisniewska J, Hamann T, Ljung K, Woody S, Sandberg G, Scheres B, Jürgens G, Palme K** (2002). AtPIN4 mediates sink-driven auxin gradients and root patterning in Arabidopsis. *Cell* 108(5):661-73.
- Friml J, Palme K** (2002). Polar auxin transport - old questions and new concepts? *Plant Mol Biol* 49(3-4):273-84.
- Furuta KM, Yadav SR, Lehesranta S, Belevich I, Miyashima S, Heo JO, Vatén A, Lindgren O, De Rybel B, Van Isterdael G, Somervuo P, Lichtenberger R, Rocha R, Thitamadee S, Tähtiharju S, Auvinen P, Beeckman T, Jokitalo E, Helariutta Y** (2014). Plant development. Arabidopsis NAC45/86 direct sieve element morphogenesis culminating in enucleation. *Science* 345(6199):933-7.
- Gälweiler L, Guan C, Müller A, Wisman E, Mendgen K, Yephremov A, Palme K** (1998). Regulation of polar auxin transport by AtPIN1 in Arabidopsis vascular tissue. *Science* 282(5397):2226-30.
- Geldner N, Friml J, Stierhof Y D, Jürgens G, Palme K** (2001). Auxin transport inhibitors block PIN1 cycling and vesicle trafficking. *Nature* 413(6854):425-8.
- Goldsmith MH, Goldsmith TH** (1981). Quantitative predictions for the chemiosmotic uptake of auxin. *Planta* 153(1):25-33.
- Goldsmith MH, Goldsmith TH, Martin MH** (1981). Mathematical analysis of the chemosmotic polar diffusion of auxin through plant tissues. *Proc Natl Acad Sci U S A* 78(2):976-80.
- Guilfoyle TJ, Hagen G** (2007). Auxin response factors. *Curr Opin Plant Biol* 10(5):453-60.
- Gujas B, Alonso-Blanco C, Hardtke CS** (2012). Natural Arabidopsis brx loss-of-function alleles confer root adaptation to acidic soil. *Curr Biol* 22(20):1962-8.
- Gujas B, Kastanaki E, Sturchler A, Cruz TMD, Ruiz-Sola MA, Dreos R, Eicke S, Truernit E, Rodriguez-Villalon A** (2020). A Reservoir of Pluripotent Phloem Cells Safeguards the Linear Developmental Trajectory of Protophloem Sieve Elements. *Curr Biol* 30(5):755-766.e4.
- Halle F** (1986). Modular Growth in Seed Plants. *Philos T Roy Soc B* 313, 77-87.
- Hardtke CS, Berleth T** (1998). The Arabidopsis gene MONOPTEROS encodes a transcription factor mediating embryo axis formation and vascular development. *EMBO J* 17(5):1405-11.

- Hazak O, Brandt B, Cattaneo P, Santiago J, Rodriguez-Villalon A, Hothorn M, Hardtke CS** (2017). Perception of root-active CLE peptides requires CORYNE function in the phloem vasculature. *EMBO Rep* 18(8):1367-1381.
- Holbrook NM, Knoblauch M** (2018). Editorial overview: Physiology and metabolism: Phloem: a supracellular highway for the transport of sugars, signals, and pathogens. *Curr Opin Plant Biol* 43, iii-vii.
- Jaillais Y, Hothorn M, Belkhadir Y, Dabi T, Nimchuk ZL, Meyerowitz EM, Chory J** (2011). Tyrosine phosphorylation controls brassinosteroid receptor activation by triggering membrane release of its kinase inhibitor. *Genes Dev* 25(3):232-7.
- Kang YH, Hardtke CS** (2016). Arabidopsis MAKR5 is a positive effector of BAM3-dependent CLE45 signaling. *EMBO Rep* 17(8):1145-54.
- Kleine-Vehn J, Dhonukshe P, Swarup R, Bennett M, Friml J** (2006). Subcellular trafficking of the Arabidopsis auxin influx carrier AUX1 uses a novel pathway distinct from PIN1. *Plant Cell* 18(11):3171-81.
- Kramer EM** (2004). PIN and AUX/LAX proteins: their role in auxin accumulation. *Trends Plant Sci* 9(12):578-82.
- Krogan NT, Berleth T** (2012). A dominant mutation reveals asymmetry in MP/ARF5 function along the adaxial-abaxial axis of shoot lateral organs. *Plant Signal Behav* 7(8):940-3.
- Krogan NT, Ckurshumova W, Marcos D, Caragea AE, Berleth T** (2012). Deletion of MP/ARF5 domains III and IV reveals a requirement for Aux/IAA regulation in Arabidopsis leaf vascular patterning. *New Phytol* 194(2):391-401.
- Krogan NT, Marcos D, Weiner AI, Berleth T** (2016). The auxin response factor MONOPTEROS controls meristem function and organogenesis in both the shoot and root through the direct regulation of PIN genes. *New Phytol* 212(1):42-50.
- Ljung K** (2013). Auxin metabolism and homeostasis during plant development. *Development* 140(5):943-50.
- Ljung K, Hull AK, Celenza J, Yamada M, Estelle M, Normanly J, Sandberg G** (2005). Sites and regulation of auxin biosynthesis in Arabidopsis roots. *Plant Cell* 17(4):1090-104.
- Marchant A, Bhalerao R, Casimiro I, Eklöf J, Casero PJ, Bennett M, Sandberg G** (2002). AUX1 promotes lateral root formation by facilitating indole-3-acetic acid distribution between sink and source tissues in the Arabidopsis seedling. *Plant Cell* 14(3):589-97.
- Marchant A, Kargul J, May ST, Muller P, Delbarre A, Perrot-Rechenmann C, Bennett MJ** (1999). AUX1 regulates root gravitropism in Arabidopsis by facilitating auxin uptake within root apical tissues. *EMBO J* 18(8):2066-73.
- Marhava P, Aliaga Fandino AC, Koh SWH, Jelínková A, Kolb M, Janacek DP, Breda AS, Cattaneo P, Hammes UZ, Petrášek J, Hardtke CS** (2020). Plasma Membrane Domain Patterning and Self-Reinforcing Polarity in Arabidopsis. *Dev Cell* 52(2):223-235.e5.
- Marhava P, Bassukas AEL, Zourelidou M, Kolb M, Moret B, Fastner A, Schulze WX, Cattaneo P, Hammes UZ, Schwechheimer C, Hardtke CS** (2018). A molecular rheostat adjusts auxin flux to promote root protophloem differentiation. *Nature* 558(7709):297-300.
- Milne RJ, Grof CP, Patrick JW** (2018). Mechanisms of phloem unloading: shaped by cellular pathways, their conductances and sink function. *Curr Opin Plant Biol* 43, 8-15.
- Mouchel CF, Briggs GC, Hardtke CS** (2004). Natural genetic variation in Arabidopsis identifies BREVIS RADIX, a novel regulator of cell proliferation and elongation in the root. *Genes Dev* 18(6):700-14.
- Mouchel CF, Osmont KS, Hardtke CS** (2006). BRX mediates feedback between brassinosteroid levels and auxin signalling in root growth. *Nature* 443(7110):458-61.
- Nagawa S, Sawa S, Sato S, Kato T, Tabata S, Fukuda H** (2006). Gene trapping in Arabidopsis reveals genes involved in vascular development. *Plant Cell Physiol* 47(10):1394-405.
- Péret B, Swarup K, Ferguson A, Seth M, Yang Y, Dhondt S, James N, Casimiro I, Perry P, Syed A, Yang H, Reemmer J, Venison E, Howells C, Perez-Amador MA, Yun J, Alonso J, Beemster GT, Laplaze L, Murphy A, Bennett MJ, Nielsen E,**

- Swarup R** (2012). AUX/LAX genes encode a family of auxin influx transporters that perform distinct functions during Arabidopsis development. *Plant Cell* 24(7):2874-85.
- Petersson SV, Johansson AI, Kowalczyk M, Makoveychuk A, Wang JY, Moritz T, Grebe M, Benfey PN, Sandberg G, Ljung K** (2009). An auxin gradient and maximum in the Arabidopsis root apex shown by high-resolution cell-specific analysis of IAA distribution and synthesis. *Plant Cell* 21(6):1659-68.
- Petrásek J, Friml J** (2009). Auxin transport routes in plant development. *Development* 136, 2675-2688.
- Petrásek J, Mravec J, Bouchard R, Blakeslee JJ, Abas M, Seifertová D, Wisniewska J, Tadele Z, Kubes M, Covanová M, Dhonukshe P, Skupa P, Benková E, Perry L, Krecek P, Lee OR, Fink GR, Geisler M, Murphy AS, Luschnig C, Zazimalová E, Friml J** (2006). PIN proteins perform a rate-limiting function in cellular auxin efflux. *Science* 312(5775):914-8.
- Przemeck GK, Mattsson J, Hardtke CS, Sung ZR, Berleth T** (1996). Studies on the role of the Arabidopsis gene MONOPTEROS in vascular development and plant cell axialization. *Planta* 200(2):229-37.
- Rademacher EH, Lokerse AS, Schlereth A, Llavata-Peris CI, Bayer M, Kientz M, Freire Rios A, Borst JW, Lukowitz W, Jürgens G, Weijers D** (2012). Different auxin response machineries control distinct cell fates in the early plant embryo. *Dev Cell* 22(1):211-22.
- Rademacher EH, Möller B, Lokerse AS, Llavata-Peris CI, van den Berg W, Weijers D** (2011). A cellular expression map of the Arabidopsis AUXIN RESPONSE FACTOR gene family. *Plant J* 68(4):597-606.
- Rodriguez-Villalon A, Gujas B, Kang YH, Breda AS, Cattaneo P, Depuydt S, Hardtke CS** (2014). Molecular genetic framework for protophloem formation. *Proc Natl Acad Sci U S A* 111(31):11551-6.
- Rodriguez-Villalon A, Gujas B, van Wijk R, Munnik T, Hardtke CS** (2015). Primary root protophloem differentiation requires balanced phosphatidylinositol-4,5-bisphosphate levels and systemically affects root branching. *Development* 142(8):1437-46.
- Ross-Elliott TJ, Jensen KH, Haaning KS, Wager BM, Knoblauch J, Howell AH, Mullendore DL, Monteith AG, Paultre D, Yan D, Otero S, Bourdon M, Sager R, Lee JY, Helariutta Y, Knoblauch M, Oparka KJ** (2017). Phloem unloading in Arabidopsis roots is convective and regulated by the phloem-pole pericycle. *Elife* 6. pii: e24125.
- Rubery PH, Sheldrake AR** (1973). Effect of pH and surface charge on cell uptake of auxin. *Nat New Biol* 244(139):285-8.
- Rubery PH, Sheldrake AR** (1974). Carrier-mediated auxin transport. *Planta* 118(2):101-21.
- Sabatini S, Beis D, Wolkenfelt H, Murfett J, Guilfoyle T, Malmay J, Benfey P, Leyser O, Bechtold N, Weisbeek P, Scheres B** (1999). An auxin-dependent distal organizer of pattern and polarity in the Arabidopsis root. *Cell* 99(5):463-72.
- Santuari L, Scacchi E, Rodriguez-Villalon A, Salinas P, Dohmann EM, Brunoud G, Vernoux T, Smith RS, Hardtke CS** (2011). Positional information by differential endocytosis splits auxin response to drive Arabidopsis root meristem growth. *Curr Biol* 21(22):1918-23.
- Sarkar AK, Luijten M, Miyashima S, Lenhard M, Hashimoto T, Nakajima K, Scheres B, Heidstra R, Laux T** (2007). Conserved factors regulate signalling in Arabidopsis thaliana shoot and root stem cell organizers. *Nature* 446(7137):811-4.
- Scacchi E, Osmont KS, Beuchat J, Salinas P, Navarrete-Gómez M, Trigueros M, Ferrándiz C, Hardtke CS** (2009). Dynamic, auxin-responsive plasma membrane-to-nucleus movement of Arabidopsis BRX. *Development* 136(12):2059-67.
- Scacchi E, Salinas P, Gujas B, Santuari L, Krogan N, Ragni L, Berleth T, Hardtke CS** (2010). Spatio-temporal sequence of cross-regulatory events in root meristem growth. *Proc Natl Acad Sci U S A* 107(52):22734-9.
- Sultan SE** (2000). Phenotypic plasticity for plant development, function and life history. *Trends Plant Sci* 5, 537-542.
- Swarup K, Benková E, Swarup R, Casimiro I, Péret B, Yang Y, Parry G, Nielsen E, De Smet I, Vanneste S, Levesque MP, Carrier D, James N, Calvo V, Ljung K, Kramer E, Roberts R, Graham N, Marillonnet S, Patel K, Jones JD, Taylor CG, Schachtman DP, May S, Sandberg G, Benfey P, Friml J, Kerr I, Beeckman T, Laplaze L, Bennett MJ** (2008). The auxin influx carrier LAX3 promotes lateral root emergence. *Nat Cell Biol* 10(8):946-54.

- Swarup R, Friml J, Marchant A, Ljung K, Sandberg G, Palme K, Bennett M** (2001). Localization of the auxin permease AUX1 suggests two functionally distinct hormone transport pathways operate in the Arabidopsis root apex. *Genes Dev* 15(20):2648-53.
- Swarup R, Kargul J, Marchant A, Zadik D, Rahman A, Mills R, Yemm A, May S, Williams L, Millner P, Tsurumi S, Moore I, Napier R, Kerr ID, Bennett MJ** (2004). Structure-function analysis of the presumptive Arabidopsis auxin permease AUX1. *Plant Cell* 16(11):3069-83.
- Swarup R, Kramer EM, Perry P, Knox K, Leyser HM, Haseloff J, Beemster GT, Bhalerao R, Bennett MJ** (2005). Root gravitropism requires lateral root cap and epidermal cells for transport and response to a mobile auxin signal. *Nat Cell Biol* 7(11):1057-65.
- Swarup R, Péret B** (2012). AUX/LAX family of auxin influx carriers-an overview. *Front Plant Sci* 3:225.
- Thimann KV, Koepfli JB** (1935). Identity of the Growth-Promoting and Root-Forming Substances of Plants. *Nature* 135(3403):101-102.
- Truernit E, Bauby H, Belcram K, Barthélémy J, Palauqui JC** (2012). OCTOPUS, a polarly localised membrane-associated protein, regulates phloem differentiation entry in Arabidopsis thaliana. *Development* 139(7):1306-15.
- Vanneste S, Friml J** (2009). Auxin: a trigger for change in plant development. *Cell* 136(6):1005-16.
- Wallner ES, López-Salmerón V, Belevich I, Poschet G, Jung I, Grünwald K, Sevilem I, Jokitalo E, Hell R, Helariutta Y, Agustí J, Lebovka I, Greb T** (2017). Strigolactone- and Karrikin-Independent SMXL Proteins Are Central Regulators of Phloem Formation. *Curr Biol* 27(8):1241-1247.
- Wang R, Estelle M** (2014). Diversity and specificity: auxin perception and signaling through the TIR1/AFB pathway. *Curr Opin Plant Biol* 21:51-58.
- Weijers D, Benkova E, Jäger KE, Schlereth A, Hamann T, Kientz M, Wilmoth JC, Reed JW, Jürgens G** (2005). Developmental specificity of auxin response by pairs of ARF and Aux/IAA transcriptional regulators. *EMBO J*. 24(10):1874-85.
- Wildwater M, Campilho A, Perez-Perez JM, Heidstra R, Blilou I, Korthout H, Chatterjee J, Mariconti L, Grissem W, Scheres B** (2005). The RETINOBLASTOMA-RELATED gene regulates stem cell maintenance in Arabidopsis roots. *Cell* 123(7):1337-49.
- Wisniewska J, Xu J, Seifertová D, Brewer PB, Ruzicka K, Blilou I, Rouquié D, Benková E, Scheres B, Friml J** (2006). Polar PIN localization directs auxin flow in plants. *Science* 312(5775):883.
- Zhao Y, Christensen SK, Fankhauser C, Cashman JR, Cohen JD, Weigel D, Chory J** (2001). A role for flavin monooxygenase-like enzymes in auxin biosynthesis. *Science* 291(5502):306-9.

Annex 1: A molecular rheostat adjusts auxin flux to promote root protophloem differentiation (Marhava et al., 2018)

LETTER

<https://doi.org/10.1038/s41586-018-0186-z>

A molecular rheostat adjusts auxin flux to promote root protophloem differentiation

P. Marhava^{1,5}, A. E. L. Bassukas^{2,5}, M. Zourelidou², M. Kolb^{2,3}, B. Moret¹, A. Fastner³, W. X. Schulze⁴, P. Cattaneo¹, U. Z. Hammes^{2,3}, C. Schwechheimer^{2*} & C. S. Hardtke^{1*}

Auxin influences plant development through several distinct concentration-dependent effects¹. In the *Arabidopsis* root tip, polar auxin transport by PIN-FORMED (PIN) proteins creates a local auxin accumulation that is required for the maintenance of the stem-cell niche^{2–4}. Proximally, stem-cell daughter cells divide repeatedly before they eventually differentiate. This developmental gradient is accompanied by a gradual decrease in auxin levels as cells divide, and subsequently by a gradual increase as the cells differentiate^{5,6}. However, the timing of differentiation is not uniform across cell files. For instance, developing protophloem sieve elements (PPSEs) differentiate as neighbouring cells still divide. Here we show that PPSE differentiation involves local steepening of the post-meristematic auxin gradient. BREVIS RADIX (BRX) and PROTEIN KINASE ASSOCIATED WITH BRX (PAX) are interacting plasma-membrane-associated, polarly localized proteins that co-localize with PIN proteins at the rootward end of developing PPSEs. Both *brx* and *pax* mutants display impaired PPSE differentiation. Similar to other AGC-family kinases, PAX activates PIN-mediated auxin efflux, whereas BRX strongly dampens this stimulation. Efficient BRX plasma-membrane localization depends on PAX, but auxin negatively regulates BRX plasma-membrane association and promotes PAX activity. Thus, our data support a model in which BRX and PAX are elements of a molecular rheostat that modulates auxin flux through developing PPSEs, thereby timing PPSE differentiation.

Auxin is a concentration-dependent permissive–restrictive signal in plant cell proliferation and differentiation–elongation that directly impinges on adaptive processes and growth rates^{1,2}. Local auxin accumulations are important cues for organ organization. For example, high auxin concentration specifies the stem-cell niche in the *Arabidopsis* root tip^{2–4}. Proximally, auxin concentration decreases gradually as stem-cell daughters repeatedly divide before they eventually differentiate. Notably, differentiation is accompanied by a renewed rise in auxin levels^{5,6}. The underlying auxin distribution is generated by plasma-membrane-integral PINs, which are auxin efflux carriers with a coordinated asymmetric cellular localization that gives rise to directional polar auxin transport^{2–4}. In root vasculature, PINs generally localize to the rootward end of cells, transporting auxin towards the root tip³. PINs are regulated by auxin, predominantly post-translationally^{7–9}. Moreover, the AGC-family kinases D6 PROTEIN KINASE (D6PK) and PINOID (PID) activate auxin efflux through PIN phosphorylation^{10–12}.

The proximo-distal auxin profile in root meristems intersects with differential auxin activity in the radial dimension. For example, developing PPSEs (Extended Data Fig. 1a, b) display higher auxin accumulation than surrounding cells⁶ (Extended Data Fig. 2a–d) and differentiate, whereas neighbouring cells still remain meristematic^{6,13,14} (Extended Data Fig. 2e). To explore whether PPSE differentiation depends on auxin activity, we manipulated the auxin response by expressing a constitutively active variant of an auxin-response factor, MONOPTEROS (MP^Δ)¹⁵, under the control of PPSE-specific

COTYLEDON VASCULAR PATTERN 2 (CVP2) promoter^{13,16}. *CVP2::MP^Δ* accelerated PPSE differentiation, indicating that auxin responses critically determine the differentiation process (Extended Data Fig. 2f, g).

How differential auxin activity is achieved in PPSEs remained unclear. BRX is plasma-membrane-associated, polarly localized and specifically expressed in developing PPSEs^{13,17}. In *brx* mutants, PPSEs frequently fail to differentiate¹³. These cells lack the characteristic cell-wall changes and appear as gaps in the PPSE differentiation zone^{13,16,18} (Extended Data Fig. 2h). A similar phenotype is observed in *octopus (ops)* mutants^{13,17}, which are affected in a parallel genetic pathway required for PPSE differentiation¹⁹. Whereas OPS localizes to the shootward end of PPSEs, BRX co-localizes with PINs at the rootward end^{2,6,13,18}. Auxin negatively regulates BRX protein abundance and plasma-membrane association, but induces BRX transcription^{18,20}. Thus, BRX is a candidate for mediating auxin effects in PPSE differentiation. In *brx* PPSEs, auxin accumulation as compared to neighbouring cells was markedly lower and more variable than in the wild type (Extended Data Fig. 2i, j). Although *CVP2::MP^Δ* expression in *brx* did not reduce the proportion of PPSE strands with gaps (Extended Data Fig. 2k), it significantly stimulated root growth (Extended Data Fig. 2l) and reduced gap size (Extended Data Fig. 2m). Such partial rescue was not observed with another PPSE-specific promoter that was inactive in gap cells (Extended Data Fig. 2k–n). Moreover, impaired PPSE differentiation was observed after pharmacological inhibition of auxin biosynthesis (Extended Data Fig. 2o, p), and *brx* protophloem defects were aggravated by genetic interference with auxin uptake (Extended Data Fig. 2q). These observations support the hypothesis that finely tuned auxin activity contributes to PPSE differentiation.

BRX protein is expressed only at low levels and in few cells, complicating cell-biological and biochemical investigations of BRX in its native context. However, a recently established trans-differentiation assay for sieve element formation²¹ (Extended Data Fig. 3a, b) enabled us to perform proteomics analyses in a native cell type and identify specific BRX interactors by immunoprecipitation (Extended Data Fig. 3c, d). Among them, we retrieved D6PK and several D6PK-LIKE (D6PKL) kinases as well as PINs, but by far the most abundant was a D6PK/D6PKL-related kinase (AT2G44830)²², which we named PROTEIN KINASE ASSOCIATED WITH BRX (PAX).

To examine a potential role of AGC kinases in PPSE differentiation, we analysed *d6pk/d6pkl* as well as *pax* mutants. *D6PK/D6PKL* genes display substantial genetic redundancy and, consistent with normal PIN phosphorylation in their roots^{10,11,23}, *d6pk0123* quadruple mutants had only a mild, possibly enhanced root-growth phenotype (Extended Data Fig. 4a). By contrast, *pax* loss-of-function mutants displayed reduced primary root growth (Fig. 1a), which was accompanied by PPSE differentiation defects (Fig. 1b–e). No phenotype was observed in a mutant of the closest PAX homologue, the uncharacterized PAX-LIKE (PAXL) kinase (AT5G40030)²², and *paxl* mutation only mildly enhanced the *pax* phenotype (Fig. 1b). A PAX–CITRINE fusion protein expressed

¹Department of Plant Molecular Biology, University of Lausanne, Lausanne, Switzerland. ²Plant Systems Biology, Technical University of Munich, Freising, Germany. ³Department of Cell Biology and Plant Biochemistry, Regensburg University, Regensburg, Germany. ⁴Department of Plant Systems Biology, University of Hohenheim, Stuttgart, Germany. ⁵These authors contributed equally: P. Marhava, A. E. L. Bassukas. *e-mail: claus.schwechheimer@wzw.tum.de; christian.hardtke@unil.ch

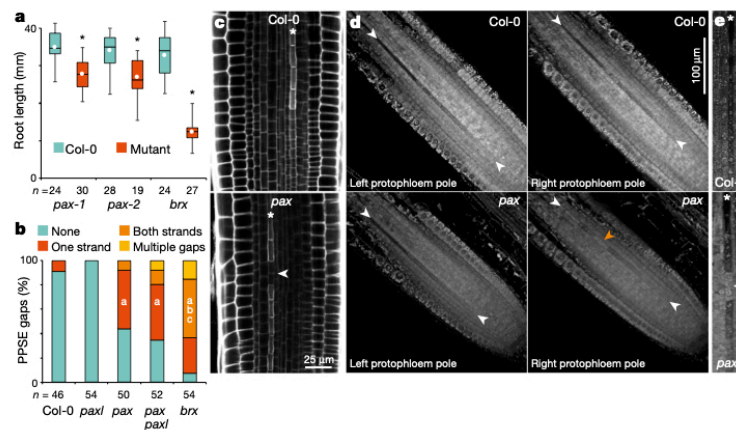


Fig. 1 | Phenotypic characterization of *pax* mutants. **a**, Root length of seven-day-old mutant and wild-type *A. thaliana* L. Heyn reference accession Columbia-0 (Col-0) seedlings. *pax-1* and *pax-2* are two independent PAX loss-of-function alleles. All data that are displayed subsequently were generated using *pax-1*. Box plots throughout show the second and third quartiles, maximum, minimum and mean (white dot). Statistically significant differences are indicated (two-sided Student's *t*-test; * $P < 0.0008$). **b**, Quantification of protophloem strands with gap cells, 6-day-old seedlings. Statistically significant differences are indicated (Fisher's exact test, two-sided, all *P* values < 0.001 ; a, significantly different

to Col-0; b, significantly different to *pax*; c, significantly different to *pax* *pax1*). **c**, Confocal microscopy of propidium iodide (PI)-stained root meristems. Asterisks indicate PPSE strands and the arrowhead indicates a gap cell in the *pax* protophloem. **d**, Confocal microscopy of Col-0 and *pax* root meristems (ClearSee fixation with PI staining), showing both protophloem poles. Note PPSE cell files (white arrowheads) that start with meristematic cells and end with mature empty sieve elements. In one *pax* pole, PPSE differentiation is perturbed (gap cells, orange arrowhead). **e**, Expanded view, highlighting a gap cell in a *pax* PPSE cell file (arrowhead). *n*, number of independent biological replicates.

under its native promoter complemented the PPSE differentiation phenotype of *pax* mutants (Extended Data Fig. 4b) and revealed PAX expression in developing protophloem, as well as weaker expression in the xylem axis (Fig. 2a). PAX displayed rootward cellular polarity (Fig. 2b) and co-localized with BRX (Fig. 2c). Exclusive expression of PAX-CITRINE in developing PPSEs, under the BRX promoter, fully rescued the *pax* protophloem phenotype (Extended Data Fig. 4c, d). As previously observed in *brx*, the *pax* PPSE differentiation defects were accompanied by impaired phloem sap delivery into the meristem¹⁶ (Extended Data Fig. 4e). In summary, *pax* mutants represent a (hypomorphic) phenocopy of *brx* mutants.

The *brx* phenotype was not enhanced in *brx pax* double mutants (Extended Data Fig. 4f), suggesting that *brx* is genetically epistatic to *pax*. In turn, the *pax* phenotype was not significantly enhanced by *d6pk/d6pk1* mutations (Extended Data Fig. 4g). However, similar to D6PK or PID, PAX (and PAXL) activated auxin efflux when co-expressed with PINs in *Xenopus laevis* oocytes¹² (Fig. 2d, Extended Data Fig. 4h). However, PAX was the weakest activator in this assay. Moreover, similar to D6PKL proteins, ADP-ribosylation factor-guanine-exchange factor (ARF-GEF) inhibition by brefeldin A (BFA) triggered rapid dissociation of PAX from the plasma membrane (Fig. 3a, Extended Data Fig. 4i). BRX is also BFA-sensitive¹⁸, yet in direct comparison, BFA-induced BRX plasma-membrane dissociation was slower than for PAX (Fig. 3a, Extended Data Fig. 4j, k). Consistently, BFA treatment also triggered PPSE differentiation defects in a dosage-dependent manner (Extended Data Fig. 4l, m). Moreover, BRX abundance, but not PIN abundance, was severely reduced in *pax* PPSEs (Fig. 3b–g). By contrast, PAX abundance or localization did not substantially depend on BRX (Extended Data Fig. 4n). In protoplasts, BRX localized evenly at the plasma membrane, whereas PAX accumulated in large patches²⁴ (Extended Data Fig. 4o). Their co-expression recruited BRX into PAX patches. However, a cytoplasmic PAX variant²⁴ did not disrupt the even plasma-membrane distribution of BRX. These results suggest that PAX is required for efficient BRX plasma-membrane recruitment.

Auxin activity is systemically reduced throughout *brx* root meristems¹⁶. We thus sought to monitor PIN activity in *brx* or *pax*. We focused our analysis on the dominant PIN in developing PPSEs, PIN1 (Extended

Data Fig. 5a). Corroborating the PIN1-green fluorescent protein (GFP) results, PIN1 abundance and localization in both the protophloem and the meristem were not affected in *pax* or *brx* mutants (Extended

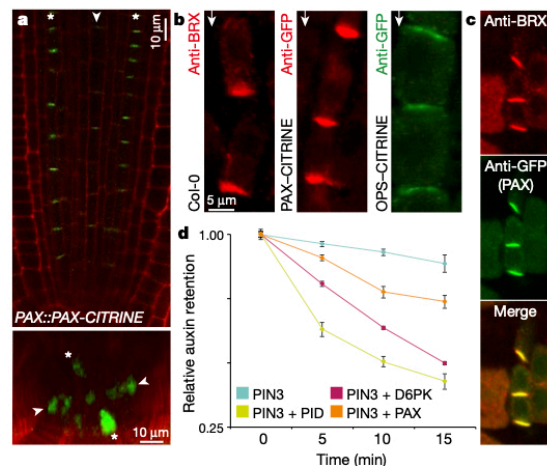


Fig. 2 | Expression analysis of PAX protein. **a**, Top, Confocal microscopy of the PAX-CITRINE fusion protein (green fluorescence) expressed under its native promoter in the meristem (longitudinal plane). Bottom, optical cross section. Asterisks indicate PPSE cell files and arrowheads indicate the xylem axis. **b**, Detection of endogenous BRX (red) using anti-BRX antibody staining, or PAX-CITRINE (red) or OPS-CITRINE (green) using anti-GFP antibody staining, in protophloem of fixed meristems (squashed after fixation). Arrows point rootward. **c**, Simultaneous detection of PAX-CITRINE (green) and BRX (red) by immunostaining, demonstrating co-localization. **d**, Auxin transport assays, average retention of radio-labelled auxin in *X. laevis* oocytes expressing the indicated heterologous plant proteins ($n = 10$ per time point; error bars, s.e.m.).

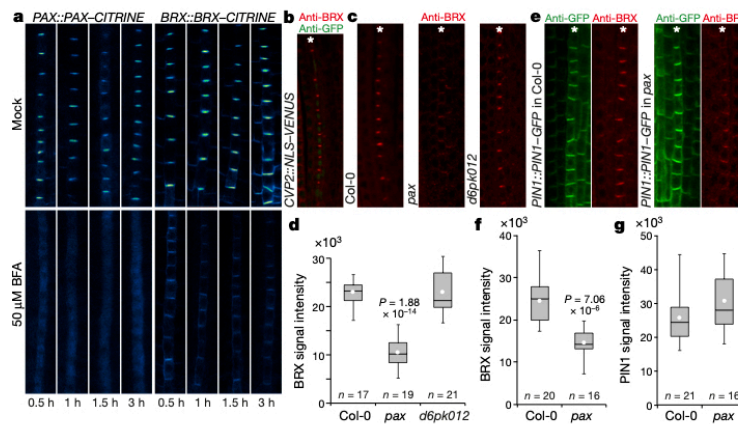


Fig. 3 | PAX-dependence of efficient BRX plasma-membrane association. **a**, Plasma-membrane dissociation of PAX–CITRINE and BRX–CITRINE in response to BFA treatment. **b**, Simultaneous detection of nuclear NLS–VENUS protein (green) expressed under the control of PPSE-specific *CVP2* promoter and BRX (red) by antibody staining. Asterisks in all microscopy images indicate the PPSE cell file. **c**, Detection of BRX (red) by antibody staining. **d**, BRX signal intensity quantification (anti-BRX antibody detection) in PPSEs (mean from approximately ten

cells per root, arbitrary units). **e**, Simultaneous immunolocalization of PIN1–GFP (anti-GFP, green) expressed under its native promoter and BRX (anti-BRX, red) by antibody staining in Col-0 and *pax*. **f**, **g**, BRX signal intensity quantification (**f**, anti-BRX antibody detection) and PIN1–GFP signal intensity (**g**, anti-GFP antibody detection) in PPSEs (means from approximately ten cells per root, arbitrary units). **d–g**, Statistically significant differences from Col-0 are indicated, two-sided Student's *t*-test.

Data Fig. 5b). To survey PIN1 activity, we performed immunostaining with antibodies against PIN1 phosphosites that are critical for PIN1 activation^{11,12}. Phosphoserine S231 (J231) signal was significantly reduced in *pax* PPSEs, whereas phosphoserine S271 (J271) was not affected (Extended Data Fig. 5c–e). By contrast, both phosphoserines were barely detectable in *brx* meristems (Extended Data Fig. 5c, f). Reduced PIN1 phosphorylation was also observed in *ops* (Extended Data Fig. 5f), suggesting that meristem-wide reduced PIN1 activity is a secondary systemic consequence of severely disturbed PPSE differentiation, similar to other traits¹⁶. Yet, *brx* or *pax* protophloem defects

were aggravated in the presence of a *pin1* mutation (Extended Data Fig. 5g–i). In *brx pin1* double mutants, protophloem was frequently barely distinguishable, or even absent (approximately 20% of seedlings) (Extended Data Fig. 5i), underlining the importance of properly regulated auxin transport for PPSE differentiation.

The systemic ramifications of discontinuous protophloem on meristem development can be considered to be a post-catastrophic scenario that is triggered and enhanced by repeated PPSE differentiation failure, and is difficult to recover from once phloem sap (and thus auxin) delivery is impaired¹⁶. This complicates efforts to untangle cause and

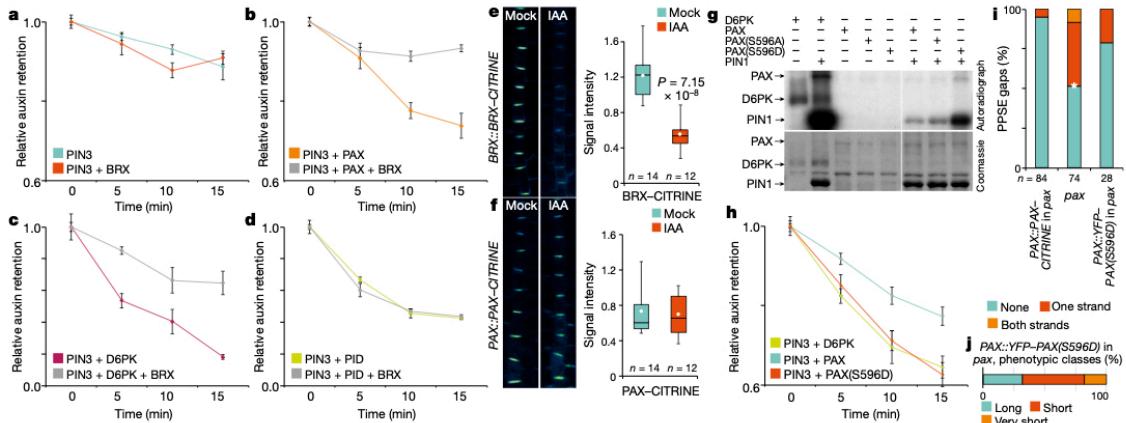


Fig. 4 | Regulatory input of auxin on PAX and BRX activity. **a–d**, Auxin transport assays in *X. laevis* oocytes expressing the indicated heterologous plant proteins ($n = 10$ per time point; error bars, s.e.m.). **e–f**, Response of BRX (**e**) or PAX (**f**) fusion protein to 5 μ M auxin (IAA) treatment (3 h), with quantification (arbitrary units; means from approximately ten cells per root). The statistically significant difference is indicated, two-sided Student's *t*-test. **g**, Radioactive in vitro kinase assays with GST fusion proteins of D6PK, PAX or the PAX(S596A) and PAX(S596D) point mutants, with the PIN1 cytosolic loop as substrate (top), and

corresponding loading controls (bottom). **h**, Auxin transport assays in *X. laevis* oocytes expressing the indicated heterologous plant proteins ($n = 10$ per time point; error bars: s.e.m.). **i**, Quantification of gap-cell frequency in PPSE strands. For PAX::YFP–PAX(S596D), only long root seedlings (see **j**) were scored. *pax* alone was significantly different from PAX::PAX–CITRINE in *pax* (two-sided Fisher's exact test, $*P < 0.0001$). PAX::YFP–PAX(S596D) was not significantly different from PAX::PAX–CITRINE in *pax* or from *pax* alone. **j**, Quantification of root phenotype classes in a PAX::YFP–PAX(S596D) line ($n = 50$).

effect in the cellular action of regulators from the multicellular context. For example, it remained unclear whether *pax* mutants display PPSE differentiation defects because of inefficient BRX plasma membrane recruitment, or whether *brx* mutants display PPSE differentiation defects because of a failure to control PAX activity. To investigate whether BRX interaction with AGC kinases affects auxin transport, we tested the effect of BRX co-expression on kinase-mediated PIN activation in oocytes. In these experiments, BRX substantially inhibited stimulation of auxin efflux by PAX or D6PK (Fig. 4a–c, Extended Data Fig. 5j, k). Because this inhibition was not observed in assays with the more distantly related PID (Fig. 4d), our findings suggest that BRX action affects a subset of related AGC kinases, and that its inhibitory effect is determined by kinase identity.

The observation that BRX inhibits auxin efflux appeared particularly interesting in light of its known auxin-induced plasma-membrane dissociation¹⁸ (Fig. 4e, Extended Data Fig. 6a, b). By contrast, neither PAX abundance nor localization were affected by auxin (Fig. 4f). However, phosphoproteomics indicated auxin-induced phosphorylation of phosphoserine S596 in the PAX activation loop (Extended Data Fig. 6c), which correlated with simultaneously increased PIN1 phosphorylation (Extended Data Fig. 6d). In vitro, recombinant PAX phosphorylated PIN1 with comparably low efficiency, and S596 was dispensable for kinase activation (Fig. 4g, Extended Data Fig. 6e). A PAX(S596D) phosphomimic variant, however, was considerably more active than wild-type PAX and displayed increased phosphorylation activity towards PIN1 (Fig. 4g, Extended Data Fig. 6e). Matching this biochemical observation, PAX(S596D) also stimulated auxin efflux considerably more in oocytes, to a level approximately equal to D6PK (Fig. 4h, Extended Data Fig. 6f). However, unlike wild-type PAX, the PAX(S596D) variant at best partially rescued the *pax* mutant (Fig. 4i, Extended Data Fig. 6g). Moreover, PAX(S596D) frequently triggered a gain-of-function phenotype of even shorter, often barely triggered roots (Fig. 4j). Consistent with the D6PK-like activity of PAX(S596D), D6PK expressed from the PAX promoter could not rescue the *pax* phenotype (Extended Data Fig. 6h, i). These findings suggest that fine-tuning of PAX activity is a feature of properly integrated PPSE development.

In a parsimonious interpretation of our results, PAX and BRX act together as a molecular rheostat to modulate auxin efflux dynamically (Extended Data Fig. 7). In this scenario, PAX recruits BRX to the plasma membrane, which inhibits PIN-mediated auxin efflux at lower auxin levels. Because of this inhibition, cellular auxin increases until BRX eventually becomes displaced from the plasma membrane. Concomitantly, PAX is activated and stimulates auxin efflux. Reinforced through auxin-induced BRX transcription^{6,18} (Extended Data Fig. 6j, k), this interplay could reach a dynamic steady-state equilibrium, which would impair higher local auxin activity in the multicellular context to properly time PPSE differentiation.

Online content

Any Methods, including any statements of data availability and Nature Research reporting summaries, along with any additional references and Source Data files, are available in the online version of the paper at <https://doi.org/10.1038/s41586-018-0186-z>.

Received: 14 September 2017; Accepted: 24 April 2018;
Published online 6 June 2018.

- Benjamins, R. & Scheres, B. Auxin: the looping star in plant development. *Annu. Rev. Plant Biol.* **59**, 443–465 (2008).
- Bilou, I. et al. The PIN auxin efflux facilitator network controls growth and patterning in *Arabidopsis* roots. *Nature* **433**, 39–44 (2005).
- Grieneisen, V. A., Xu, J., Marée, A. F., Hogeweg, P. & Scheres, B. Auxin transport is sufficient to generate a maximum and gradient guiding root growth. *Nature* **449**, 1008–1013 (2007).
- Sabatini, S. et al. An auxin-dependent distal organizer of pattern and polarity in the *Arabidopsis* root. *Cell* **99**, 463–472 (1999).

- Brunoud, G. et al. A novel sensor to map auxin response and distribution at high spatio-temporal resolution. *Nature* **482**, 103–106 (2012).
- Santuari, L. et al. Positional information by differential endocytosis splits auxin response to drive *Arabidopsis* root meristem growth. *Curr. Biol.* **21**, 1918–1923 (2011).
- Sauer, M. et al. Canalization of auxin flow by Aux/IAA-ARF-dependent feedback regulation of PIN polarity. *Genes Dev.* **20**, 2902–2911 (2006).
- Geldner, N., Friml, J., Stierhof, Y. D., Jürgens, G. & Palme, K. Auxin transport inhibitors block PIN1 cycling and vesicle trafficking. *Nature* **413**, 425–428 (2001).
- Paciorek, T. et al. Auxin inhibits endocytosis and promotes its own efflux from cells. *Nature* **435**, 1251–1256 (2005).
- Barbosa, I. C., Zourelidou, M., Willige, B. C., Weller, B. & Schwechheimer, C. D6 PROTEIN KINASE activates auxin transport-dependent growth and PIN-FORMED phosphorylation at the plasma membrane. *Dev. Cell* **29**, 674–685 (2014).
- Weller, B. et al. Dynamic PIN-FORMED auxin efflux carrier phosphorylation at the plasma membrane controls auxin efflux-dependent growth. *Proc. Natl Acad. Sci. USA* **114**, E887–E896 (2017).
- Zourelidou, M. et al. Auxin efflux by PIN-FORMED proteins is activated by two different protein kinases, D6 PROTEIN KINASE and PINOID. *eLife* **3**, e02860 (2014).
- Rodríguez-Villalón, A. et al. Molecular genetic framework for protophloem formation. *Proc. Natl Acad. Sci. USA* **111**, 11551–11556 (2014).
- Furuta, K. M. et al. *Arabidopsis* NAC45/86 direct sieve element morphogenesis culminating in enucleation. *Science* **345**, 933–937 (2014).
- Ckurshumova, W., Smirnova, T., Marcos, D., Zayed, Y. & Berleth, T. Irrepressible *MONOPTEROS/ARF5* promotes *de novo* shoot formation. *New Phytol.* **204**, 556–566 (2014).
- Rodríguez-Villalón, A., Gujas, B., van Wijk, R., Munnik, T. & Hardtke, C. S. Primary root protophloem differentiation requires balanced phosphatidylinositol-4,5-bisphosphate levels and systemically affects root branching. *Development* **142**, 1437–1446 (2015).
- Truernit, E., Bauby, H., Belcram, K., Barthélémy, J. & Palauqui, J. C. OCTOPUS, a polarly localised membrane-associated protein, regulates phloem differentiation entry in *Arabidopsis thaliana*. *Development* **139**, 1306–1315 (2012).
- Scacchi, E. et al. Dynamic, auxin-responsive plasma membrane-to-nucleus movement of *Arabidopsis* BRX. *Development* **136**, 2059–2067 (2009).
- Breda, A. S., Hazak, O. & Hardtke, C. S. Phosphosite charge rather than shootward localization determines OCTOPUS activity in root protophloem. *Proc. Natl Acad. Sci. USA* **114**, E5721–E5730 (2017).
- Mouchel, C. F., Osmont, K. S. & Hardtke, C. S. BRX mediates feedback between brassinosteroid levels and auxin signalling in root growth. *Nature* **443**, 458–461 (2006).
- Kondo, Y. et al. Vascular cell induction culture system using *Arabidopsis* leaves (VISUAL) reveals the sequential differentiation of sieve element-like cells. *Plant Cell* **28**, 1250–1262 (2016).
- Galván-Ampudia, C. S. & Offringa, R. Plant evolution: AGC kinases tell the auxin tale. *Trends Plant Sci.* **12**, 541–547 (2007).
- Willige, B. C. et al. D6PK AGCVIII kinases are required for auxin transport and phototropic hypocotyl bending in *Arabidopsis*. *Plant Cell* **25**, 1674–1688 (2013).
- Barbosa, I. C. et al. Phospholipid composition and a polybasic motif determine D6 PROTEIN KINASE polar association with the plasma membrane and tropic responses. *Development* **143**, 4687–4700 (2016).

Acknowledgements We thank the University of Lausanne Protein Analysis Facility for mass spectrometry services, the Swiss National Science Foundation for Grant 31003A_166394 (C.S.H.), the German-Israeli Foundation for I-236-203.17-2014 (C.S.) and the Deutsche Forschungsgemeinschaft for SCHW751/12-2 (C.S.), HA 3468/6-1 and SFB924 (U.Z.H.).

Reviewer information Nature thanks A. P. Mahonen, D. Weijers and the other anonymous reviewer(s) for their contribution to the peer review of this work.

Author contributions P.M., A.E.L.B., M.Z., M.K., B.M., A.F., W.X.S. and P.C. performed experiments and analysed data. P.M., A.E.L.B., M.Z., W.X.S., U.Z.H., C.S. and C.S.H. designed experiments. P.M., A.E.L.B., U.Z.H., C.S. and C.S.H. wrote the manuscript.

Competing interests The authors declare no competing interests.

Additional information Extended data is available for this paper at <https://doi.org/10.1038/s41586-018-0186-z>.

Supplementary information is available for this paper at <https://doi.org/10.1038/s41586-018-0186-z>.

Reprints and permissions information is available at <http://www.nature.com/reprints>.

Correspondence and requests for materials should be addressed to C.S. and C.S.H.

Publisher's note: Springer Nature remains neutral with regard to jurisdictional claims in published maps and institutional affiliations.

METHODS

No statistical methods were used to predetermine sample size. The experiments were not randomized and investigators were not blinded to allocation during experiments and outcome assessment. Experiments were repeated two to four times. All attempts at replication were successful.

Plant materials and growth conditions. The wild-type *Arabidopsis* line used in this study was the *A. thaliana* L. Heynh reference accession Columbia-0 (Col-0), which was also the genetic background for the mutants and transgenic lines. For plant tissue culture, seeds were surface-sterilized, stratified for 2 days in the dark at 4 °C, and germinated in vertically placed Petri dishes on 0.9% agar and 0.5 × Murashige and Skoog (1/2 MS) medium (Duchefa) with 0.3% sucrose at 22 °C under continuous light. The mutant *pax-1* and *pax-2* alleles (T-DNA insertion lines SAIL_688_B04 and GABI_274F04, respectively) were identified from available collections and obtained from the Nottingham *Arabidopsis* Stock Centre. The following transgenic and mutant lines have been described elsewhere: *BRX::BRX-CITRINE*¹³, *PIN1::PIN1-GFP*²⁵, *PIN3::PIN3-GFP*²⁶, *PIN7::PIN7-GFP*²⁷, *CVP2::NLS-VENUS*¹⁶, *35S::DII-NLS-VENUS* and *35S::mDII-NLS-VENUS*⁵, *brx-2*¹³, *ops-2*¹⁷, *pin1-613*²⁸, *aux1-729*, *d6pk*, *d6pk11*, *d6pk12*, *d6pk13*, as well as their *d6pk12* triple and *d6pk123* quadruple mutants¹². Primers used for genotyping are summarized in Extended Data Table 1.

Constructs and generation of transgenic lines. Transgenes for plant transformation were created in suitable binary vectors and produced using standard molecular biology procedures and/or the NEBuilder HiFi DNA Assembly Reaction Protocol. The *35S::mDII-VENUS* and *35S::DII-VENUS* lines in Col-0 and *brx-2* backgrounds have previously been described⁶. For the *CVP2::MP^A* or *CLE45::MP^A* constructs, a 2.6-kb genomic promoter fragment upstream of the initiation codon of the *CVP2* gene¹⁶ or a 2.0-kb genomic promoter fragment upstream of the initiation codon of the *CLAVATA3/EMBRYO SURROUNDING REGION 45 (CLE45)* gene¹⁶ was amplified, combined with amino acids 1–794 of the *MP* open reading frame¹⁵ and introduced into the pCAMBIA1305.1 binary vector. To generate the translational *PAX::PAX-CITRINE* fusion, the *PAX* promoter region (4.5-kb upstream of the ATG start codon) was amplified and cloned into pDONR P4P1R as well as a genomic fragment of the *PAX* transcript region without a STOP codon into pDONR 221. The entry clones together with *CITRINE* in pDONR P2RP3 were cloned into the destination vector pH7m34GW by the multisite Gateway recombination system. To create *UBQ10::PAX-CITRINE*, the entry clones containing the *UBQ10* promoter in pDONR P4P1R, the *PAX* coding sequence without a STOP codon in pDONR 221, and the *CITRINE* coding sequence in pDONR P2RP3 were combined into binary vector pH7m34GW. The binary constructs were introduced into *Agrobacterium tumefaciens* strain GV3101^{MP90} and transformed into the pertinent *Arabidopsis* genotypes using the floral dip method. For recombinant expression of the glutathione-S-transferase N-terminally tagged fusion proteins *GST-PAX*, *GST-PAX(S596D)* and *GST-PAX(S596A)*, a Gateway-compatible attB-flanked PCR product of *PAX* coding sequence was amplified from cDNA and cloned into the Gateway-compatible donor vector pDONR 201 (Invitrogen). The mutagenesis leading to *PAX(S596D)* phosphomimetic or *PAX(S596A)* phospho-mutant variants in the activation loop of the *PAX* coding sequence was achieved using site-directed mutation PCR on a pDONR 201 entry clone carrying the *PAX* coding sequence insert. The resulting pDONR 201 entry clones served as substrate to recombine the *PAX* coding sequences into the pDEST15 (Life Technologies) destination vector that was ultimately used for recombinant protein expression. The expression vectors pDEST15 containing *GST-D6PK* and *GST-PIN1* cytosolic loop have previously been described¹². Primers used for cloning are summarized in Extended Data Table 1.

Microscopy. To visualize reporter genes and staining signals, fluorescence for *CITRINE* (excitation 514 nm, emission 529 nm), *VENUS* (excitation 515 nm, emission 528 nm), propidium iodide (PI) (excitation 536 nm, emission 617 nm), Alexa Fluor 488 (excitation 498 nm, emission 520 nm) and Alexa Fluor 546 (excitation 556 nm, emission 573 nm) were detected in seedlings examined under Zeiss LSM 700 or 710 inverted confocal scanning microscopes. Pictures were taken with 20× or 40× water/oil immersion objectives. PI staining of seven-day-old seedlings was used for quantification of protophloem cell size. For presentation, composite images had to be assembled in various instances. Sequential scanning was used for co-localization studies to avoid any interference between fluorescence channels. For image analyses, ImageJ (NIH; <https://rsb.info.nih.gov/ij/>), Zeiss Zen (black edition) and Imaris software were used. If necessary, images were processed using the 'sharpen' tool for clearer visualization of cellular organization. For signal quantifications, all samples were analysed in the same area of the root meristem, and the average signal intensity per transgenic line was calculated as the mean of means. Statistical significance was evaluated with Student's *t* test.

Pharmacological and hormonal treatments. For treatments, 5–7-day-old seedlings were either grown on, or transferred either onto solid or into liquid 1/2 MS

medium with or without the chemicals and incubated for the indicated time. Drugs and hormones used were as follows: BFA (dissolved in DMSO), IAA (dissolved in DMSO), L-kynurenine (dissolved in DMSO), PI (1 mg ml⁻¹ in water, diluted 1:25).

VISUAL assay and proteomics. The VISUAL protocol²¹ was performed as previously described¹⁹ with subsequent BRX-CITRINE or YFP pull down. In brief, cotyledons of six-day-old transgenic *Arabidopsis* seedlings were cultured for 3 days in induction medium and subsequently ground in extraction buffer. Supernatants (4 mg of total protein extract in two technical replicates) were incubated with anti-GFP beads (GFP-Trap_MA, Chromotek). Beads were magnetically separated and protein was eluted in 2× SDS sample buffer, loaded on an SDS-PAGE gel for electrophoresis, and subsequently analysed by liquid chromatography with tandem mass spectrometry.

Protein immunolocalization. Whole mount immunolocalization on five-day-old seedlings was performed as described previously⁷. The primary antibody dilutions were: 1:600 for anti-GFP mouse (Roche), 1:500 for anti-BRX rabbit (this study), 1:100 for anti-PIN1 S1-P rabbit¹¹, 1:300 for anti-PIN1 S4-P rabbit¹¹ and 1:100 for anti-PIN1 goat (Santa Cruz Biotechnology). The secondary antibody dilutions were: 1:600 for Alexa Fluor 488 anti-mouse (Molecular Probes) and 1:600 for Alexa Fluor 546 anti-rabbit (Molecular Probes). The anti-BRX antibody was obtained by custom antibody production directed against the keyhole-limpet hemocyanin (KLH)-conjugated BRX peptide GGSSNYGPGSYHGGC with affinity purification (Agrisera).

Oocyte experiments. Auxin transport assays in *X. laevis* oocytes were carried out as described^{12,30}. The oocytes were obtained from the animal facility of the Technical University of Munich, Department of Nutritional Physiology. The animals were kept in accordance with local guidelines and regulations. To monitor expression levels, post-assay immunoblots were performed with anti-PIN1 sheep and anti-PIN3 sheep primary antibodies (Nottingham *Arabidopsis* Stock Centre, used at 1:5,000 dilution), and anti-GFP rabbit (custom antibody³¹, 1:2,000 dilution). The secondary antibodies were anti-sheep from donkey (1:5,000, Santa Cruz Biotechnology) and anti-rabbit from goat (1:10,000, Santa Cruz Biotechnology).

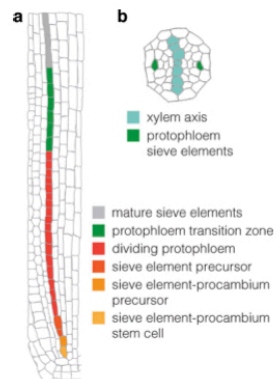
Protoplast transformation. Protoplasts were isolated from *Arabidopsis* suspension-cultured cells (Col-0) five to seven days after subculturing by incubation of 2 g of cell culture with 1% Cellulase R-10 (SERVA) and 0.25% Macerzyme R-10 (SERVA). Typically, protoplasts were transformed with 20 μg of plasmid DNA using polyethylene glycol-mediated transformation and analysed after 16 to 20 h of incubation as described²⁴.

In vitro kinase assay. The in vitro kinase assay was performed using recombinant glutathione-S-transferase N-terminally tagged fusion proteins *GST-PIN1*¹² CL (cytosolic loop), *GST-D6PK*¹², *GST-BRX*¹⁸, *GST-PAX*, *GST-PAX(S596D)* and *GST-PAX(S596A)*, expressed in the *Escherichia coli* strain BL21(DE3) and purified using Glutathione Sepharose 4B (GE Healthcare). The kinase reactions were performed by incubating the purified GST-fusion proteins for 60 min at 28 °C in the kinase reaction buffer (25 mM Tris HCl pH 7.5, 5 mM MgCl₂, 0.2 mM EDTA, 1× cComplete protease inhibitor cocktail (Roche)), supplemented with 10 μCi [^γ-³²P] ATP (370 Mbq, specific activity 185 Tbq, Hartmann Analytics). The reactions were stopped by boiling the protein samples mixed with 5× concentrated Laemmli buffer for 10 min. Subsequently, the protein mixtures were separated by SDS-PAGE. After samples had been run, the SDS-PAGE gel was vacuum-dried and used for autoradiography. The same gel was later rehydrated and stained with Commae Brilliant Blue to serve as a loading control.

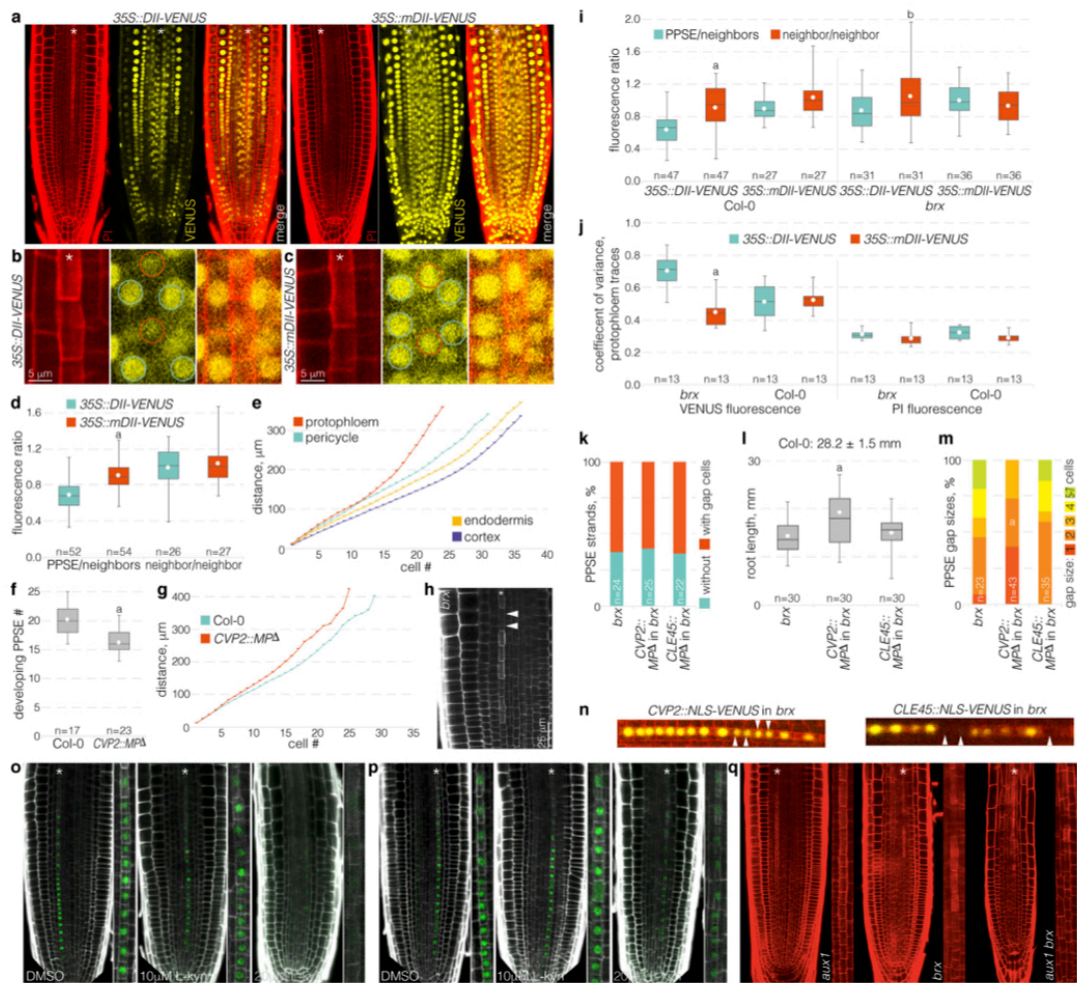
Reporting summary. Further information on experimental design is available in the Nature Research Reporting Summary linked to this paper.

Data availability. The datasets displayed in the current study are available from the corresponding authors upon reasonable request. For gel source images, see Supplementary Fig. 1.

- Benková, E. et al. Local, efflux-dependent auxin gradients as a common module for plant organ formation. *Cell* **115**, 591–602 (2003).
- Zádníková, P. et al. Role of PIN-mediated auxin efflux in apical hook development of *Arabidopsis thaliana*. *Development* **137**, 607–617 (2010).
- Friml, J. et al. Efflux-dependent auxin gradients establish the apical-basal axis of *Arabidopsis*. *Nature* **426**, 147–153 (2003).
- Bennett, T. et al. The *Arabidopsis* MAX pathway controls shoot branching by regulating auxin transport. *Curr. Biol.* **16**, 553–563 (2006).
- Marchant, A. et al. AUX1 promotes lateral root formation by facilitating indole-3-acetic acid distribution between sink and source tissues in the *Arabidopsis* seedling. *Plant Cell* **14**, 589–597 (2002).
- Fastner, A., Absmanner, B. & Hammes, U. Z. Use of *Xenopus laevis* oocytes to study auxin transport. *Methods Mol. Biol.* **1497**, 259–270 (2017).
- Absmanner, B., Stadler, R. & Hammes, U. Z. Phloem development in nematode-induced feeding sites: the implications of auxin and cytokinin. *Front. Plant Sci.* **4**, 241 (2013).



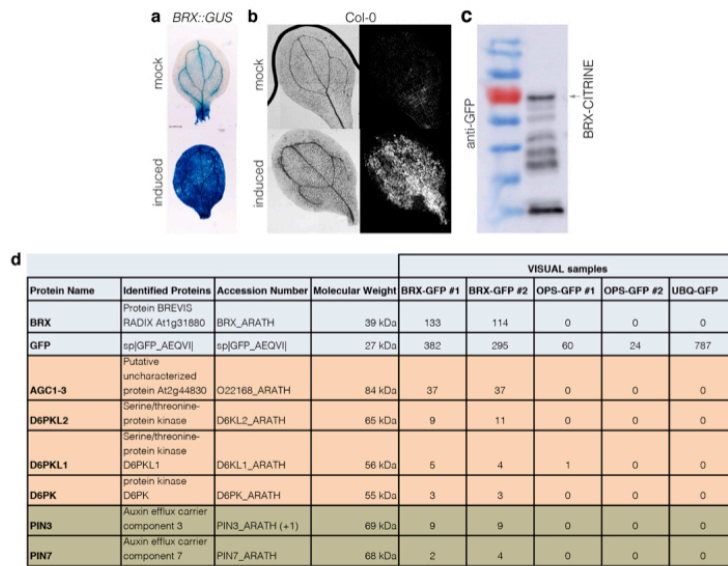
Extended Data Fig. 1 | Overview of protophloem development. **a**, Illustration of protophloem development from the stem cell to the mature sieve element in the *Arabidopsis* root meristem. **b**, Illustration of a cross section through the stele of an *Arabidopsis* root meristem, highlighting the arrangement of the two sieve element strands and the xylem axis.



Extended Data Fig. 2 | See next page for caption.

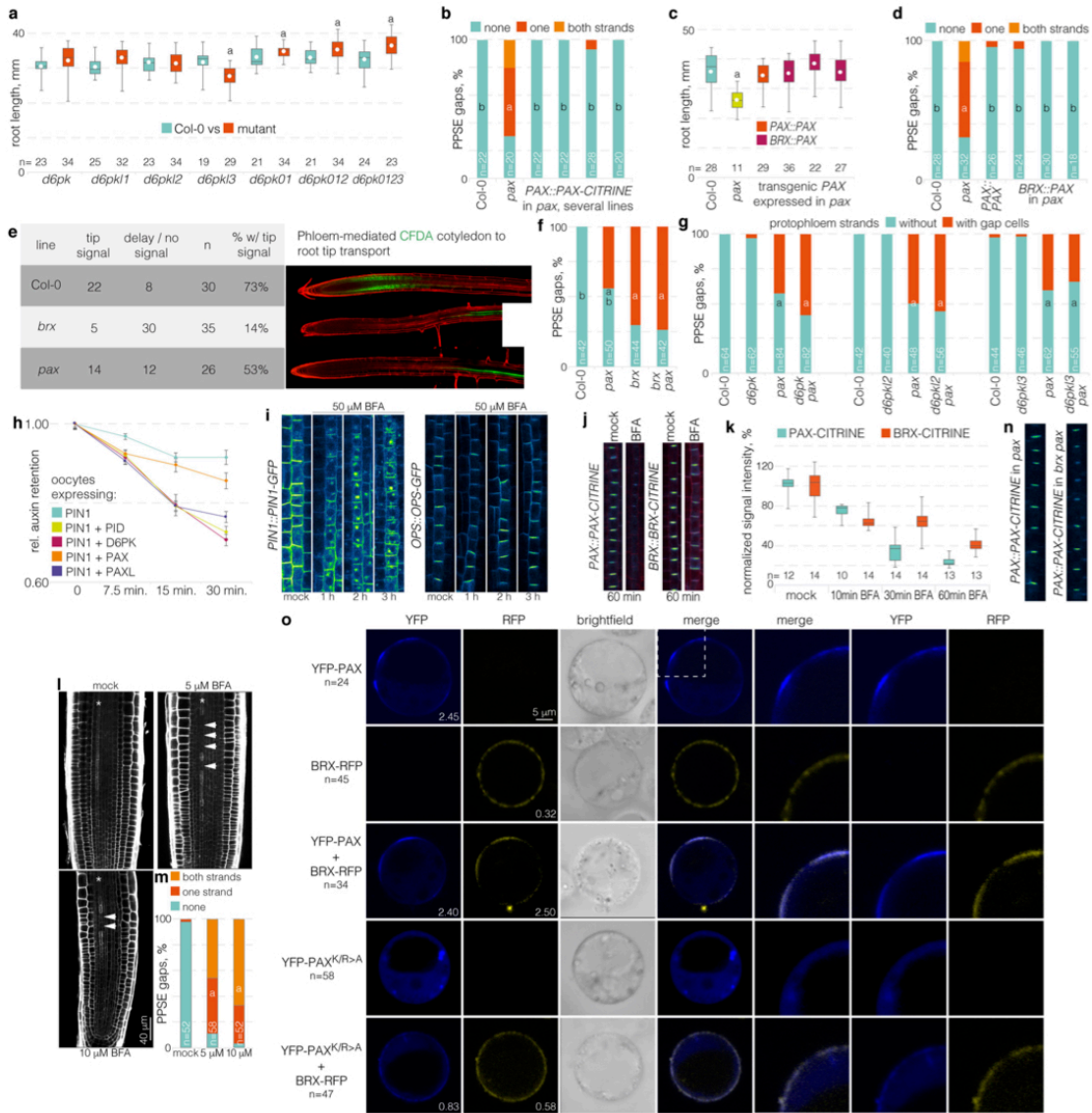
Extended Data Fig. 2 | Auxin activity in developing PPSEs. **a**, Confocal microscopy of the inverse auxin activity reporter DII-VENUS and its negative control mDII-VENUS (yellow fluorescence) in the root meristem (PI staining, red) of wild-type Col-0 plants. Asterisks indicate sieve element cell files. **b**, Confocal microscopy of constitutively expressed DII-VENUS in developing PPSEs and neighbouring cell files. Left, PI cell-wall staining (red); middle, DII-VENUS fluorescence (yellow; PPSE nuclei marked with red circles, nuclei in neighbouring cell files with blue circles); right, overlay. **c**, As in **b**, for mDII-VENUS. **d**, Relative intensity of the DII-VENUS reporter and its mDII-VENUS control in the nuclei of Col-0 PPSEs as compared to the nuclei of directly neighbouring cells. The statistically significant difference between DII-VENUS and mDII-VENUS in the PPSE/neighbours group is indicated (two-sided Student's *t*-test; a , $P = 5.86 \times 10^{-11}$). **e**, Cumulative average cell length in different root cell files, starting from the respective first stem-cell daughters (cell #1) ($n = 11$ wild-type Col-0 roots). **f**, Number of developing PPSEs from the first stem-cell daughter up to the first transition zone PPSE (protophloem length) in seven-day-old Col-0 seedlings, and transgenic seedlings expressing a constitutively active derivative of the auxin response factor MONOPTEROS (MP^{Δ}) under control of the PPSE-specific *CVP2* promoter. a , $P = 3.16 \times 10^{-6}$; two-sided Student's *t*-test. **g**, Cumulative average cell length in the developing protophloem, starting from the first stem-cell daughter (cell #1) ($n = 23$ each). Elongation occurs prematurely in *CVP2::MP^{\Delta}* plants. **h**, Confocal microscopy of a *brx* root meristem, focused on one of the sieve element strands (asterisk). Arrowheads point out gap cells, which fail to build up the characteristic PPSE cell wall owing to a failure to differentiate. **i**, Relative intensity of the DII-VENUS reporter and its mDII-VENUS control in the nuclei of Col-0 and *brx* PPSEs as

compared to nuclei of cells in directly neighbouring files. Statistically significant differences between PPSE/neighbours and neighbour/neighbour in the Col-0 and *brx* DII-VENUS groups are indicated (two-sided Student's *t*-test; a , $P = 2.49 \times 10^{-7}$; b , $P = 0.026$). **j**, Coefficient of variance for fluorescence traces of the DII-VENUS reporter and its mDII-VENUS control (left) and PI staining (right) along protophloem cell files. The statistically significant difference in VENUS fluorescence in the *brx* group is indicated (two-sided Student's *t*-test; a , $P = 2.30 \times 10^{-7}$). **k**, Quantification of PPSE strands with gaps in roots of indicated genotypes. **l**, Root length in seven-day-old seedlings for indicated genotypes. The statistically significant differences between *CVP2::MP^{\Delta}* in *brx* and *brx* alone ($P = 0.0017$) and between *CVP2::MP^{\Delta}* in *brx* and *CLE45::MP^{\Delta}* in *brx* ($P = 0.0052$) are indicated by the character α . **m**, Distribution of gap size in protophloem strands of seven-day-old seedlings with gaps of indicated genotypes. The statistically significant differences between *CVP2::MP^{\Delta}* in *brx* and *brx* alone ($P = 0.0008$) and between *CVP2::MP^{\Delta}* in *brx* and *CLE45::MP^{\Delta}* in *brx* ($P = 0.0051$) are indicated by the character α (two-sided χ^2 test). **n**, Expression of fluorescent NLS-VENUS reporter in PPSEs of *brx* mutants, driven by either *CVP2* or *CLE45* promoter. Arrowheads indicate gap cells. **o**, **p**, Expression of *CVP2::NLS-VENUS* reporter (green fluorescence) in PPSE cell files (asterisks) of six-day-old Col-0 root meristems (PI staining, white) grown in the presence of (**o**), or transferred for 48 h onto (**p**), increasing amounts of the auxin biosynthesis inhibitor L-kynurenine (L-kyn). On the higher concentration, PPSE cell files (magnified) were barely distinguishable. **q**, Confocal microscopy of seven-day-old root meristems (PI staining, red). Asterisks indicate sieve element cell files (magnified, barely distinguishable in *aux1 brx*).



Extended Data Fig. 3 | Identification of BRX interactors. **a**, Induction of *BRX* expression in cotyledons in the VISUAL transdifferentiation assay, as indicated by a *BRX::GUS* reporter gene. **b**, Visualization of successful tracheary element differentiation using polarized light

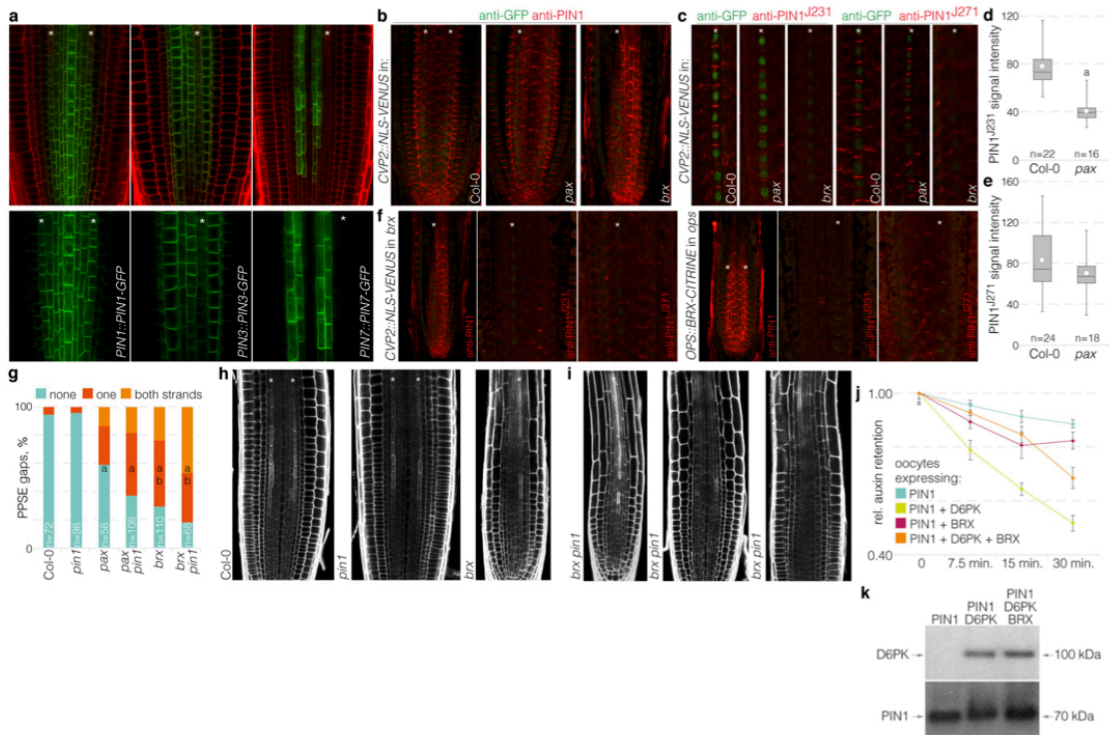
microscopy. **c**, Western analysis of BRX-CITRINE fusion protein after immunoprecipitation. **d**, List of the top BRX interactors, indicating the number of peptides isolated as compared to controls.



Extended Data Fig. 4 | See next page for caption

Extended Data Fig. 4 | Phenotypic analysis of *pax*-related mutants and transgenic lines. **a**, Root length in seven-day-old seedlings for indicated mutants and parallel Col-0 controls. Statistically significant differences between Col-0 and mutants are indicated (Student's *t*-test, two-sided; *a*, $P < 0.02$). **b**, Quantification of gap-cell frequency in protophloem strands of six-day-old seedlings. Statistically significant differences are indicated (two-sided Fisher's exact test; *a*, *pax* versus Col-0; *b*, others versus *pax*; all P values < 0.001). **c**, Root length in seven-day-old seedlings for Col-0, *pax* and transgenic lines in the *pax* mutant background that expressed *PAX* under the control of its native promoter or the *BRX* promoter. The statistically significant difference between *pax* and Col-0 is indicated (two-sided Student's *t*-test; *a*, $P = 0.00016$). **d**, Quantification of gap-cell frequency in protophloem strands of six-day-old seedlings. Statistically significant differences are indicated (two-sided Fisher's exact test; *a*, *pax* versus Col-0; *b*, others versus *pax*; all P values < 0.001). **e**, Phloem-mediated translocation of carboxyfluorescein diacetate succinimidyl ester (CFDA) dye (green fluorescence) into the phloem-unloading zone of the root tip 45 min after CFDA application to the cotyledons of four-day-old seedlings, and corresponding classification of CFDA signal at the end of the experiment. **f**, Quantification of gap-cell frequency in protophloem strands of six-day-old seedlings. Statistically significant differences are indicated (two-sided Fisher's exact test; *a*, others versus Col-0; *b*, Col-0 and *pax* versus *brx*; all P values < 0.01). **g**, Quantification of gap-cell frequency in protophloem strands of six-day-old seedlings. Statistically significant

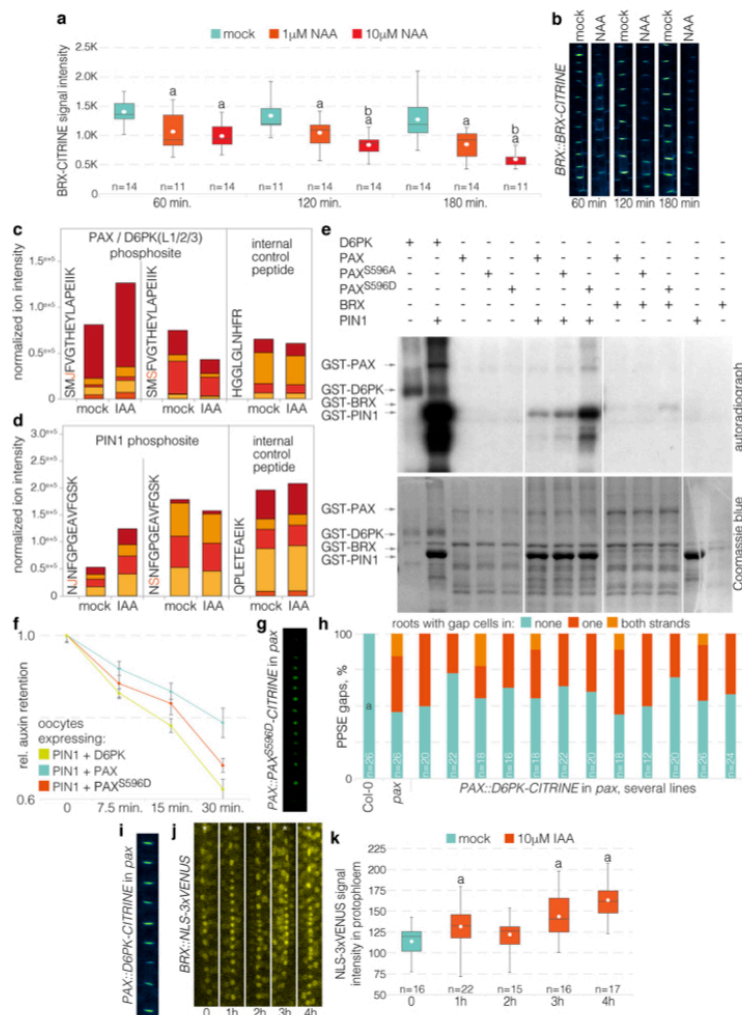
differences are indicated (two-sided Fisher's exact test; *a*, others versus Col-0, all P values < 0.001). **h**, Auxin transport assays performed in *X. laevis* oocytes expressing the indicated heterologous plant proteins ($n = 10$ oocytes per time point; error bars, s.e.m.). **i**, BFA control experiments. Accumulation of PIN1-GFP fusion protein in BFA compartments (left), and comparative BFA insensitivity of OPS-GFP fusion protein (right). **j**, Dissociation of PAX-CITRINE and BRX-CITRINE fusion proteins from the plasma membrane in response to 5 μ M BFA treatment. **k**, Quantification of PAX-CITRINE and BRX-CITRINE fluorescence signal at the plasma membrane in response to 5 μ M BFA treatment, normalized to allow direct comparison (means of approximately ten cells per root). **l**, Confocal microscopy of six-day-old PI-stained root meristems grown on mock or low BFA concentration as indicated. Asterisks indicate PPSE cell files and arrowheads indicate gap cells. **m**, Quantification of gap-cell frequency in PPSE strands of roots shown in **l**. Statistically significant differences are indicated (two-sided Fisher's exact test; *a*, others versus mock, $P < 0.0001$). **n**, Expression of PAX-CITRINE fusion protein under its native promoter, in *pax* single or *brx pax* double mutants. **o**, Transient expression of the indicated fusion proteins, alone or in combination, in *Arabidopsis* protoplasts. The PAX^{K^R>A} variant carries point mutations in a polybasic stretch that is required for plasma membrane interaction²⁴. The average number of patches per protoplast is indicated.



Extended Data Fig. 5 | PIN activity in the root protophloem.

a, Confocal microscopy of indicated reporter genes (green fluorescence) in the root meristem (PI staining, red) of Col-0 wild-type plants (top), and magnification without PI background (bottom). Asterisks indicate sieve element cell files. **b**, Immunolocalization of nuclear localized NLS-VENUS (green) expressed under control of PPSE-specific *CVP2* promoter, and PIN1 (red) by antibody staining. Asterisks indicate PPSE cell files. **c**, Simultaneous immunolocalization of *CVP2*-driven NLS-VENUS (green) with different anti-PIN1 antibodies that specifically detect phosphorylated PIN1 residues S231 (J231) or S271 (J271). **d**, Quantification of the J231 phosphosite signal intensity (means from approximately ten cells per root, arbitrary units). The statistically significant difference is indicated (two-sided Student's *t*-test; a, $P = 1.2 \times 10^{-9}$). **e**, Quantification of the J271 phosphosite signal intensity (means from approximately ten cells per root, arbitrary units). **f**, Immunolocalization of PIN1, and the J231 and J271 PIN1 phosphosites (red) in *brx* (left) or *ops* (right) by antibody staining, with an *OPS::BRX-CITRINE*

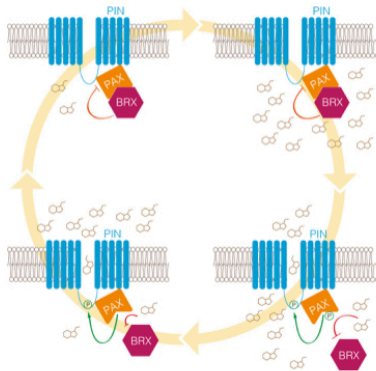
or *CVP2::NLS-VENUS* reporter in the background for the identification of PPSE cell files (asterisks). **g**, Quantification of gap-cell frequency in protophloem strands of six-day-old seedlings for the indicated genotypes. Statistically significant differences are indicated (two-sided Fisher's exact test; a, Col-0 and *pin1* versus others, $P < 0.0001$; b, *brx* or *pax* single mutant versus *brx pin1* or *pax pin1* double mutants, $P < 0.02$). **h**, Confocal microscopy of representative six-day-old Col-0, *pin1*, and *brx* root meristems (PI staining, white). Asterisks indicate PPSE cell files. **i**, Different phenotypic classes occurring in *brx pin1* double mutant root meristems (PI staining, white). PPSE cell files were frequently barely distinguishable or missing. **j**, Auxin transport assays performed in *X. laevis* oocytes expressing the indicated heterologous plant proteins ($n = 10$ oocytes per time point; error bars, s.e.m.). **k**, Western blot analysis of the oocytes used in **j**, demonstrating that BRX expression does not interfere with D6PK or PIN1 expression or stability (detection of YFP-D6PK and PIN1 with anti-GFP and anti-PIN1 antibodies, respectively).



Extended Data Fig. 6 | BRX auxin response and PAX specificity.

a, b, Response of BRX–CITRINE fusion protein to treatment with 1 μM or 10 μM auxin (NAA), time course experiment (**b**) with quantification (**a**, means from approximately ten cells per root, arbitrary units). Statistically significant differences are indicated (two-sided Student's *t*-test; **a**, mock versus others, $P < 0.0094$; **b**, 1 μM versus 10 μM auxin, $P < 0.0028$). **c,** Phosphoproteomics of auxin-treated seedlings, showing normalized abundance of a conserved phosphosite in PAX, D6PK, D6PKL1-3, and AGC1-6, with subfragments indicated in different colours. **d,** Same as **c**, for a PIN1 phosphosite. **e,** Radioactive in vitro kinase assays with GST fusion proteins of D6PK, PAX, or PAX(S596A) and PAX(S596D) point mutants, with BRX or the PIN1 cytosolic loop as substrate (top) and corresponding loading controls (bottom). **f,** Auxin transport assays performed in *X. laevis* oocytes expressing the indicated heterologous

plant proteins ($n = 10$ oocytes per time point; error bars, s.e.m.). **g,** Polar localization of the YFP–PAX(S596D) variant in developing PPSEs of a *pax* mutant. **h,** Quantification of gap-cell frequency in protophloem strands of seven-day-old *pax* mutant seedlings that express a D6PK–CITRINE fusion protein under the control of the PAX promoter. The statistically significant difference is indicated (two-sided Fisher's exact test; **a**, Col-0 versus *pax* and transgenic lines, $P < 0.0001$). **i,** Polar localization of D6PK–CITRINE fusion protein in developing PPSEs of a *pax* mutant. **j, k,** Auxin induction of BRX transcription in developing PPSE cell files (asterisks) visualized using an NLS–3 \times VENUS reporter gene (**j**), with corresponding quantification of nuclear fluorescence signal (**k**). Statistically significant differences are indicated (one-sided Student's *t*-test; **a**, versus preceding time point, $P < 0.0153$).



Extended Data Fig. 7 | Molecular rheostat model for PAX-BRX action in the regulation of auxin efflux. Proposed model for the cellular action of PAX and BRX as elements of a molecular rheostat. BRX interacts with PAX at the plasma membrane, where it inhibits PIN-mediated auxin efflux at lower auxin levels. Because of reduced PIN-mediated auxin efflux, cellular auxin levels increase so that, eventually, BRX becomes displaced from the plasma membrane. Concomitantly, PAX becomes activated and increasingly stimulates auxin efflux. Reinforced through auxin-induced *BRX* transcription and decreasing cellular auxin levels, BRX can return to the plasma membrane and again inhibit auxin efflux. This interplay would lead to a dynamic steady-state equilibrium that fine-tunes auxin levels along a cell file.

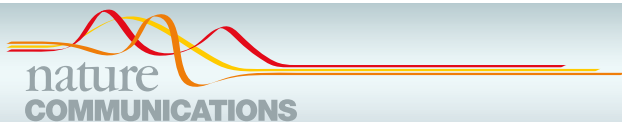
Extended Data Table 1 | List of oligonucleotides used in this study**Genotyping T-DNA insertion lines 5'→3'**

LB3 Sail	TAGCATCTGAATTTTCATAACCAATCTCGATACAC
LB Gabi o8474	ATAATAACGCTGCGGACATCTACATTTT
LBb1.3 Salk	ATT TTG CCG ATT TCG GAA C
brx-2_F417	GTCAGTGTTTGCTTCTCTCTATG
brx-2_R650	TATTTCTTGTCTAGGTAAGAATCC
brx-2_ski3	TGATCCATGTAGATTTCCGGACATGAA
pax_Sail_RP	ATAGTAGCGCCTAAGCGAAG
pax_Sail_LP	CTGCATAGCTAGTTGCTGGT
pax_Sail_LP_UTR	CTACTACGGAACCAATCTTGG
pax_GK_LP	GTAATCCGAGAAATGCTTCCC
pax_GK_RP	AAATTGGAGCTGCTGATGATG
d6pk LP	CAA GAT CAA CCG GTT TAG GAA TCT
d6pk RP	GGC TCA AAC TGA AAG AGA GAT ATT GC
d6pkI1 LP	CATTTCCATGGAAGGAAGGTGATGAGCT
d6pkI1 RP	ACTCCAGAACCATACTTCGAGGCCAT
d6pkI2 LP	CTTCGCCTTTGATGATCTCTG
d6pkI2 RP	AGTGACGAGAGTAGCTGCAGC
d6pkI3 LP	CGGACACTAATCGGATCGGA
d6pkI3 RP	GGCAAGAAAGGATGATCTAACG
pin1_SALK047613_F	CAAAAAACCCCCAAAATTTCTCT
pin1_SALK047613_RP	AATCATCACAGCCAATGATCC

Cloning 5'→3'

attB1_PAX	GGGGACAAGTTTGTACAAAAAAGCAGGCTTTATGCTGGAATGGAAAGAGTTGC
attB2_PAX	GGGGACCACCTTTGTACAAGAAAGCTGGGTGAAAACTCAAAGTCTAGAAATTTACC
attB1r_prPAX	GGGGACTGCTTTTTTGTACAAACTGTTTCATGCGATTTTAAACCAACAC
attB4_prPAX	GGGGACAACCTTTGTATAGAAAAGTTGTTCCGGACCAATTCATTCTTCAGAC
prCVP2	CGCAGAGCTTGAGTAAATCAAG
prCVP2	AACACAAGACAATGAAGCCATCATTGTTGCTTCTTCTGCAAGTG
prCLE45	CATCAAAGATCTGATTGGTCACATC
prCLE45	AACACAAGACAATGAAGCCATCATTCTGCTTTAGGCAGACAAGA
mpd-2	ATGATGGCTTCATTGTCTTGTGT
mpd-2	TGGTCACCAATTCACACGTGTTAGGTTCCGGACGCGGGTG
attB1_PAX	GGGGACAAGTTTGTACAAAAAAGCAGGCTTAATGCTGGAATGGAAAGAGTTG
attB2_PAX with stop codon	GGGGACCACCTTTGTACAAGAAAGCTGGGTATTAGAAAACTCAAAGTCTAGAAATTTACC
PAX_S596Dmut	[Phos]-GGGTTCCAACAAAGTCCATGGACCGTG
PAX_S596Amut	[Phos]-GGGTTCCAACAAATGCCATGGACCGTG

Annex 2: Local auxin competition explains fragmented differentiation patterns (Moret et al., 2020)






ARTICLE



<https://doi.org/10.1038/s41467-020-16803-7>

OPEN

Local auxin competition explains fragmented differentiation patterns

Bernard Moret¹, Petra Marhava¹, Ana Cecilia Aliaga Fandino ¹, Christian S. Hardtke ¹✉ & Kirsten H. W. ten Tusscher ²✉

Trajectories of cellular ontogeny are tightly controlled and often involve feedback-regulated molecular antagonism. For example, sieve element differentiation along developing proto-phloem cell files of *Arabidopsis* roots requires two antagonistic regulators of auxin efflux. Paradoxically, loss-of-function in either regulator triggers similar, seemingly stochastic differentiation failures of individual sieve element precursors. Here we show that these patterning defects are distinct and non-random. They can be explained by auxin-dependent bistability that emerges from competition for auxin between neighboring cells. This bistability depends on the presence of an auxin influx facilitator, and can be triggered by either flux enhancement or repression. Our results uncover a hitherto overlooked aspect of auxin uptake, and highlight the contributions of local auxin influx, efflux and biosynthesis to proto-phloem formation. Moreover, the combined experimental-modeling approach suggests that without auxin efflux homeostasis, auxin influx interferes with coordinated differentiation.

¹Department of Plant Molecular Biology, University of Lausanne, Biophore Building, CH-1015 Lausanne, Switzerland. ²Theoretical Biology, Department of Biology, Utrecht University, 3584 CH Utrecht, The Netherlands. ✉email: christian.hardtke@unil.ch; K.H.W.J.tenTusscher@uu.nl

Development of multicellular organisms entails tightly orchestrated cellular differentiation in response to temporal and spatial cues. Accordingly, trajectories of cellular ontogeny and their plasticity are under firm molecular-genetic control. Postembryonic plant development is highly plastic and modular in order to adapt to environmental conditions¹. Nevertheless, once initiated, plant organs develop in stereotypic patterns, similar to animals². Their sustained growth is driven by apical meristems, and requires phloem sap delivery from source organs^{3,4}. Phloem sap contains sugars and other metabolites, as well as developmental signals, such as the phytohormone auxin⁵. It is transported through the phloem sieve tubes, which consist of interconnected sieve elements. In the sink tissues, for example in root apical meristems, the mature phloem sieve tubes connect to the early, so-called protophloem. Protophloem is continuously produced by the meristem's stem cell niche, and is essential for meristem growth and maintenance⁶. In *Arabidopsis thaliana* root meristems, development of protophloem sieve elements (PPSEs) is laid out in a spatiotemporal gradient that comprises a meristematic zone where stem cell daughters divide, followed by a differentiation zone where elongating cells rearrange their cell walls and organelles, and eventually enucleate^{6,7} (Fig. 1a). The trajectory is overlaid by auxin accumulation around the stem cells, followed by gradual auxin decrease as cells divide and gradual auxin increase as they differentiate^{8–10}. This auxin pattern emerges from polar auxin transport dynamics, with a key role for plasma-membrane-integral PIN-FORMED (PIN) auxin efflux carriers. PINs are rootward localized (i.e., at the plasma membrane that faces the root tip) in developing protophloem cells^{11,12}, similar to most inner cell files^{13,14}, and transport shoot-derived auxin delivered by bulk transport through mature phloem to the periphery of the meristem, as well as locally synthesized auxin, and auxin redirected by the root tip reflux loop^{15,16}.

Controlled PIN activity is required for correct timing of PPSE differentiation^{10,12}. This control is exerted by a “molecular rheostat” that connects two antagonistic regulators of auxin efflux, BREVIS RADIX (BRX) and PROTEIN KINASE ASSOCIATED WITH BRX (PAX)¹². Both are polar plasma-membrane-associated proteins that co-localize with PINs. Whereas PAX stimulates PIN-mediated auxin efflux, BRX inhibits this activation. Because threshold auxin levels negatively regulate BRX plasma-membrane association and also stimulate PAX activity through phosphorylation^{11,12,17}, a dynamic steady-state equilibrium ensues that fine-tunes PIN activity and thereby auxin flux through PPSE cell files. Yet, counterintuitively, both *brx* and *pax* loss-of-function mutants display discontinuous protophloem, which manifests in reduced root growth and other systemic effects^{6,12,18}. This phenotype arises from seemingly stochastic failure of developing PPSEs to differentiate. Such cells stand out as morphological “gaps” that interrupt differentiation zone continuity (Fig. 1b–d). Here, we show that these patterning defects are distinct, non-random, and can be explained by a bistability in fate determination that emerges from competition for auxin between neighboring cells.

Results and discussion

Protophloem differentiation failures in *brx* and *pax* mutants show a non-random pattern. Upon phenotyping larger samples, we found that although the overall gap cell frequency was similar in *brx* and *pax* (Fig. 1e), larger (≥ 4 -cell) gaps were significantly more abundant, and smaller (1-cell) gaps less abundant, in *pax* (Fig. 1f). Yet, in both genotypes, 2-cell gaps were most frequent. To investigate the nature of this pattern, we developed a simple 1D model that decided for each cell in a cell file independently whether it will become a gap cell or a differentiated cell. To

simulate a random distribution, the chances of an individual cell to be assigned gap cell fate were set to the fraction of experimentally observed gap cells. This produced a gap cell distribution that was strongly skewed toward 1-cell gaps (Fig. 1g). These results suggest that loss of either auxin efflux inhibition or activation triggers distinct yet similar protophloem phenotypes that represent non-random disturbance of PPSE differentiation.

To determine which conditions could produce a preponderance of 2-cell gaps, we attributed a higher chance to attain gap fate if the preceding cell was a gap cell, while keeping the overall gap cell fraction constant. These conditions increased the frequency of 2-cell gaps, but also of larger-sized gaps beyond what was observed experimentally (Fig. 1g). Finally, predominantly 2-cell gaps without many larger gaps occurred when cells were assigned a higher chance to become a gap cell only if a single preceding cell was a gap cell (Fig. 1g). These combined results pointed to a potential interdependence of pairs of neighboring cells.

Auxin flux acceleration or deceleration can trigger similar auxin-level reductions in the meristem. To investigate whether this could reflect auxin flux disturbance, we developed a mechanistic model for cellular auxin efflux regulation (Fig. 1h). In this model, ordinary differential equations describe the known auxin-dependent dynamics of BRX, PAX, and PINs (i.e., auxin-dependence of plasma membrane BRX levels and PAX activity, dependence of PIN activity on PAX activity, repression of PAX-mediated PIN stimulation by membrane-bound BRX, and auxin efflux resulting from PIN activation; see “Methods”). To investigate auxin efflux dependence on auxin levels, intracellular auxin levels were varied as a control parameter. *brx* and *pax* mutants were simulated by setting their gene product rates to zero. This model produced low steady-state PIN-mediated auxin export rates at low intracellular auxin levels, which increased with increasing auxin levels (Supplementary Fig. 1a). Virtual *brx* mutation did not simply lower the auxin level required to achieve the same efflux rate, but rather increased the minimum efflux rates at low auxin levels (Supplementary Fig. 1b), which can be understood from the dominant PAX baseline activity at lower auxin levels. In contrast, the absence of PAX resulted in constant low efflux rates, independent of cellular auxin level (Supplementary Fig. 1c).

We next implemented a spatial extension representing a developing PPSE strand that receives auxin from shootward (not explicitly modeled) mature phloem as well as lateral tissues (Fig. 1h). Assuming constant auxin influx as well as constant PIN levels, this model recreated auxin decrease away from the stem cell niche (Fig. 1i). In the virtual *brx* mutant, elevated auxin transport rates resulted in an overall reduction of auxin levels. In contrast, virtual *pax* mutation resulted in substantial auxin accumulation in shootward cells because of an auxin traffic jam arising in the absence of PIN phosphorylation, while more rootward cells displayed lower auxin levels. Thus, in both virtual mutants, a similar-sized integrated auxin reduction occurred across the spatial range of early meristematic cells (Fig. 1i). This could explain the paradoxically similar *brx* and *pax* phenotypes: whereas differentiation zone gaps are easy morphological read-outs, incipient differentiation or specification might already fail in the meristematic zone¹². However, the question how decreased auxin levels translate into the observed pattern of gap cells interspersed with normally differentiating cells remained open.

Gap cell patterning depends on AUX1-mediated bistability and lateral inhibition. The pattern suggested that individual developing PPSEs could be bistable, either attaining a stably

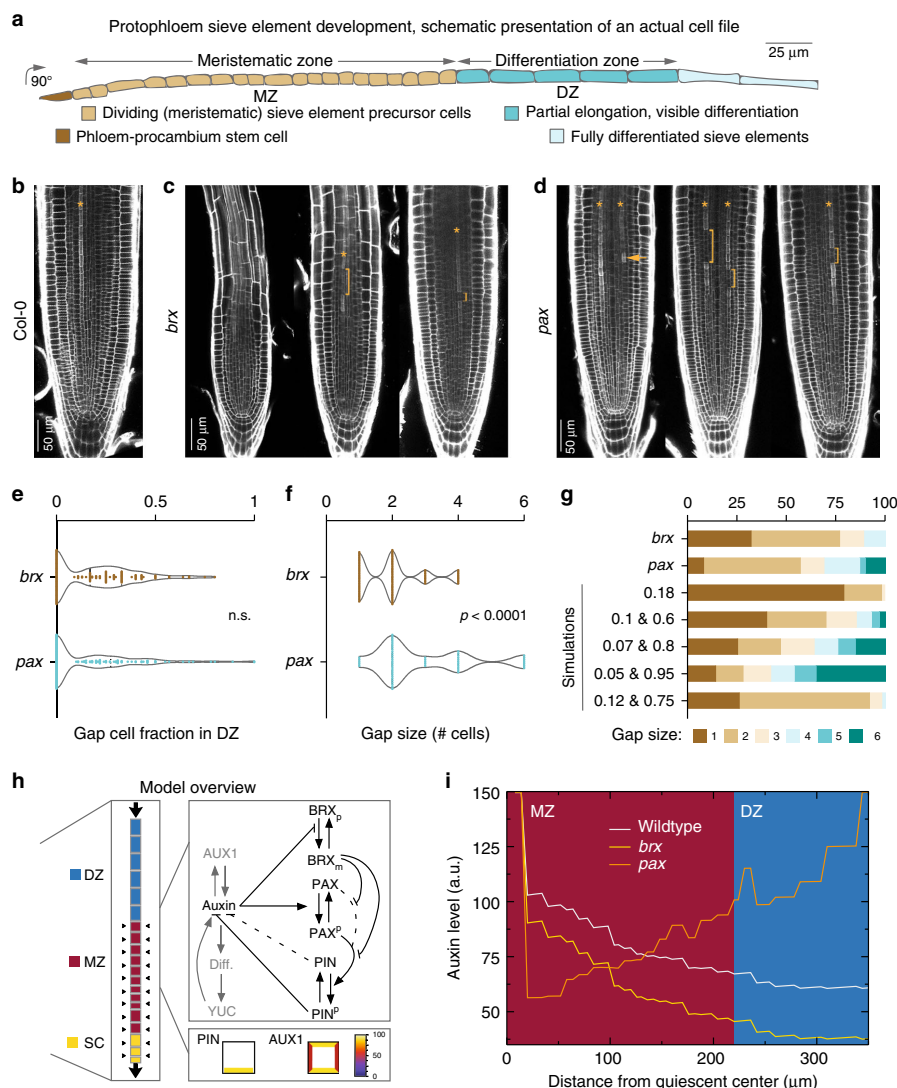


Fig. 1 Antagonistic auxin efflux impairments trigger similar non-random protophloem differentiation failures. **a** Schematic overview of a developing protophloem sieve element (PPSE) cell file in the *Arabidopsis* root meristem. **b** Confocal microscopy image of a 7-day-old wild type (Col-0) root meristem, propidium iodide (PI) cell wall staining (protophloem cell file marked by an asterisk, as hereafter). **c, d** Phenotypic range of *brx* or *pax* mutant root meristems. Brackets point out protophloem “gaps”, i.e., PPSE precursors that fail to differentiate. Arrowheads highlight an isolated differentiated PPSE. **e, f** Quantification of gap cell frequency (**e**) and gap size (**f**) in indicated genotypes. **g** Comparison of experimentally observed simulated gap-size distributions. Simulation of y-axis values indicates differentiation failure probability of an individual cell, total or split, as a function of differentiation failure in the preceding cell. **h** Overview of the models developed in this study. Left: idealized PPSE strand (SC stem cells, MZ meristematic zone, DZ differentiation zone). Cellular PIN and AUX1 levels dictate auxin transport dynamics (shoot-derived auxin supplied to the differentiation zone via bulk phloem sap). The model incorporates cellular growth, division, early expansion, and differentiation dynamics, causing individual cells to move from the meristematic to the differentiation zone. Stem cells undergo slow, meristematic cells rapid divisions; differentiation zone cells undergo early phases of elongation. Right, top: individual model cells contain a regulatory network governing BRX membrane occupancy, PAX and PIN phosphorylation, and auxin efflux dynamics (black). This model network is incrementally augmented with auxin-dependent AUX1 expression, then differentiation, and finally differentiation-dependent YUCCA expression (gray). Right, bottom: individual model cells have a polar PIN pattern, and an apolar AUX1 pattern. **i** Steady-state auxin profiles in wild type, *brx*, and *pax* mutant settings in the initial PSSE model. Dark red indicates the meristematic zone, blue the differentiation zone. Discrete jumps in auxin levels reflect the transition between distinct cells. Within cells, more graded auxin changes occur. Plots display individual values (dots) and their density distribution. See Source Data for raw measurements and statistical test details.

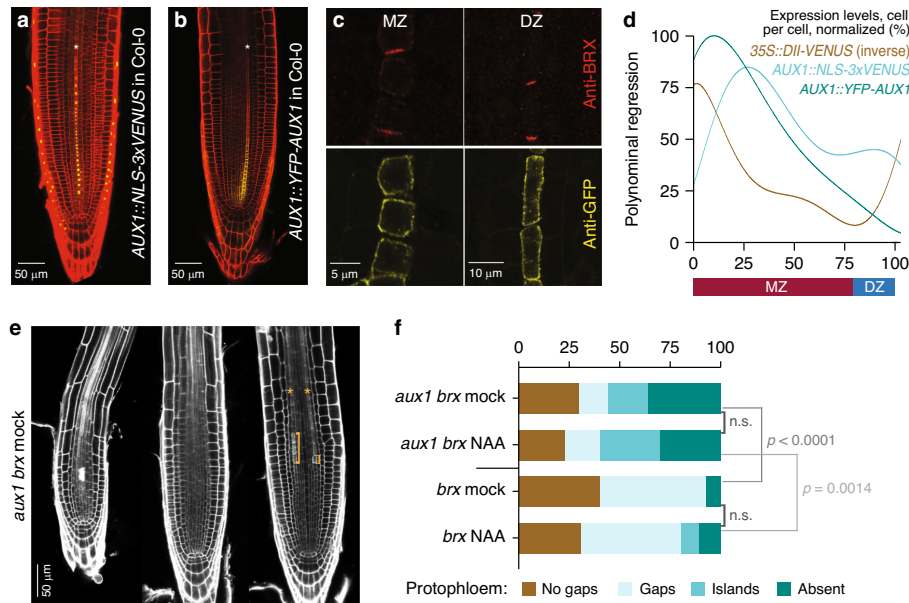


Fig. 2 Intermittent gap cell patterning depends on the auxin influx facilitator AUX1. **a, b** Confocal imaging (PI staining, red) of AUX1 transcriptional (**a**) and translational (**b**) reporter genes (yellow). **c** Anti-GFP immunostaining of YFP-AUX1 fusion protein (yellow) in developing PPSEs, with simultaneous anti-BRX staining (red) for PPSE identification. **d** Relative expression levels of AUX1 reporters and the inverse auxin sensor DII-VENUS along developing PPSE cell files, fitted from experimental data (see Supplementary Fig. 3). **e** Phenotypic range of *aux1 brx* double-mutant root meristems, including isolated “islands” of differentiation (brackets). **f** Quantification of phenotype classes in *aux1 brx* double and *brx* single mutants, in mock conditions or upon treatment with 50 nM of the membrane-soluble synthetic auxin 1-naphthylacetic acid (NAA). Statistical significance of differences (chi-square test) are indicated. See Source Data for raw measurements and statistical test details.

differentiated or non-differentiated, gap cell state. Moreover, the intermittence of differentiated and non-differentiated cells suggested lateral inhibition-type patterning^{19–21}, in which a state promotes itself while simultaneously repressing that same state in neighboring cells. An interesting candidate in this context is the auxin influx facilitator AUX1, whose auxin-dependent expression has been implicated in amplifying auxin patterning during lateral root initiation²² and root tropism²³. AUX1 expression could cause lateral inhibition, because auxin import is further enhanced through AUX1 induction, thereby generating the positive feedback that is essential for bistability, while auxin uptake of a particular cell depletes directly neighboring cells of that same auxin. Besides the columella-root cap, where it is required for root gravitropism, AUX1 is specifically expressed in developing protophloem²⁴, all around PPSEs (Fig. 2a–c, Supplementary Fig. 2a), essentially apolar but with possibly slightly higher abundance along the apical–basal axis (Supplementary Fig. 2b, c). *aux1* loss-of-function mutants do not display discernible root phenotypes apart from agravitropism²⁵. However, *aux1* mutation exacerbates the *brx* phenotype¹². In ca. one-third of *aux1 brx* double mutants, distinguishable protophloem was missing, while otherwise an “inverse gap phenotype” of isolated differentiated cells occurred frequently (Fig. 2e, f). To investigate whether AUX1 could affect PPSE bistability, we developed a second differential equation-based single-cell model that focused on the interplay between intracellular auxin and AUX1. For simplicity, we assumed constant, PIN-mediated auxin efflux, and incorporated dependence of AUX1 levels on intracellular auxin (Fig. 2d, Supplementary Fig. 3a–d), as well as AUX1-dependent auxin uptake. To investigate potential

bistability of intracellular auxin and AUX1 levels, we varied external auxin levels as a control parameter. When the experimentally observed nonlinear positive dependence of AUX1 on auxin levels was implemented, this model created two alternative stable states separated by an auxin threshold. Cells that started out with below-threshold auxin levels converged on a low auxin-low AUX1 (LALA) state, and cells that started out with above-threshold auxin levels converged on a high auxin-high AUX1 (HAHA) state (Fig. 3a). Bistability only arose at intermediate external auxin levels (Fig. 3b), with lower or higher auxin resulting in exclusive accessibility of the LALA or HAHA state, respectively.

In agreement, three alternatives emerged in a simple spatial model extension to a cell file (Fig. 3c). At low auxin availability, all cells converged to a LALA state. At higher external auxin availability, all cells converged to a HAHA state. However, intermediate levels of auxin availability resulted in an alternating pattern of HAHA and LALA cells, because AUX1-mediated auxin influx mostly impaired auxin uptake capacity of directly neighboring cells. Next, we kept auxin influx constant and implemented BRX- and PAX-regulated PIN activity. In this model, simulated *brx* and *pax* mutations resulted in alternating HAHA–LALA phenotypes (Fig. 3d), consistent with the limited auxin-level decrease they induced in the earlier PPSE-strand model. Still, whereas virtual *brx* mutants showed highly regular and temporally constant HAHA–LALA patterning, virtual *pax* mutants displayed a temporally variable, alternating pattern rootward, with a stretch of HAHA cells shootward. In summary, the modeling suggested that local auxin reductions in both *brx* and *pax* protophloem cause AUX1-dependent competition for

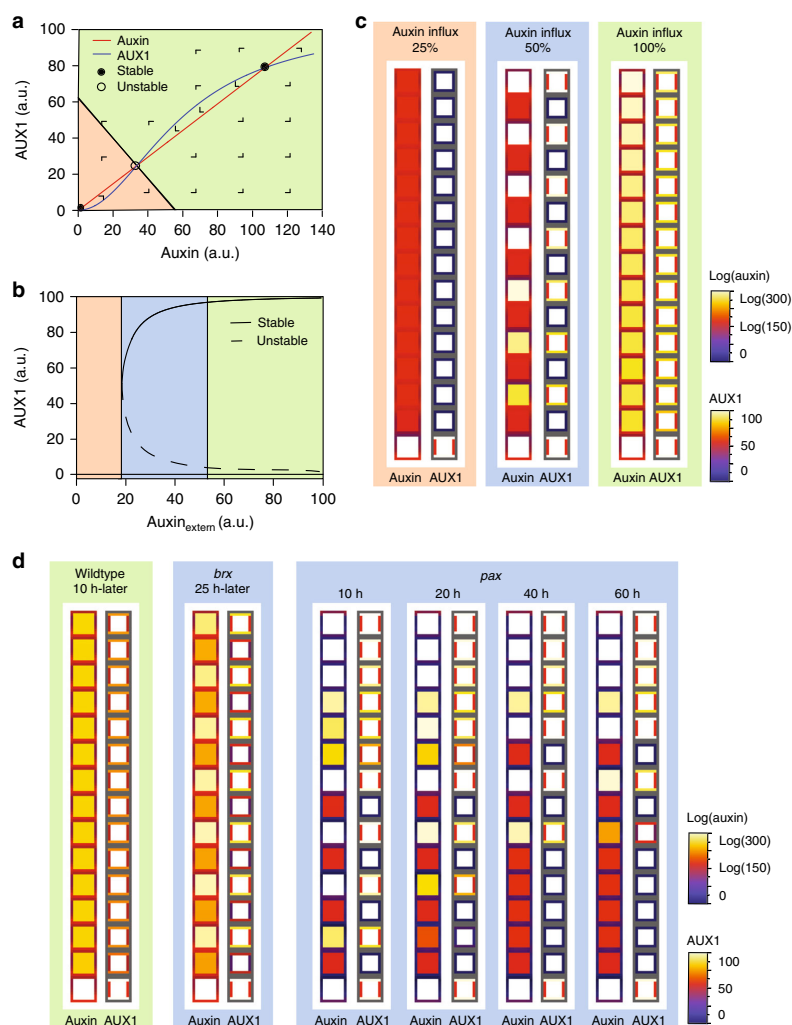


Fig. 3 **AUX1-dependent bistability.** **a** Phase portrait of the auxin-AUX1 single-cell model for intermediate external auxin levels, showing auxin- and AUX1-null clines, the stable and unstable equilibrium intersection points, and the basins of attraction for low auxin-low AUX1 (LALA) (orange) and high auxin-high AUX1 (HAHA) (green) stable equilibria. **b** Bifurcation diagram of the auxin-AUX1 single-cell model using external auxin as the bifurcation parameter. Note the bistable parameter domain in which both the LALA and HAHA equilibria exist (blue). **c** Snapshots of steady-state auxin and AUX1 patterns in a 15-cell strand auxin-AUX1 model for varying levels of shoot-derived auxin influx. Background colors indicate correspondence with parameter regions shown in (b). **d** Snapshots for simulated *brx* mutants, *pax* mutants and wild type under constant shoot auxin influx (showing steady-state dynamics for *brx* and wild type, and patterning dynamics for *pax*).

auxin, and generate intermittent HAHA-LALA patterning. These results matched experimental observations. For example, both *AUX1* transcription and AUX1 protein levels were typically reduced in *brx* gap cells (Fig. 4a-d). Moreover, local AUX1 reductions were also frequently observed in the *brx* meristematic zone (Fig. 4e). These findings were also consistent with reported higher fluctuation of cellular auxin levels along developing *brx* protophloem¹², and lower auxin content in *brx* gap cells as determined by the DII-VENUS auxin sensor (Supplementary Fig. 4a-d). Finally, to confirm the causal role of AUX1 rather than mere auxin availability in creating the bistability of developing PPSEs, we treated *aux1 brx* double mutants with a membrane-

diffusible synthetic auxin that does not require active import. Consistent with our model predictions, this treatment could not revert *aux1 brx* double mutants to the typical *brx* single-mutant gap pattern phenotype (Fig. 2f).

Early meristematic fate specification drives gap-non-gap distribution. While models incorporating AUX1 generated intermittent gaps, these regular, 1-cell gaps did not match observations. However, because of the inherent tendency for alternation, this pattern was substantially perturbed once we moved to the PPSE-strand model that incorporated divisions.

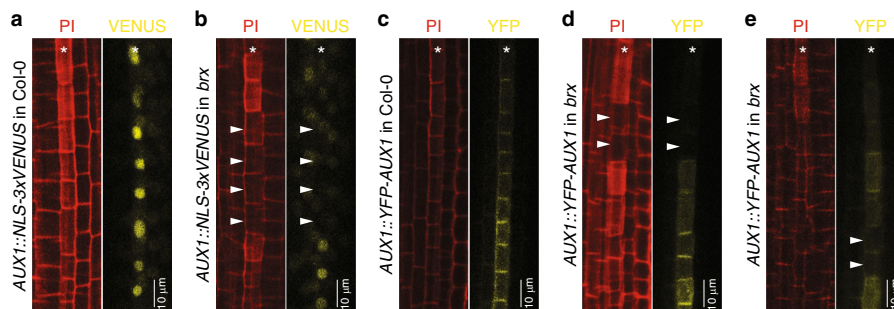


Fig. 4 AUX1 expression in *brx* mutants. **a–e** Confocal microscopy images of developing PPSE cell files (asterisks); left panels: propidium iodide cell wall staining (red); right panels: reporter fluorescence (yellow). **a, b** Transcriptional reporter of AUX1 gene expression in developing PPSEs of Col-0 wild type (**a**) or *brx* (**b**). **c–e** Expression of YFP-AUX1 fusion protein in wild type (**c**), the *brx* differentiation zone (**d**), and the *brx* early meristematic zone (**e**). Gap cells in *brx* are marked by arrowheads in **b** and **d**, cells with low AUX1 are marked by arrowheads in **e**.

Upon cell division, single LALA (or HAHA) cells were transiently transformed into a LALA (or HAHA) pair, followed by dynamic readjustment of auxin–AUX1 patterning (Fig. 5a). Based on this observation of transient cell pairs, we hypothesized that the timing of fate determination onset may be important for gap cell patterning. We therefore refined the PPSE-strand model by including an abstract description of auxin-dependent differentiation, where cells that remain below a certain threshold level of the simulated differentiation factor become gap cells, whereas cells that pass this threshold will become PPSEs. The latter is consistent with the observation that PPSE differentiation can no longer be suppressed, once a cell has committed to this fate^{6,26}. In the first scenario, we assumed that fate determination occurs once cells are distant enough from the stem cell niche (early scenario), and is fixed when cells enter the differentiation zone. In an alternative scenario, we assumed that fate is only determined once cells exit the meristematic zone (late scenario). While approximately similar final differentiation levels were achieved in both wild type scenarios (Fig. 5b–d), clear differences arose for the virtual *brx* mutant: whereas the late scenario produced an alternating 1-cell gap pattern (Fig. 5e), the early scenario regularly produced the experimentally observed 2- as well as 1-cell gaps (Fig. 5f). Moreover, consistent with experimental observations, gaps were interspersed with larger numbers of differentiated cells. This asymmetry resulted from the different dynamics of auxin and AUX1 versus differentiation. Whereas auxin and AUX1 levels can both increase and decrease, differentiation merely increases, albeit at considerably slower rates for lower auxin levels. As a consequence, daughter cells of early meristematic HAHA cells start with a differentiation head start, and although division-induced LALA–HAHA repatterning (Fig. 5a) may cause auxin and AUX1 levels to decrease at later stages, they mostly differentiate (Fig. 5f). In contrast, daughter cells of early meristematic LALA cells start out with a differentiation delay, and only those that gain higher auxin early enough in the meristem due to division-induced LALA–HAHA repatterning differentiate, while others become gap cells (Fig. 5f). Thus, early meristematic LALA cells produced both gap cell pairs and differentiated daughter cells, whereas early meristematic HAHA cells produced mostly differentiated cells (Fig. 5f).

Unlike the virtual *brx* mutant, the virtual *pax* mutant produced a large number of 1-, 2-, and 3-cell gaps in the late scenario (Fig. 5g). In the early scenario, virtual *pax* regularly produced 2- as well as 4-cell gaps interspersed with larger non-gap regions (Fig. 5h), matching experimental observations. These dynamics were more easily observed when a positive feedback of

differentiation on itself was incorporated (Supplementary Fig. 5a–c). Note that division frequency or asynchrony were not tuned to more precisely match our models, since experimental data to realistically constrain these parameters are currently unavailable. Yet, our models provide proof-of-principle that early fate determination is necessary for a 2-cell gap pattern interspersed with longer stretches of differentiated cells, matching the experimentally observed early loss of distinct PPSE markers¹².

Auxin flux homeostasis buffers auxin level fluctuations. To gauge the role of auxin levels and sources, we next investigated local biosynthesis. Interestingly, we found that among potentially protophloem-expressed *YUCCA* genes, which encode the rate-limiting enzymes in auxin biosynthesis^{27,28}, only *YUC5* was expressed in the protophloem, specifically in the differentiation zone (Supplementary Fig. 3e–f; Supplementary Fig. 6a). However, *yuc5* loss-of-function mutants displayed at best somewhat delayed PPSE differentiation (Supplementary Fig. 6b), but no gap or root phenotype. *yuc5* mutation also did not enhance *brx* defects (Supplementary Fig. 6c), consistent with strongly reduced *YUC5* expression in *brx* protophloem (Supplementary Fig. 6d). Although we could not determine whether auxin levels in protophloem are indeed reduced in *yuc5* mutants, these effects were reproduced by our model, and could be ascribed to an overall lower auxin level (Supplementary Fig. 7a–d). This indicates that mere reduction of auxin level through either reduced production (Supplementary Fig. 7b) or uptake (Supplementary Fig. 7e, f) is insufficient to generate gap cells. Supporting this notion, simulations of auxin reduction in wild type merely delayed differentiation (Supplementary Fig. 7g). A functional auxin efflux homeostasis caused auxin efflux to increase with higher and decrease with lower intracellular auxin levels, and thereby counteracted AUX1-mediated competition for auxin and hence prevented bistability. On a similar note, the failure to rescue *brx* mutants by application of a synthetic membrane-diffusible auxin indicated that mere auxin addition is insufficient to prevent gap cell formation (Fig. 2f). Again, these results were reproduced by our model (Supplementary Fig. 7h), and can be explained by the cells' diminished capacity to hold on to auxin in the absence of BRX, and hence its incapacity to prevent AUX1-mediated bistability. Collectively, the results thus indicate that gap cells emerge from a combination of auxin-level reduction and absent flux homeostasis, which triggers AUX1-induced competition for auxin and causes bistable cell fate acquisition. This also means that the BRX–PAX auxin flux rheostat protects the protophloem from differentiation failure when auxin levels fluctuate, by

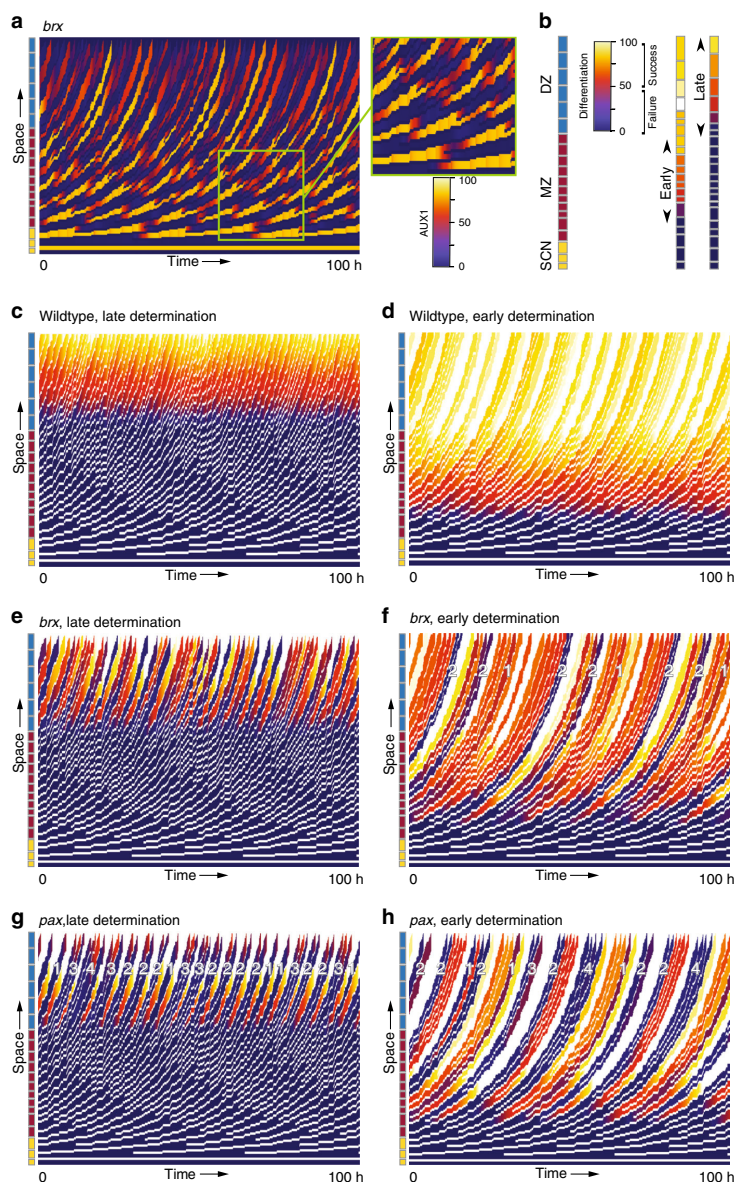


Fig. 5 Early fate determination explains differentiation patterns. **a** Kymograph of cellular AUX1 expression levels for a *brx* mutant in the PPSE-strand model. The inset shows details of AUX1 dynamics in the meristematic zone, highlighting the transient presence of single, double-sized cells just prior to division, and slightly later divided cell pairs with differential AUX1 expression. **b** Snapshots of differentiation dynamics for wild type in the case of early and late fate determination, respectively. Arrows indicate the PPSE zone in which fate is determined for the respective differentiation scenarios. **c-g** Differentiation kymographs for wild type, *brx*, and *pax* mutants in the two scenarios. Numbers in **e-h** indicate gap sizes. For *brx*, only 1-cell gaps (not marked) are observed in the late scenario.

increasing efflux from high auxin-content cells and decreasing efflux from low auxin-content cells.

In summary, our combined experimental-modeling approach explains the paradoxical observation that both genetic flux enhancement and repression trigger a similar protophloem phenotype. The data suggest that once auxin availability and

flux homeostasis are severely disrupted, cells that lose out in competition for auxin spiral into a low auxin uptake capacity state that prevents their timely differentiation. In this scenario of auxin-dependent bistability, facilitator-driven auxin uptake gains in importance, and explains the non-random differentiation failure pattern observed in the mutants. Yet, our findings also

corroborate that as long as auxin efflux homeostasis is functional, impaired auxin influx or local biosynthesis have little effect on differentiation capacity. It appears possible however that auxin influx facilitation into developing protophloem gains importance in more challenging conditions than unobstructed root growth in tissue culture, for example upon extreme root tip bending to avoid obstacles in the soil. Here, it might protect developing protophloem from the dynamic, adaptive auxin flux adjustments throughout the root meristem by maintaining its auxin sourcing and thereby proper differentiation of an essential tissue.

Methods

Plant material and growth conditions. The *A. thaliana* wild type line used in this study was Col-0, which was also the genetic background for the mutants and transgenic lines. For plant tissue culture, seeds were surface-sterilized, stratified for 2 days in the dark at 4 °C, and germinated in vertically placed Petri dishes on 0.7% agar and 0.5× Murashige and Skoog (½ MS) medium (Duchefa) with 0.3% sucrose at 22 °C under continuous light. The following transgenic and mutant lines have been described before: *aux1-7* and *AUX1::YFP-AUX1*²⁸, *brx*, *aux1-7 brx-2*, and *pax*¹².

Generation of constructs, transgenic lines, and *yuc5* mutants. Transgenes for plant transformation were created in suitable binary vectors and produced through standard molecular biology procedures and/or NEBuilder HiFi DNA Assembly Reaction Protocol. For the cloning of the *pX::NLS-3xVENUS* constructs, the following primer combinations were used to insert the amplified promoters into a version of the pCambia1305.1 binary vector containing a *NLS-3xVENUS* reporter downstream of a multicloning site. The restriction sites that were used were *KpnI* or *Eco53kI* for the forward primers and *SbfI* for the reverse primers (Supplementary Table 1). The *yuc5* mutant lines were generated using the CRISPR/Cas9 technology and targeting the *YUC5* reference sequence (AT5G43890). Guides were designed with the help of the CRISPR-P website (<http://crispr.hzau.edu.cn/cgi-bin/CRISPR2/CRISPR>) (Supplementary Table 2).

Plant transformation. The binary constructs were introduced into *Agrobacterium tumefaciens* strain GV3101 pMP90 and transformed into *A. thaliana* using the standard floral dip method. At least three independent transgenic lines were used for each construct to perform experiments and verify reproducibility.

Protein immunolocalization. Immunostaining was performed on 5-day-old seedlings as previously described¹¹. Samples were imaged by confocal laser-scanning microscopy. YFP-AUX1 fusion protein was detected with rabbit polyclonal anti-GFP antibody (Abcam, Cat# ab290; dilution 1:500), and endogenous AUX1 was detected with goat polyclonal anti-AUX1 antibody (Agrisera, Cat# AS16 3957; dilution 1:600). Alexafluor anti-rabbit/goat 546 donkey secondary antibodies (Molecular Probes; dilution 1:500) were used for primary antibody detection.

Microscopy. To visualize reporter genes and staining signals, fluorescence for VENUS (excitation 515 nm, emission 528 nm), YFP (excitation 512 nm, emission 529 nm), and propidium iodide (excitation 536 nm, emission 617 nm) was detected in seedlings examined under a Zeiss LSM 700 inverted confocal scanning microscope. Seven days after germination, seedlings were used for quantifications. For presentation, composite images had to be assembled in various instances. Sequential scanning was used to avoid any interference between fluorescence channels of simultaneously detected probes. For image analyses, ImageJ (NIH; <https://rsb.info.nih.gov/ij/>) and Zeiss Zen (black edition) were used.

Modeling. To investigate whether gap cells follow a random distribution or not, we developed a gap-frequency model, consisting of a one-dimensional strand of cells, the length of a typical protophloem cell file, in which individual cells could be assigned normal or gap cell fate, such that the final gap cell frequencies fit experimental observations in *brx* and *pax* mutants. We varied whether the chances of individual cells to be assigned gap cell fate depend on the fate of preceding cells or not. To investigate how the interplay between BRX, PAX, and PIN impacts auxin flux and patterning, we developed a single-cell ordinary differential equation-based model (parameter settings described in Supplementary Table 3), and subsequently extended this to a one-dimensional protophloem tissue-strand model incorporating cell growth, division, expansion, and differentiation. To investigate auxin-dependent AUX1 expression-mediated bistability, we developed a second ordinary equation-based model (parameter settings described in Supplementary Table 4), which subsequently was incorporated first in a simplified, non-growing, non-zonated tissue-strand model, and then in the protophloem tissue-strand model. Parameter settings for the protophloem tissue-strand model and auxin dynamics (Supplementary Fig. 8) are described in Supplementary Table 5. For a full description of the models including equations see Supplementary Methods.

Reporting summary. Further information on research design is available in the Nature Research Reporting Summary linked to this article.

Data availability

All data in this study are available in the main text or the Supplementary materials. This file also contains the statistical test details. Source data are provided with this paper.

Code availability

The source codes for the different models described here are available on <http://bioinformatics.bio.uu.nl/khwjtuss/ProtophloemModel>.

Received: 2 March 2020; Accepted: 20 May 2020;

Published online: 11 June 2020

References

- Sultan, S. E. Phenotypic plasticity for plant development, function and life history. *Trends Plant Sci.* **5**, 537–542 (2000).
- Halle, F. Modular Growth in Seed. *Plants Philos. Trans. R. Soc. B* **313**, 77–87 (1986).
- Holbrook, N. M. & Knoblauch, M. Editorial overview: physiology and metabolism: phloem: a supracellular highway for the transport of sugars, signals, and pathogens. *Curr. Opin. Plant Biol.* **43**, iii–vii (2018).
- Milne, R. J., Grof, C. P. & Patrick, J. W. Mechanisms of phloem unloading: shaped by cellular pathways, their conductances and sink function. *Curr. Opin. Plant Biol.* **43**, 8–15 (2018).
- Teale, W. D., Paponov, I. A. & Palme, K. Auxin in action: signalling, transport and the control of plant growth and development. *Nat. Rev. Mol. Cell Biol.* **7**, 847–859 (2006).
- Rodriguez-Villalon, A. et al. Molecular genetic framework for protophloem formation. *Proc. Natl Acad. Sci. USA* **111**, 11551–11556 (2014).
- Furuta, K. M. et al. Plant development. Arabidopsis NAC45/86 direct sieve element morphogenesis culminating in enucleation. *Science* **345**, 933–937 (2014).
- Brunoud, G. et al. A novel sensor to map auxin response and distribution at high spatio-temporal resolution. *Nature* **482**, 103–106 (2012).
- Sabatini, S. et al. An auxin-dependent distal organizer of pattern and polarity in the Arabidopsis root. *Cell* **99**, 463–472 (1999).
- Santuari, L. et al. Positional information by differential endocytosis splits auxin response to drive Arabidopsis root meristem growth. *Curr. Biol.* **21**, 1918–1923 (2011).
- Marhava, P. et al. Plasma membrane domain patterning and self-reinforcing polarity in arabidopsis. *Dev. Cell* **52**, 223–235 (2020).
- Marhava, P. et al. A molecular rheostat adjusts auxin flux to promote root protophloem differentiation. *Nature* **558**, 297–300 (2018).
- Adamowski, M. & Friml, J. PIN-dependent auxin transport: action, regulation, and evolution. *Plant Cell* **27**, 20–32 (2015).
- Petrasek, J. & Friml, J. Auxin transport routes in plant development. *Development* **136**, 2675–2688 (2009).
- Bliou, I. et al. The PIN auxin efflux facilitator network controls growth and patterning in Arabidopsis roots. *Nature* **433**, 39–44 (2005).
- Grieneisen, V. A., Xu, J., Maree, A. F., Hogeweg, P. & Scheres, B. Auxin transport is sufficient to generate a maximum and gradient guiding root growth. *Nature* **449**, 1008–1013 (2007).
- Scacchi, E. et al. Dynamic, auxin-responsive plasma membrane-to-nucleus movement of Arabidopsis BRX. *Development* **136**, 2059–2067 (2009).
- Anne, P. & Hardtke, C. S. Phloem function and development-biophysics meets genetics. *Curr. Opin. Plant Biol.* **43**, 22–28 (2018).
- Greenwald, I. & Ruben, G. M. Making a difference: the role of cell-cell interactions in establishing separate identities for equivalent cells. *Cell* **68**, 271–281 (1992).
- Oster, G. F. Lateral inhibition models of developmental processes. *Math. Biosci.* **90**, 265–286 (1988).
- Raible, D. W. & Eisen, J. S. Lateral specification of cell fate during vertebrate development. *Curr. Opin. Genet. Dev.* **5**, 444–449 (1995).
- Laskowski, M. et al. Root system architecture from coupling cell shape to auxin transport. *PLoS Biol.* **6**, e307 (2008).
- van den Berg, T., Korver, R. A., Testerink, C. & Ten Tusscher, K. H. Modeling halotropism: a key role for root tip architecture and reflux loop remodeling in redistributing auxin. *Development* **143**, 3350–3362 (2016).
- Swarup, R. et al. Localization of the auxin permease AUX1 suggests two functionally distinct hormone transport pathways operate in the Arabidopsis root apex. *Genes Dev.* **15**, 2648–2653 (2001).
- Bennett, M. J. et al. Arabidopsis AUX1 gene: a permease-like regulator of root gravitropism. *Science* **273**, 948–950 (1996).
- Hazak, O. et al. Perception of root-active CLE peptides requires CORYNE function in the phloem vasculature. *EMBO Rep.* **18**, 1367–1381 (2017).

27. Stepanova, A. N. et al. The Arabidopsis YUCCA1 flavin monooxygenase functions in the indole-3-pyruvic acid branch of auxin biosynthesis. *Plant Cell* **23**, 3961–3973 (2011).
28. Zhao, Y. et al. A role for flavin monooxygenase-like enzymes in auxin biosynthesis. *Science* **291**, 306–309 (2001).
29. Swarup, R. et al. Structure-function analysis of the presumptive Arabidopsis auxin permease AUX1. *Plant Cell* **16**, 3069–3083 (2004).

Acknowledgements

This work was supported by Swiss National Science Foundation grant 310030B_185379 awarded to C.S.H., and the Netherlands Scientific Organization grant 864.14.003 awarded to K.H.W.J.T.T.

Author contributions

B.M., P.M., and A.C.A.F. performed the experiments. K.H.W.J.T.T. performed the modeling. B.M., P.M., A.C.A.F., and C.S.H. analyzed the experimental data. B.M., C.S.H., and K.H.W.J.T.T. designed the study and wrote the paper together.

Competing interests

The authors declare no competing interests.

Additional information

Supplementary information is available for this paper at <https://doi.org/10.1038/s41467-020-16803-7>.

Correspondence and requests for materials should be addressed to C.S.H. or K.H.W.J.T.T.

Peer review information *Nature Communications* thanks the anonymous reviewers for their contribution to the peer review of this work.

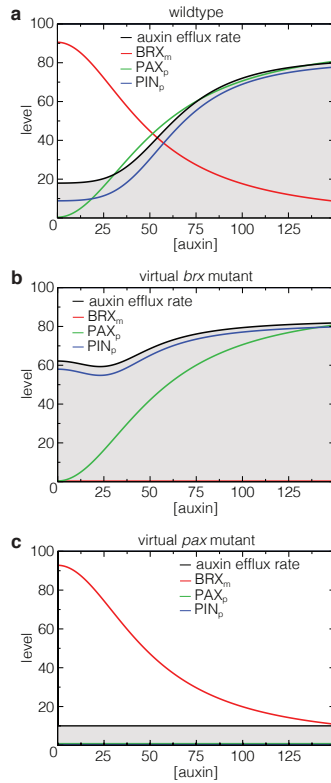
Reprints and permission information is available at <http://www.nature.com/reprints>

Publisher's note Springer Nature remains neutral with regard to jurisdictional claims in published maps and institutional affiliations.

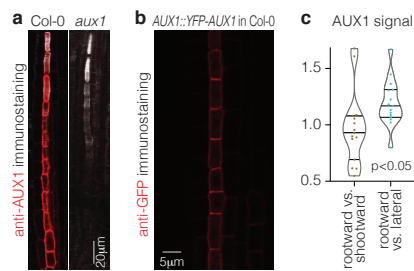


Open Access This article is licensed under a Creative Commons Attribution 4.0 International License, which permits use, sharing, adaptation, distribution and reproduction in any medium or format, as long as you give appropriate credit to the original author(s) and the source, provide a link to the Creative Commons license, and indicate if changes were made. The images or other third party material in this article are included in the article's Creative Commons license, unless indicated otherwise in a credit line to the material. If material is not included in the article's Creative Commons license and your intended use is not permitted by statutory regulation or exceeds the permitted use, you will need to obtain permission directly from the copyright holder. To view a copy of this license, visit <http://creativecommons.org/licenses/by/4.0/>.

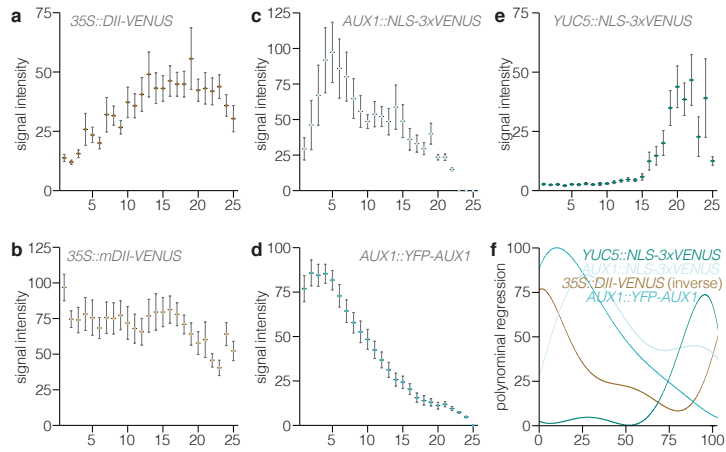
© The Author(s) 2020



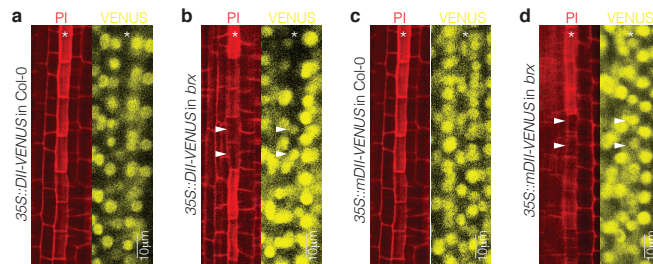
Supplementary Fig. 1. Single cell model of the BRX-PAX auxin efflux rheostat. Steady-state membrane-associated BRX (BRX_m), phosphorylated PAX (PAX_p) and PIN (PIN_p) levels, and resulting PIN-mediated auxin efflux, as a function of internal auxin level for simulated **a**, wildtype, **b**, *brx* mutant, and **c**, *pax* mutant.



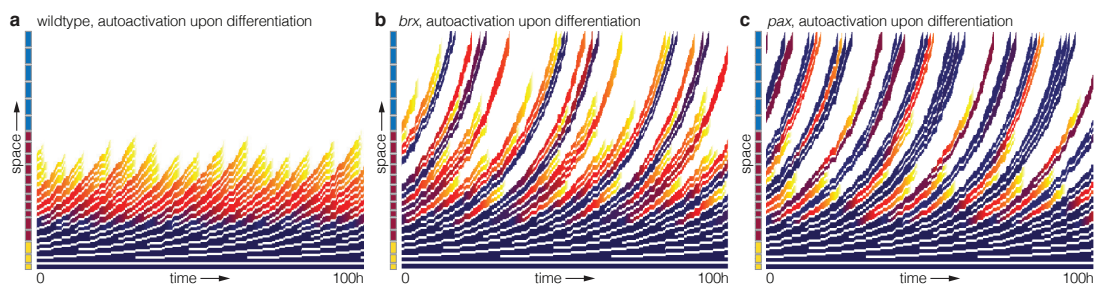
Supplementary Fig. 2. Apolar AUX1 localization in PPSEs. **a**, Detection of endogenous AUX1 in developing PPSEs of Col-0 wildtype with anti-AUX1 immunostaining, overlaid with calcofluor white cell staining (grey). A staining of the *aux1-21* null mutant is shown as a negative control. **b**, YFP-AUX1 detection by anti-GFP immunostaining in developing PPSEs. Note seemingly higher AUX1 levels shootward and rootward due to adjacency of the membranes. **c**, Quantification AUX1 signal ratios between shoot-/rootward and lateral membranes, obtained exclusively from detached PPSEs. Plots display individual values (dots) and their density distribution. See Source Data for raw measurements and statistical test details.



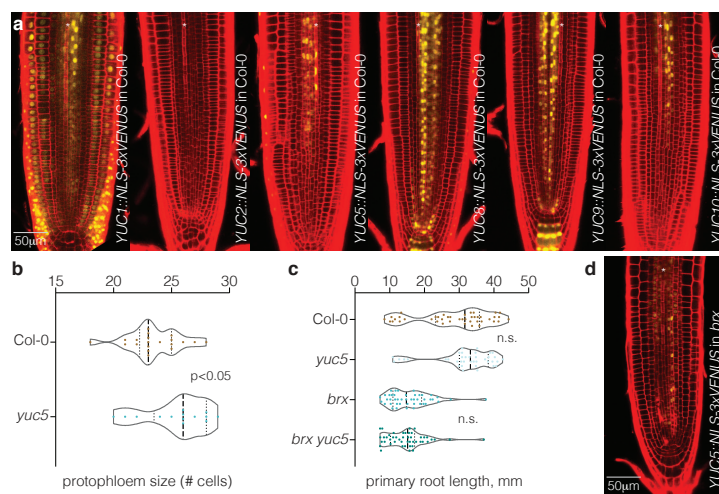
Supplementary Fig. 3. Expression profiles in PPSEs. a-e, Quantification of reporter gene expression levels along developing PPSE cell files, determined cell-by-cell in pertinent regions of interest (nucleus or plasma membrane). DII-VENUS is an inverse reporter of cellular auxin levels, mDII-VENUS its inert control. f, Fitted polynomial regression curves for the expression patterns, normalized along the cell files for the spread between highest (100%) and lowest (0%) raw expression values. See Source Data for raw measurements.



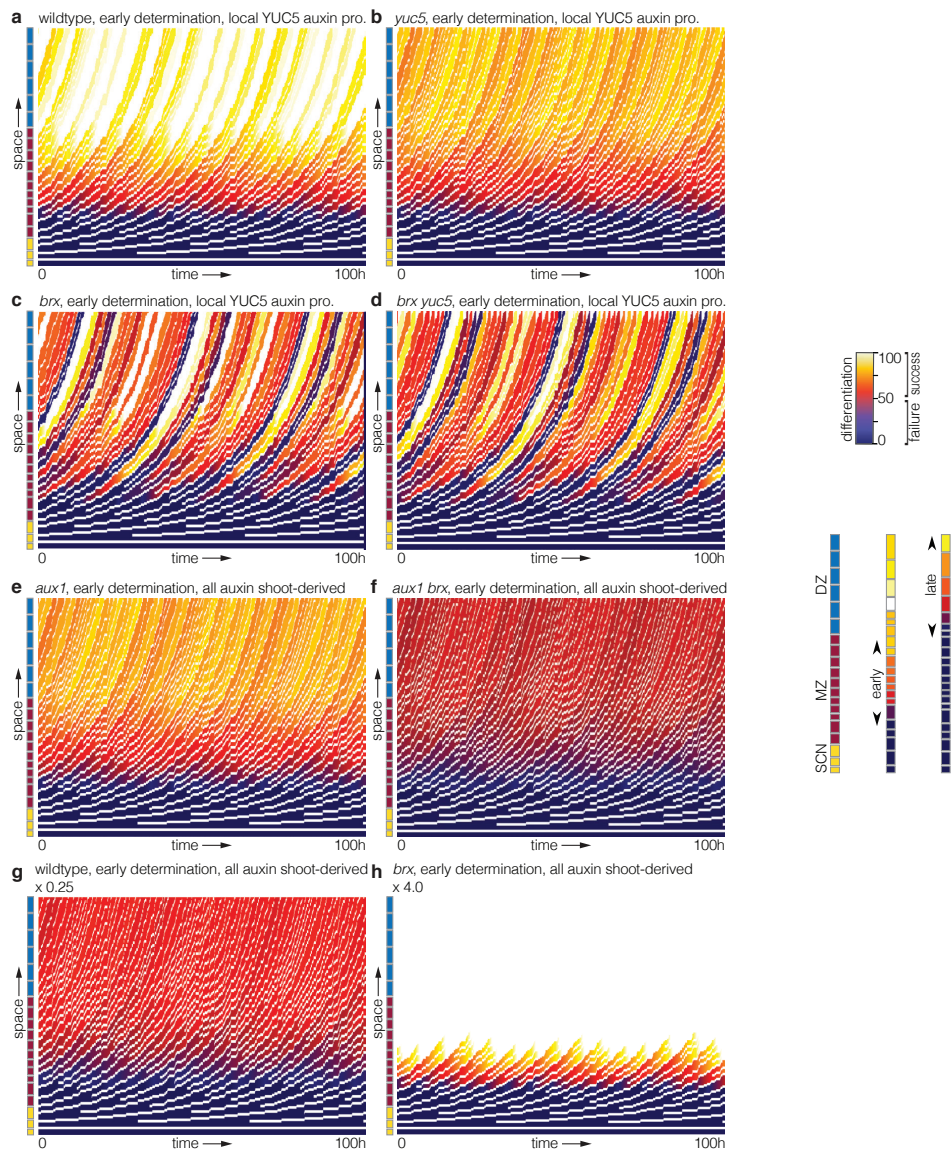
Supplementary Fig. 4. DII-VENUS expression in developing PPSEs. a-d, Confocal microscopy images of developing PPSE cell files (asterisks); left panels: propidium iodide cell wall staining (red); right panels: reporter fluorescence (yellow). a-b, Expression of the inverse auxin sensor DII-VENUS in developing PPSEs of Col-0 wildtype (a) or *brx* (b). c-d, Corresponding expression of the auxin-insensitive negative control reporter protein mDII-VENUS. Gap cells in *brx* are marked by arrowheads in b and d.



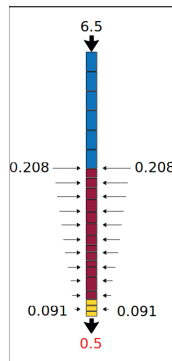
Supplementary Fig. 5. Early specification explains differentiation patterns. a-c, Differentiation kymographs for wildtype, *brx* and *pax* mutants in the early scenario (see Figure 5), with additional implementation of a positive feedback of differentiation on itself.



Supplementary Fig. 6. Local auxin biosynthesis in developing PPSEs. a, Confocal imaging (PI staining, red) of transcriptional reporters (yellow) for different YUCCA genes in Col-0 wildtype. **b**, Protophloem cell file length (counted from the first cell adjacent to the QC up to the last cell of the differentiation zone) in Col-0 and a *yuc5* knock-out mutant. **c**, Root length for 7-day-old seedlings of indicated genotypes. **d**, Confocal imaging of the transcriptional *YUC5* reporter in *brx* mutant background. Plots display individual values (dots) and their density distribution. See Source Data for raw measurements and statistical test details.



Supplementary Fig. 7. PPSE differentiation as a function of local auxin biosynthesis. a-h, Differentiation kymographs for indicated simulated genotypes, in the early scenario.



Supplementary Fig. 8. Overview of auxin influx and efflux into the simulated protophloem strand. Top influx, bottom efflux (fat arrows), emulated reflux loop influx (normal arrows). Influx/efflux rates indicated with black/red numbers.

	Forward primer	Reverse primer
pAUX1 (KpnI/SbfI)	5'- CTC GGT ACC CAA GAG ATT TTG AAG ACT CTT C -3'	5'- CAG CC TGC AGG TTT TTT AGC TTC TAG ATC TGA GA -3'
pYUC1 (Eco53KI/SbfI)	5'- CTC GAG CTC AAG CTT AAC AAA CTG CAA GGA AGT G -3'	5'- CAG CC TGC AGG TCT TGA TGG ATG ATG GAA AAT GTT TTA AA -3'
pYUC2 (Eco53KI/SbfI)	5'- CTC GAG CTC TTA GCA TAA TGA AAT TTT AGT TAC TAG AC -3'	5'- CAG CC TGC AGG GAA AGA GAG AAA GAG AAG AAA AAA GA -3'
pYUC5 (Eco53KI/SbfI)	5'- CTC GAG CTC CTA CAA CTA CAA AGG GAG CTT TC -3'	5'- CAG CC TGC AGG CTT TAG GGG TGA GTT TGA TCG A -3'
pYUC8 (Eco53KI/SbfI)	5'- CTC GAG CTC GCA TAT ATA AGG TTC TAC CAC GA -3'	5'- CAG CC TGC AGG TCT TTT TTT ATA AGT TTC TTT AAT AAG TAT TG -3'
pYUC9 (Eco53KI/SbfI)	5'- CTC GAG CTC AGA CGA TCA CTG AAC CTA ACC -3'	5'- CAG CC TGC AGG TTT CTT GAG TGA GTT TTT GAA TGA AAG -3'
pYUC10 (Eco53KI/SbfI)	5'- CTC GAG CTC GTA AAG TGA CTA ATT TTC CAA TTA AGT T -3'	5'- CAG CC TGC AGG TTC TTG TGT TTA GTT TGA TAG ATT CTC -3'

Supplementary Table 1: List of the primers used for promoter amplification prior to integration into *NLS-3xVENUS* pCAMBIA1205.1 construct templates.

ID	Score	Sequence		%GC
guide2	0.849	5'-ATA TTC CAT CTC CGA CCC CGA GG-3'	CDS	55%
guide5	0.8146	5'-AGT CAC GTG GAG CTA GTA GAC GG-3	CDS	50%
guide9	0.7393	5'-CAC GGC AGC CTG CCT CCG CGA GG-3	CDS	80%

Supplementary Table 2: List of the RNA guides used for the generation of the *ymc5* mutant lines.

Parameter	Meaning	Value	Units
BRX_{tot}	Total cellular amount of BRX protein	100	[]
brx_{exo}	Maximum rate of BRX exocytosis	0.1	s^{-1}
brx_{endo}	Rate of BRX endocytosis	0.01	s^{-1}
K_{brx}	Auxin level at which exocytosis rate is half maximal	15	[]
PAX_{tot}	Total cellular amount of PAX protein	100	[]
pax_{act}	Maximum rate of PAX phosphorylation	0.1	s^{-1}
pax_{deact}	Rate of PAX dephosphorylation	0.01	s^{-1}
K_{pax}	Auxin level at which phosphorylation rate is half maximal	180	[]
$PIN1_{tot}$	Total cellular amount of PIN1 protein	100	[]
$pin1_{act}$	Maximum rate of PIN1 phosphorylation	0.1	s^{-1}
$pin1_{deact}$	Rate of PIN1 dephosphorylation	0.001	s^{-1}
$K_{PIN1,pax}$	(weighted) PAX level at which PIN1 phosphorylation rate is half maximal	250	[]
$K_{pin1,brx}$	BRX level at which PIN1 phosphorylation rate is half maximal	25	[]
enh_{paxp}	Relative effectiveness of PAXp versus PAX	2.5	dimensionless
enh_{pinp}	Relative effectiveness of PINp versus PIN	10	dimensionless

Supplementary Table 3: Default parameter values for the single cell BRX PAX PIN model.

Parameter	Meaning	Value	Units
p_{aux1}	Maximum rate of AUX1 production	0.04	$[]s^{-1}$
d_{aux1}	Rate of AUX1 degradation	0.0004	s^{-1}
K_{aux1}	Auxin level at which AUX1 production is half maximal	60	$[]$
i_{aux1}	Rate of active AUX1 dependent auxin influx	0.20	$[AUX1]^{-1}s^{-1}$
$PIN1$	Total cellular amount of PIN1 protein	100	$[]$
e_{pin1}	Rate of active PIN1 dependent efflux	0.04	$[PIN1]^{-1}s^{-1}$
p_{auxin}	Rate of auxin production	0	$[]s^{-1}$
d_{auxin}	Rate of auxin degradation	0.0000725	s^{-1}

Supplementary Table 4: Default parameter values for the auxin-AUX1 single cell model.

Parameter	Meaning	Value	Units
D_{wall}	Apoplasmic auxin diffusion rate	40	$\mu m^2 s^{-1}$
D_{cell}	Cytoplasmic auxin diffusion rate	600	$\mu m^2 s^{-1}$
p_{Aux}	<i>Rate of auxin production</i>	0	$[]s^{-1}$
d_{Aux}	<i>Rate of auxin degradation</i>	0.0000725	s^{-1}
i_{pas}	Rate of passive auxin influx	2	$[]s^{-1}$
i_{aux1}	<i>Maximum rate of active AUX1 dependent auxin influx</i>	0.2	$\mu m^2 s^{-1}$
$K_{sataux1}$	Intracellular auxin level at which AUX1 influx rate is half maximal	60	$[]$
e_{PIN}	<i>Maximum rate of active PIN1 dependent auxin efflux</i>	0.04	$\mu m^2 s^{-1}$
K_{satpin}	Extracellular auxin level at which PIN1 efflux rate is half maximal	60	$[]$

Supplementary Table 5: Default parameters of the simple cell strand model.

Supplementary Methods

Modelling

Gap frequency model

To investigate whether the observed gap size frequency distributions in *brx* and *pax* mutants are the likely result of a random process or not, we made a simple model of a protophloem cell file in which cells can be either a gap (non-differentiated) or non-gap (differentiated) cell, by varying the chances for individual cells of being a gap cell. Protophloem cell file length was drawn from a range of 6.8 to 10.8 cells, resulting in an average of 8.8 cells, based on our experimental observations (average differentiation zone size of 8.8 for *pax* and 6.7 for *brx* mutants). We compared three model variants:

- 1) Each cell has the same, independent chance P of being a gap cell. The chance of being a gap cell was set to the fraction of gap cells observed experimentally in *brx* mutants (P=0.18).
- 2) There is an independent chance P1 for cells to be a gap cell. Additionally there is a chance P2 for a cell to be a gap cell given that the previous cell is a gap cell. P1 and P2 are set such that the resulting fraction of gap cells equals the fraction observed experimentally. Various combinations fulfilling this constraint were investigated (P1=0.1 and P2=0.6; P1=0.07 and P2=0.8; P1=0.05 and P2=0.95).
- 3) This is a variation on 2. Again there are chances P1 and P2. However, P2 now is the chance for a cell to be a gap cell given that the previous cell is a gap cell and the one before is not a gap cell. Again, P1 and P2 are set such that the resulting fraction of gap cells matches the fraction observed experimentally (P1=0.12 and P2=0.75).

To investigate the gap size frequency distribution each of these scenarios would result in, we randomly generated a total of 100,000 protophloem strands per scenario, quantifying them in the same way as our *in planta* protophloem strands.

Single cell BRX, PAX, PIN model

In this single cell model we assume that overall BRX (BRX_{tot}), PAX (PAX_{tot}) and PIN1 ($PIN1_{tot}$) levels stay constant, and model the dynamics of auxin dependent membrane occupancy of BRX (BRX_{mem}), the auxin dependent phosphorylation of PAX (PAX^p), the BRX- and PAX-dependent phosphorylation of PIN1 ($PIN1_p$), and how average PIN1 efflux rate depends on the fraction of phosphorylated PIN1 using the following set of equations:

$$\frac{dBRX_{mem}}{dt} = brx_{exo} \frac{K_{brx}^2}{K_{brx}^2 + auxin_i^2} (BRX_{tot} - BRX_{mem}) - brx_{endo} BRX_{mem} \quad \text{Eq. 1}$$

$$\frac{dPAX^p}{dt} = pax_{act} \frac{auxin_i^2}{auxin_i^2 + K_{pax}} (PAX_{total} - PAX^p) - pax_{deact} PAX^p \quad \text{Eq. 2}$$

$$\frac{dPIN1^p}{dt} = pin1_{act} f(PAX, PAX^p) g(BRX_{mem}) (PIN1_{total} - PIN1^p) - pin1_{deact} PIN1^p \quad \text{Eq. 3}$$

$$f(PAX, PAX^p) = \frac{(PAX_{total} - PAX^p)^2 + enh_{paxp} PAX^p^2}{(PAX_{total} - PAX^p)^2 + enh_{paxp} PAX^p^2 + K_{PIN1, PAX^p}^2} \quad \text{Eq. 3b}$$

$$g(BRX_{mem}) = \frac{K_{pin1, brx}^2}{K_{pin1, brx}^2 + BRX_{mem}^2} \quad \text{Eq. 3c}$$

$$pinexport = ppump \frac{(PIN1_{total} - PIN1^p) + enh_{pinp} PIN^p}{enh_{pinp}} \quad \text{Eq. 4}$$

Note that we kept intracellular auxin as a control parameter external to the model to investigate the effect of auxin levels on PIN1-mediated export. In the multi-cellular, 1D strand models, intra- and extracellular auxin dynamics were modelled as independent variables (see below).

Note that in the equation for BRX_{mem} , the negative effect of auxin on BRX_{mem} levels is incorporated through a repression of BRX exocytosis. The alternative, auxin-induced BRX endocytosis would lead to similar outcomes. In the equation for PAX_p , we incorporated that PAX phosphorylation rate is enhanced in the presence of auxin. For the equation of PIN_p , we incorporated the PAX dependence of PIN phosphorylation ($f(PAX, PAX_p)$), and the enhanced PIN ($enh_{pax>1}$) phosphorylation potential of phosphorylated PAX. Additionally, for PIN_p we incorporate the repression of PAX mediated phosphorylation by BRX_{mem} ($g(BRX_{mem})$). Finally, average PIN transport rate depends on the fraction of highly active ($enh_{pin>1}$) phosphorylated and less active, non-phosphorylated PINs.

With regard to parameter values, experimental data suggest a 2-3 fold increase in auxin efflux due to PIN phosphorylation¹, thus providing us with a ballpark figure for the value of parameter enh_{pinp} . For other parameters, no quantitative experimental data were available and robustness of results against variation in parameter values was investigated. The qualitative shape of the dependence of PIN1 efflux rate on auxin levels remained the same for 2-fold changes in the parameters controlling the efficiency of PAX versus PAX_p in PIN phosphorylation and of PIN versus PIN_p in transporting auxin, as well as 33% increases or decreases in saturation constants. See Supplementary Table 3 for an explanation of parameter meaning, default values and units.

Total cellular levels of BRX, PAX and PIN proteins (BRX_{tot} , PAX_{tot} , $PIN1_{tot}$) were normalized to an arbitrary value of 100. Ratios between BRX exo- and endocytosis rates (brx_{exo} , brx_{endo}) as well as PAX (pax_{act} , pax_{deact}) and PIN ($pin1_{act}$, $pin1_{deact}$) phosphorylation and dephosphorylation rates were set to 10 to ensure that under optimal conditions (very low auxin; very high auxin; and very low BRX_{mem} and high PAX_p , respectively) a near to 100% (10/11) fraction of BRX can reside on the membrane, or PAX and PIN can be phosphorylated, respectively. In addition to choosing this ratio, rates are set such that they exceed the rates of *AUX1* and *PIN1* gene expression used later in described cell strand models. Saturation constants for auxin dependent BRX endocytosis K_{brx} and auxin dependent PAX phosphorylation K_{pax} were (because of the opposing effects of BRX_{mem} and PAX_p on PIN_p levels) chosen to lie near the opposite ends of the auxin range occurring in our models. Additionally, saturation constants mediating the effects of BRX_{mem} and PAX_p on PIN phosphorylation rate ($K_{pin1,brx}$, $K_{pin1,pax}$) were set such that BRX_{mem} starts having an effect at low levels, whereas for PAX effects to become strong considerably higher concentrations are needed. Combined this ensures that PIN_p levels can gradually vary over a wide range of auxin levels, enabling effective BRX-PAX-PIN-mediated auxin homeostasis. As explained above enh_{pinp} is based on experimental data and enh_{pax} is chosen to have a similar order of magnitude.

Changes in membrane occupancy of BRX, as well as in PAX and PIN phosphorylation levels will occur rapidly relative to changes in transcription, as well as processes of cell growth, division and expansion. Therefore, rather than using the dynamic equations 1-3 we used a quasi-steady-state assumption, enabling us to apply the following algebraic expressions:

$$BRX_m = \frac{BRX_{total}}{1 + \frac{brx_{endo}}{brx_{exo} \frac{K_{brx}^2}{K_{brx}^2 + auxin_i^2}}} \quad \text{Eq. 5}$$

2

$$PAX^p = \frac{PAX_{total}}{1 + \frac{pax_{inact} \cdot auxin_i^2}{pax_{act} \cdot auxin_i^2 + K_{pax}^2}} \quad \text{Eq. 6}$$

$$PIN1_p = \frac{PIN1_{total}}{1 + \frac{pin_{deact}}{pin_{act} f(PAX, PAX^p) g(BRX_m)}} \quad \text{Eq. 7}$$

brx mutants were simulated by setting $BRX_{total} = 0$, while *pax* mutants were simulated by setting $PAX_{total} = 0$.

Single cell AUX1 model

In this single cell model we solely focused on the auxin-dependence of AUX1 expression and its effect on intracellular auxin levels ($auxin_i$). Extracellular auxin levels ($auxin_e$) are set constant and are used as a control parameter. PIN1 phosphorylation and its effect on PIN1 efflux rate are ignored. Based on our observation of a positive relation between auxin and AUX1 protein levels as well as earlier results², we modeled a positive effect of auxin on AUX1 protein production:

$$\frac{dAUX1}{dt} = P_{AUX1} \frac{auxin_i^2}{auxin_i^2 + K_{AUX1}^2} - d_{AUX1} AUX1 \quad \text{Eq. 8}$$

Note that incorporating a negative effect of auxin on AUX1 degradation instead would yield similar results.

We initially make the simplifying assumption that PIN1 and AUX1 auxin transport increases linearly with levels of available auxin. Together this results in the following auxin dynamics:

$$\frac{dauxin_i}{dt} = i_{aux1} AUX1 auxin_e - e_{pin} PIN1 auxin_i + p_{auxin} - d_{auxin} auxin_i \quad \text{Eq. 9}$$

See Supplementary Table 4 for an explanation of parameter meaning and default values.

Rate of AUX1 mediated influx i_{aux1} and auxin degradation d_{auxin} are similar as in previous models^{2,3}, while for simplicity (given the dominance of shoot and reflux loop-derived auxin) local auxin production p_{aux1} is ignored. PIN1-mediated efflux rate e_{pin1} was reduced 5-fold relative to previous models, to prevent all auxin from accumulating in the lowermost cell. AUX1 production p_{aux1} and decay rates d_{aux1} were taken to result in a maximum expression level of 100, equal to the total amount of *PIN1* present in a cell. Additionally, values were taken such that AUX1 transcriptional and translational dynamics are slower than BRX endo/exocytosis and PAX/PIN phosphorylation/dephosphorylation. The saturation constant for AUX1 expression K_{aux1} was set to approximately half-way the maximally occurring auxin values.

Applying steady state assumptions this results in the following equations for the auxin and AUX1 null-clines:

$$AUX1 = \frac{e_{pin} \frac{PIN1}{d_{PIN1}} + d_{auxin}}{i_{AUX1} auxin_e} auxin_i - \frac{p_{auxin}}{i_{AUX1} auxin_e} \quad \text{Eq. 10}$$

$$AUX1_{ss} = \frac{p_{AUX1}}{d_{AUX1}} \frac{auxin_i^2}{auxin_i^2 + K_{AUX1}^2} \quad \text{Eq. 11}$$

This enabled us to draw the phase plane diagram. The auxin nullcline is a straight line. Assuming that auxin transport rates exceed auxin production and degradation rates, the slope approximates $\frac{e_{pin} PIN1_{ss}}{i_{AUX1} auxin_e}$, and the negative intercept $\frac{p_{auxin}}{i_{AUX1} auxin_e}$ will be very small (we used $p_{auxin} = 0$ resulting in an intercept at zero). The AUX1 null-cline corresponds to a second order Hill function that

approaches $\frac{p_{AUX1}}{d_{AUX1}}$ for large values of auxin, and its point of half maximum occurs for auxin equal to K_{AUX1} . For all parameter values, the two null-clines will intersect at a point close to (auxin=0,AUX1=0) (or at this point for $p_{auxin} = 0$), which corresponds to a stable state of the system. If the slope of the auxin null-cline is high, only this single intersection point will occur, resulting in a single low auxin-low AUX1 equilibrium. For parameter values resulting in a more shallow slope of the auxin null-cline two additional intersection points arise, the higher one of which is an alternative high auxin-high AUX1 stable state, and the lower one an unstable state separating the two stable equilibria. Finally, if parameter values result in very shallow slopes, although the lower stable equilibrium remains present, the unstable equilibrium will lie infinitesimally nearby, enabling the system to only converge to the higher stable equilibrium.

Note that if we instead assume that PIN1 and AUX1 auxin transport are not proportionate to auxin levels, but saturate with increasing auxin levels (as we did for the spatial, 1D cell strand models described below) the auxin equation changes into:

$$\frac{d_{auxin}}{dt} = i_{AUX1}AUX1 \frac{auxin_e}{auxin_e + K_e} - e_{pin1}PIN1 \frac{auxin}{auxin + K_i} + p_{auxin} - d_{auxin}auxin \quad \text{Eq. 12}$$

This changes the equation for the auxin null-cline into:

$$AUX1 = \frac{e_{pin1}PIN1 \frac{auxin}{auxin + K_i}}{i_{AUX1} \frac{auxin_e}{auxin_e + K_e}} + \frac{d_{auxin}}{i_{AUX1} \frac{auxin_e}{auxin_e + K_e}} auxin - \frac{p_{auxin}}{i_{AUX1} \frac{auxin_e}{auxin_e + K_e}} \quad \text{Eq. 13}$$

Since external auxin is a control parameter, the saturation terms with $auxin_e$ in them merely represent constants, with higher external auxin values resulting in division by a larger number. Thus, this leaves only the new saturating dependence on internal auxin as being relevant for null-cline shape, and we see that the auxin null-cline now depends on internal auxin levels with both a saturating and a linear dependence term, whereas earlier we only had a linear dependence. Despite this change in null-cline shape we still get the following sequence of situations for increasing external auxin: For low external auxin (division by small number) this auxin null-cline intersects the AUX1 null-cline only in a single low auxin low AUX1 point, overshooting it for higher internal auxin values. If instead external auxin is higher (division by larger number), the null-clines intersect three times resulting in a low and high stable equilibrium separated by an instable intermediate equilibrium. Finally, if external auxin levels are even higher (division by very large number) the lower and middle intersection points lie very close together, and only the high auxin high AUX1 equilibrium is accessible. Thus, qualitative model behavior remains the same. Null-cline and bifurcation analysis was performed using Grind in R, developed by R. De Boer at Utrecht University (<http://theory.bio.uu.nl/rdb/grind.html>).

Simple cell strand model

This model describes a simple strand of 15 cells, ignoring cell growth, division, expansion and differentiation processes and the resulting zonation. The model incorporates for each individual cell the BRX_m, PAX_p, and PIN_p dynamics as well as the AUX1 dynamics described in the previous two single cell models. Additionally, the model dynamically describes intracellular and extracellular auxin dynamics, in a manner similar to previous models²⁻⁵.

For a grid point i,j inside the wall bordered by only wall grid points we write:

$$\frac{\delta Aux_{i,j}}{\delta t} = \frac{D_{wall}}{\Delta x} (Aux_{i+1,j} + Aux_{i-1,j} + Aux_{i,j+1} + Aux_{i,j-1} - 4Aux_{i,j}) \quad \text{Eq. 14}$$

Here D_{wall} is the diffusion rate for auxin in the apoplast and Δx is the spatial resolution of the simulation. For a grid point i,j inside the cytoplasm bordered by only other cytoplasmic grid points we write:

$$\frac{\delta \text{Aux}_{i,j}}{\delta t} = p_{\text{Aux}} - d_{\text{Aux}} \text{Aux}_{i,j} + \frac{D_{\text{cell}}}{\Delta x} (\text{Aux}_{i+1,j} + \text{Aux}_{i-1,j} + \text{Aux}_{i,j+1} + \text{Aux}_{i,j-1} - 4\text{Aux}_{i,j}) \quad \text{Eq. 15}$$

Here p_{Aux} is the rate at which auxin is produced per cell, d_{Aux} is the rate at which auxin is degraded per cell, and D_{cell} is the diffusion rate for auxin inside cells.

For a grid point i,j inside the wall, bordered by three other wall grid points and one cytoplasmic grid point $(i,j-1)$ and hence membrane grid point we write:

$$\frac{\delta \text{Aux}_{i,j}}{\delta t} = -i_{\text{pas}} - i_{\text{aux1}} \text{AUX1}_{i,j} f(\text{Aux}_{i,j}) + e_{\text{PIN}} \text{PIN}_{i,j} g(\text{Aux}_{i,j-1}) + \frac{D_{\text{wall}}}{\Delta x} (\text{Aux}_{i+1,j} + \text{Aux}_{i-1,j} + \text{Aux}_{i,j+1} - 3\text{Aux}_{i,j}) \quad \text{Eq. 16}$$

$$\text{with } f(\text{Aux}_{i,j}) = \frac{\text{Aux}_{i,j}}{\text{Aux}_{i,j} + K_{\text{sataux1}}} \text{ and } g(\text{Aux}_{i,j}) = \frac{\text{Aux}_{i,j}}{\text{Aux}_{i,j} + K_{\text{satpin}}}$$

Here, i_{pas} is the rate of passive auxin influx from walls to cytoplasm, i_{aux1} is the maximum rate of active auxin influx through AUX1 from walls to cytoplasm, K_{sataux1} is the internal auxin level at which AUX1 operates at its half maximum rate, e_{PIN} is the maximum rate of active pumping of auxin through PINs from cytoplasm to walls, and K_{satpin} is the external auxin level at which PIN operates at its half maximum rate. Finally, for a point i,j inside the cytoplasm, neighboring three other cytoplasmic grid points and one cell wall grid point $(i,j-1)$ we write:

$$\frac{\delta \text{Aux}_{i,j}}{\delta t} = i_{\text{pas}} + i_{\text{aux1}} \text{AUX1}_{i,j} f(\text{Aux}_{i,j-1}) - e_{\text{PIN}} \text{PIN}_{i,j} g(\text{Aux}_{i,j}) + \frac{D_{\text{cell}}}{\Delta x} (\text{Aux}_{i+1,j} + \text{Aux}_{i-1,j} + \text{Aux}_{i,j+1} - 3\text{Aux}_{i,j}) \quad \text{Eq. 17.}$$

Note that auxin dynamics are solved on a subcellular grid level, incorporating both transmembrane transport processes as well as intracellular and intra-wall diffusional auxin transport, similar to earlier models^{2,3}. Note as well that the amount of auxin transported by a single PIN or AUX1 protein saturates with increasing levels of auxin, something that is usually ignored. Finally note that e_{PIN} is not a parameter, but instead a constant rate parameter multiplied by a term that is dependent on the fraction of phosphorylated PIN (Eq. 4).

Based on experimental data from protophloem cells, we assume a highly rootward polarized PIN1 pattern, with limited auxin exporter levels at lateral and shootward membrane faces (10% of downward oriented PIN1). Also based on our experimental data, we assume an apolar AUX1 pattern, with AUX1 levels highest at the apical and basal membranes, and lower (50%) at the lateral membranes. Finally, we incorporate influx of auxin at the top of the cell file (applying $p_{\text{aux}} = 10 [\text{ }] s^{-1}$ in the top-most horizontal cell wall), a small auxin influx at the sides of the cell file (applying $p_{\text{aux}} = \frac{10}{\text{tissue length}} [\text{ }] s^{-1}$ for each lateral cell wall grid point), as well as an auxin efflux at the bottom of the cell file (applying $d_{\text{aux}} = 0.25 s^{-1}$ in the bottom-most horizontal cell wall).

Parameter settings for auxin dynamics can be found in Supplementary Table 5. Auxin dynamics were solved using an alternating direction implicit (ADI) integration scheme⁶, using a timestep of 0.2ms and a spacstep of 2 micrometer.

Parameter values for auxin diffusion D_{wall} and D_{cell} , and passive influx i_{pas} are similar to those of earlier studies^{2,3}. Saturation constants for AUX1 and PIN1 transport rates K_{sataux1} and K_{satpin} were set to approximately halfway the maximally observed auxin concentrations. e_{PIN} was set to a 5 times lower value than in our previous models based on our recent observation of donut-shaped PIN1 patterns in protophloem cells, which effectively reduces PIN1-mediated auxin export⁷. Other parameters (in italics) were already discussed in Table 2.

For the simulations with BRX_{mem} , PAX_{p} , and PIN_{p} dynamics disabled, a constant level of $\text{PIN}_{\text{p}}=60$ is assumed, and auxin influx from the top is varied. For the simulations with full BRX_{mem} , PAX_{p} , and PIN_{p} model dynamics a constant auxin influx from the top is applied.

Developing protophloem strand model

As a final step we extended the simple, static single strand model to a realistic, zoned and growing protophloem sieve element (PPSE) strand model.

Zonation

We built up our PPSE strand model out of 2 distinct zones: the meristematic and the differentiation zone. Additionally, within the meristem we distinguish the three most rootward cells as being slower dividing stem cells, consistent with experimental observations. Through division, individual cells will sequentially move towards and into the differentiation zone, being pushed shootward by cells newly arising from stem cell divisions as well as the expansion of existing clones lying rootward. For simplicity, we superimposed the location of the meristematic-differentiation zone boundary, with the meristematic to differentiation zone boundary at a distance of on average 15 meristematic cells from the start of the PPSE strand (since cells change size due to growth and division processes, this results in an average number of cells fitting in a constant-sized domain) and setting overall cell file length such that a differentiation zone containing an average of 6-8 cells with a maximum size of 30 micrometer arises (consistent with experimental evidence). Note that we did not explicitly incorporate the elongation zone in our PPSE strand model. In this zone, cells have become fully differentiated, and in the case of protophloem cells this means strongly reduced organelles and fully enucleated, with minimal resistance to phloem sap transport. Therefore, while auxin transport in the meristem and differentiation zone is governed by AUX1 importer and PIN exporter levels and activities, auxin transport in the differentiation zone mainly occurs through bulk flow. Therefore, this part of the auxin dynamics was represented as auxin inflow into the differentiation zone.

Growth, division and expansion

Division and elongation rates: We assume that normal meristematic cells have a division time of 12 hours, consistent when correcting classical average cell cycle measurements on the entire Arabidopsis root meristem⁸ with the more recent observation that a substantial rootward part of the meristem does not take part in active divisions^{9,10}. The applied expansion rate is the same as in earlier models¹¹. We assume that the three most rootward oriented stem cell that divide at rates that are slower than the normal meristematic cells yet increase shootward, consistent with experimental observations¹¹. We assume division in the lower-most stem cell to be so slow that we ignore them, we assume a division time of 25.2 hours for the second stem cell, and a division time of 16.8 hours for the third stem cell. These numbers were chosen such that they are neither multiples of one another nor of the normal meristematic cells, ensuring the generation of out-of-phase clones of sibling cells, also consistent with experimental observations¹².

Division and elongation on a grid: Cell growth and expansion is modeled as in Mahonen et al., 2014³. Briefly, individual cells consist of a number of rows and columns of grid points. If a cell undergoes either cytoplasmic growth or vacuolar expansion, a row of gridpoints is added to the shootward part of the cell and all rootward lying cells are shifted one row upward on the simulation grid. Auxin concentrations are diluted to compensate for the resulting instantaneous cellular volume increase, protein concentrations are only diluted in case of cytoplasmic, but not vacuolar volume increase. Cell division occurs if cells have reached twice their original size (increase from 8 to 16 micrometer). Upon cell division, cells inherit the PIN and AUX1 patterns and levels of their maternal cell. During expansion, cells can reach a maximum size of 30 micrometer, consistent with the sizes reached within the differentiation zone. Cell behavior (cytoplasmic growth and division, elongation) is dictated by the zone in which a cell resides (see previous section).

Finite grid size: Cells exceeding a threshold position from the start of the simulated PPSE strand with their apical membrane are removed from the simulation to prevent a continuous increase in the size of the simulated domain. The threshold distance is taken such that at least 5 cells in the elongation zone are contained within the simulation.

Reflux loop emulation

To correctly simulate protophloem auxin patterning, we take into account that in addition to auxin received from the auxin flux via shootward differentiated phloem, and auxin loss to more rootward tissues, auxin is also received laterally through the presence of the root tip auxin reflux loop⁵, and that this results in a predominant recycling of auxin at the top of the meristem, with influx gradually decreasing when moving closer to the root tip (see illustration for p_{aux} values (black) and d_{aux} values (red) used to emulate this reflux influx and efflux, respectively). For lateral auxin flow into the meristem, we furthermore apply:

$$influx_j = \left(a_{pinp} PINp/PINtot + (1 - a_{pinp}) \right) (b_{basal} + b_{increase} j/MZsize)$$

Where b_{basal} is the baseline influx rate occurring at the most rootward positions, and $b_{increase}$ (set at twice the value of b_{basal}) the maximum increase in influx rate occurring at the end of the meristem (see Supplementary Figure 8), and a_{pinp} is the phosphorylated PIN-dependent and $(1 - a_{pinp})$ the phosphorylated PIN-independent fraction. Thus, we take into account that *brx* and *pax* mutations that affect PIN phosphorylation level, through affecting root tip auxin delivery, will also affect auxin reflux into the protophloem strand itself. Under default conditions $a_{pinp} = 0.65$, only in case of non-auxin-dependent AUX1 expression we use $a_{pinp} = 1$ to compensate for the higher overall AUX1 levels in absence of auxin-dependent AUX1. Finally, we assume that efflux at the bottom of the protophloem strand results in a maximum auxin level (put to 150).

For the simulation results where auxin-dependent AUX1 expression was disabled, a constant AUX1 expression level of 100 was assumed. Otherwise the normal auxin-dependent AUX1 expression was applied.

Adding Differentiation

To investigate the impact of the timing of auxin-dependent protophloem cell differentiation on gap patterning, we implemented two alternative differentiation scenarios in our model. In both scenarios the increase in differentiation level as a function of auxin is modelled as:

$$\frac{dDiff}{dt} = p_{diff} \frac{auxin_i^2}{auxin_i^2 + \kappa_{diff}^2} \quad \text{Eq. 18}$$

With p_{diff} the maximum rate of differentiation level increase, and K_{Diff} the auxin level at which this rate is half maximal. Because of the considerably higher auxin levels in the division zone as compared to more shootward zones as well as the longer time cells spend in this zone, we use $K_{Diff} = 75$ []s⁻¹ and $p_{diff} = 0.002$ []s⁻¹ for the early differentiation scenario, and $K_{Diff} = 35$ []s⁻¹ and $p_{diff} = 0.004$ []s⁻¹ for the late differentiation scenario, to ensure that we are investigating differences in the timing of differentiation onset and not final differences in the differentiation level reached. Note that the differentiation dynamics equation contains no decay term. This serves to ensure that once auxin levels drop no de-differentiation will occur. If a differentiation level of 100 is reached, no further increase in differentiation is modeled.

Early starting-early ending differentiation (“early scenario”)

In this scenario, the equation for differentiation dynamics shown above is applied from 6 cell heights rootward of the bottom of the simulated PPSE strand until the end of the meristematic zone.

Late starting-late ending differentiation (“late scenario”)

In this scenario, the equation for differentiation dynamics shown above is applied from the start of the differentiation zone onwards.

Auto-activation of differentiation

We assume that once a certain threshold level of the simulated differentiation state is reached, cells will proceed to successfully differentiate into a protophloem cell, while cells failing to reach this level will become non-differentiated gap cells. Such dynamics will automatically arise if the differentiation process, in addition to being auxin-dependent, also has a positive feedback on itself. To explicitly simulate this, in a subset of simulations we replaced the equation for the differentiation factor with:

$$\frac{dDiff}{dt} = p_{diff} \max\left(\frac{auxin_i^2}{auxin_i^2 + K_{diff}^2}, \frac{Diff^4}{Diff^4 + K_{m,diff}^4}\right), \quad \text{Eq. 18b}$$

where \max indicates a maximum function, effectively implementing an OR-type logic for *the auxin* and *Diff* influence on *Diff* expression, and $K_{m,diff} = 65$ the level of *Diff* at which half-maximal auto-activation occurs. Importantly, while auxin-dependent differentiation occurs within a restricted spatio-temporal window (either early or late scenario), no such restrictions apply for auto-activated differentiation.

Adding YUCCA

To investigate the potential effect of local rather than shoot-derived auxin on protophloem differentiation, we incorporated the *YUC5* expression. Based on the observation that *YUC5* is only expressed in the differentiation zone, but not in the meristematic zone or stem cell niche, we assumed that *YUC5* expression depends on differentiation status. We therefore model *YUC5* expression as:

$$\frac{dYUC5}{dt} = p_{yucr} \frac{Diff^2}{Diff^2 + K_{yuc5}^2} - d_{yuc} YUC5 \quad \text{Eq. 19}$$

With $p_{yuc5} = 0.01$ s⁻¹ the maximum rate of *YUC5* expression, $K_{yuc5} = 65$ [] the differentiation level at which *YUC5* expression is half maximal, and $d_{yuc5} = 0.0001$ s⁻¹ the degradation rate of *YUC5*.

We assume that *YUC5* expression has the following effect on local auxin biosynthesis:

$$p_{aux} = 0.001YUC5$$

To investigate the dependence on the *source* of auxin rather than the *absolute level* of auxin, we computed the extra amount of auxin present in a wildtype simulation as compared to when no YUCCA-mediated local auxin production was incorporated. We subsequently reduced the amount of shoot-derived auxin influx to arrive at a similar amount of overall auxin as before.

Robustness of results for the simple single strand model and the developing protophloem strand model were tested both against the parameter variations also used to test robustness of the single cell protophloem model, as well as against variations in the precise AUX1 cellular pattern. For the latter, in addition to the default pattern in which basal and apical membranes have more AUX1 than the lateral membranes, also a fully apolar pattern with equal AUX1 levels on all membrane faces, and a more polar pattern with highest AUX1 levels on the apical surface were tested. In all cases only small quantitative differences were observed, while qualitative outcomes remained constant.

Source codes for the different models described here are available on:

<http://bioinformatics.bio.uu.nl/kbwjtuss/ProtophloemModel>

Supplemental References:

- 1 Marhava, P. *et al.* A molecular rheostat adjusts auxin flux to promote root protophloem differentiation. *Nature* **558**, 297-300, doi:10.1038/s41586-018-0186-z (2018).
- 2 van den Berg, T., Korver, R. A., Testerink, C. & ten Tusscher, K. H. W. J. Modeling halotropism: a key role for root tip architecture and reflux loop remodeling in redistributing auxin. *Development* **143**, 3350-3362, doi:10.1242/dev.135111 (2016).
- 3 Mahonen, A. P. *et al.* PLETHORA gradient formation mechanism separates auxin responses. *Nature* **515**, 125-129, doi:10.1038/nature13663 (2014).
- 4 Mitchison, G. J. Model for Vein Formation in Higher-Plants. *Proc R Soc Ser B-Bio* **207**, 79-109, doi:DOI 10.1098/rspb.1980.0015 (1980).
- 5 Grieneisen, V. A., Xu, J., Maree, A. F., Hogeweg, P. & Scheres, B. Auxin transport is sufficient to generate a maximum and gradient guiding root growth. *Nature* **449**, 1008-1013, doi:10.1038/nature06215 (2007).
- 6 Peaceman, D. W. & Rachford, H. H. The Numerical Solution of Parabolic and Elliptic Differential Equations. *J Soc Ind Appl Math* **3**, 28-41, doi:Doi 10.1137/0103003 (1955).
- 7 Marhava, P. *et al.* Plasma Membrane Domain Patterning and Self-Reinforcing Polarity in Arabidopsis. *Dev Cell* **52**, 223-235, doi:10.1016/j.devcel.2019.11.015 (2020).
- 8 Beemster, G. T. S. & Baskin, T. I. Analysis of cell division and elongation underlying the developmental acceleration of root growth in Arabidopsis thaliana. *Plant Physiol* **116**, 1515-1526, doi:DOI 10.1104/pp.116.4.1515 (1998).
- 9 Ivanov, V. B. & Dubrovsky, J. G. Longitudinal zonation pattern in plant roots: conflicts and solutions. *Trends in Plant Science* **18**, 237-243, doi:10.1016/j.tplants.2012.10.002 (2013).
- 10 Pacheco-Escobedo, M. A. *et al.* Longitudinal zonation pattern in Arabidopsis root tip defined by a multiple structural change algorithm. *Ann Bot-London* **118**, 763-776, doi:10.1093/aob/mcw101 (2016).
- 11 Campilho, A. *et al.* Time-lapse analysis of stem-cell divisions in the Arabidopsis thaliana root meristem. *Plant Journal* **48**, 619-627, doi:10.1111/j.1365-313X.2006.02892.x (2006).
- 12 von Wangenheim, D. *et al.* Live tracking of moving samples in confocal microscopy for vertically grown roots. *Elife* **6**, e26792 doi:10.7554/eLife.26792 (2017).